ISTANBUL TECHNICAL UNIVERSITY ★ GRADUATE SCHOOL

INVESTIGATION OF FINE AND HYPERFINE STRUCTURE ENERGY LEVELS OF HOLMIUM I USING LASER SPECTROSCOPIC TECHNIQUES

Ph.D. THESIS

Seda KIN BARKA

Department of Physics Engineering

Physics Engineering Programme

JULY 2025

ISTANBUL TECHNICAL UNIVERSITY ★ GRADUATE SCHOOL

INVESTIGATION OF FINE AND HYPERFINE STRUCTURE ENERGY LEVELS OF HOLMIUM I USING LASER SPECTROSCOPIC TECHNIQUES

Ph.D. THESIS

Seda KIN BARKA
(509052107)

Department of Physics Engineering

Physics Engineering Programme

Thesis Advisor: Prof. Dr. Günay BAŞAR

JULY 2025

İSTANBUL TEKNİK ÜNİVERSİTESİ ★ LİSANSÜSTÜ EĞİTİM ENSTİTÜSÜ

HOLMİYUM I'İN İNCE VE AŞIRI İNCE YAPI ENERJİ SEVİYELERİNİN LASER SPEKTROSKOPİK YÖNTEMLERLE İNCELENMESİ

DOKTORA TEZİ

Seda KIN BARKA
(509052107)

Fizik Mühendisliği Anabilim Dalı

Fizik Mühendisliği Programı

Tez Danışmanı: Prof. Dr. Günay BAŞAR

TEMMUZ 2025

Seda KIN BARKA, a Ph.D. student of ITU Graduate School student ID 509052107 successfully defended the thesis entitled "INVESTIGATION OF FINE AND HYPERFINE STRUCTURE ENERGY LEVELS OF HOLMIUM I USING LASER SPECTROSCOPIC TECHNIQUES", which she prepared after fulfilling the requirements specified in the associated legislations, before the jury whose signatures are below.

Thesis Advisor :	**Prof. Dr. Günay BAŞAR** Istanbul Technical University	.....
Jury Members :	**Prof. Dr. Cem Mehmet GÜÇLÜ** Istanbul Technical University	.....
	Prof. Dr. Ali GELİR Istanbul Technical University	.....
	Prof. Dr. İpek KANAT ÖZTÜRK Istanbul University	.....
	Prof. Dr. Feyza GÜZELÇİMEN Istanbul University	.....

Date of Submission : **01 July 2025**
Date of Defense : **04 August 2025**

To my spouse İlke, my son Arel and in loving memory of my father Halil.

FOREWORD

I would like to sincerely thank my advisor, Prof. Dr. Günay BAŞAR and Prof. Dr. Gönül BAŞAR at Istanbul University, who both welcomed me back to my Ph.D. studies after a prolonged interruption due to health issues and unforeseen life challenges, for their patience, support, encouragement, and guidance throughout my doctoral studies. Their knowledge and experience in the field of atomic physics helped me complete this study and taught me extensive laboratory skills.

I would like to thank my thesis progress committee members, Prof. Dr. İpek KANAT ÖZTÜRK and Prof. Dr. Mehmet Cem GÜÇLÜ, for their reading of this dissertation and valuable feedback.

Special thanks to Dr. İpek, who kindly guided me throughout my advisor's brief sabbatical leave, for her constructive criticism, which greatly contributed to shape this thesis, and for her calmness and warm-hearted talks.

Also, I sincerely thank Prof. Dr. Sophie KRÖGER at the HTW Berlin-University of Applied Sciences for being a part of the research group I was welcomed to, for her knowledge and insightful guidance in data analysis, which greatly enhanced the quality of this study, and for always being just a Zoom call away.

I would like to express my gratitude to the valued members of our research group, Prof. Dr. Feyza GÜZELÇİMEN, for her support, guidance, and encouragement, as well as to Dr. Doğukan BİNGÖL, who guided me through the experimental setup during my early days of study, and for their friendship.

In addition, I am grateful to Prof. Dr. M. Olcay ÇİZMELİ, Director of the Vocational School of Health Services at Acibadem University, for encouraging me to return to my doctoral studies and providing me with the support necessary to carry out my scientific research.

On a personal note, I would like to thank my husband, İlke, and my son, Arel, for their endless support and encouragement throughout the long hours and challenges of my studies. I truly could not have accomplished this without them. My heartfelt thanks also go to my family, my mother Gülten KIN, my mother-and father-in-law Mehveş and Günkut BARKA, especially my sister Cemre KAYAN, and my dearest cousin, Tuba USSELİ, for their constant love, belief in me, and uplifting presence along the way.

July 2025 Seda KIN BARKA

TABLE OF CONTENTS

	Page
FOREWORD	**ix**
TABLE OF CONTENTS	**xii**
ABBREVIATIONS	**xiii**
SYMBOLS	**xv**
LIST OF TABLES	**xvii**
LIST OF FIGURES	**xxiv**
SUMMARY	**xxv**
ÖZET	**xxvii**
1. INTRODUCTION	**1**
1.1 Purpose of Thesis	1
1.2 The Holmium Element	1
1.3 Literature Review	3
1.4 Summary of Theoretical Background	7
1.4.1 Application of quantum mechanics on atoms	7
1.4.2 *LS* and *JJ* couplings in atoms and their properties	11
1.4.3 *JI* coupling in atoms and their properties	12
1.4.4 Term symbol of an energy state	12
1.4.5 Fine structure	13
1.4.6 Hyperfine structure	14
1.4.7 Hamiltonian of many electron system	15
1.4.8 HFS splitting and selection rules	17
2. EXPERIMENTAL METHODS AND TECHNIQUES	**21**
2.1 Broadening of Spectral Lines	22
2.1.1 Natural line broadening	24
2.1.2 Doppler broadening	26
2.1.3 Saturation/Power broadening	29
2.1.4 Collisional/Pressure broadening	30
2.1.5 Combined line profile: Voigt profile	31
2.2 Basis of the Experiment	32
2.2.1 Hollow cathode discharge lamp	32
2.2.2 Optogalvanic spectroscopy	33
2.2.3 Laser induced fluorescence spectroscopy	34
2.2.4 Experimental setup of the study	37
2.2.5 Data analysis programs	40
2.2.5.1 Elements program	40
2.2.5.2 Fitter program	44
3. EXPERIMENTAL RESULTS	**53**
3.1 Search for New Levels	55
3.1.1 Method 1: Discovery with the lines observed in the FT spectra	55
3.1.2 Method 2: Using systematic OG scans	62
3.1.3 Discovered energy levels	68
3.2 Determination of hfs constants	93
4. Conclusion and Recommendation	**105**
REFERENCES	**107**
APPENDICES	**113**
APPENDIX A: Energy Levels of Atomic Holmium	115

CURRICULUM VITAE **142**

ABBREVIATIONS

LIF :	Laser Induced Fluorescence
LIFS :	Laser Induced Fluorescence Spectroscopy
OG :	Optogalvanic
OGS :	Optogalvanic Spectroscopy
FT :	Fourier Transform
FTS :	Fourier Transform Spectroscopy
FS :	Fine Structure
HFS :	Hyper Fine Structure
COG :	Center of Gravity
FWHM :	Full Width at Half Maximum

SYMBOLS

λ	:	Wavelength
ν	:	Frequency
σ	:	Wavenumber
P	:	Parity
A	:	Magnetic dipole hfs constant
B	:	Electric quadrupole hfs constant
Q	:	Electric quadrupole moment
μ	:	Magnetic dipole moment

LIST OF TABLES

Page

Table 1.1: Chemical and physical properties of atomic Holmium. **2**
Table 3.1: New levels together with their hyperfine structure constants *A* and *B* (in MHz). Energy values and error bars resulting from the analysis of FT lines (see Table 3.5) **82**
Table 3.2: List of experimental hyperfine structure constants *A* and *B* which were fixed during the hfs analysis. **83**
Table 3.3: List of measured Ho I lines with the LIFS method to determine new energy levels with their classification. New levels are emphasized in bold. **89**
Table 3.4: Experimental hfs constants *A* and *B* (in MHz) for already known levels, together with values from literature if available. **90**
Table 3.5: List of Holmium lines from the FT spectrum [29,34,66], classified by the new levels. **91**
Table 3.6: List of Holmium lines from the FT spectrum [29,34,66], classified by the levels already published in [41,43], but also discovered by us. **94**
Table 3.7: List of spectral lines defined in the FT spectrum and investigated with the LIFS method. Both wavelength and wave number are given as fit result of the measured lines. **95**
Table 3.8: Energy levels with their hyperfine structure constants *A* and *B* (in MHz.). Energy values and error bars were found from the analysis of multiple LIF measurements of each laser line. **104**
Table 3.9: Experimental hyperfine structure constants *A* and *B* (in MHz.) of Ho I which kept fixed during the fit procedure. **104**
Table A.1: Energy levels of Ho from the literature with their corresponding hfs constants, if available. (Ref 1 and Ref 2 indicate the references of the energy levels and hfs constants, respectively). **115**

LIST OF FIGURES

Page

Figure 1.1: Illustration of a) *LS* and b) *JJ* vector coupling for a two-electron atom. **11**
Figure 1.2: Illustration of *JI* vector coupling. **12**
Figure 1.3: LS coupling and the interaction energy of fine structure splitting (ΔE_{FS}). . **13**
Figure 1.4: *JI* coupling and the interaction energy of hyperfine structure splitting (ΔE_{HFS}). **14**
Figure 1.5: Transition and energy level spacing comparison of fs and hfs of a spectral line at $\sigma = 12964.07$ cm^{-1} ($\lambda = 771.151$ nm). **19**
Figure 2.1: Decay curve of the population density N_i of E_i with τ_i..... **22**
Figure 2.2: Spectral line profile. **23**
Figure 2.3: Natural line broadening of a transition caused by the lifetime of the energy states ΔE_1 and ΔE_2. ..... **24**
Figure 2.4: Natural line width a) Damped oscillation and b) Lorentzian line profile. .. **25**
Figure 2.5: Doppler broadening. a) Doppler effect b) Gaussian line profile. **27**
Figure 2.6: Comparison of Gaussian and Lorentzian line profiles with the same FWHM. **28**
Figure 2.7: Saturation broadening with increasing intensity of the light source. **29**
Figure 2.8: Collision-induced shift and broadening of a spectral line. **30**
Figure 2.9: Voigt profile of a spectral line formed by the combination of the Lorentzian and Gaussian line profiles. **31**
Figure 2.10: Cross section of an HC discharge lamp..... **33**
Figure 2.11: Experimental setup of Optogalvanic Spectroscopy. **34**
Figure 2.12: Energy level diagram with possible fluorescence channels for LIF..... **35**
Figure 2.13: Experimental setup of Laser-Induced Spectroscopy. **36**
Figure 2.14: Experimental setup of the combined LIF and OG spectroscopy method. .. **39**
Figure 2.15: Classification window of the Elements program, with examined line at λ= 7509.12 Å..... **42**
Figure 2.16: Simulation of the line at λ= 7509.12 Å using the simulation program, where the red spectrum shows the experimental spectral line and blue the theoretical fit. a) and b) illustrate a good and bad fit, respectively, due to altered *B* hfs value. **44**
Figure 2.17: Screen shots of the data files .mes and .par, respectively. **47**
Figure 2.18: Screen shots of the data files .mes and .lin, respectively. The raw spectrum from the LIFS measurement is given in a). Linearized spectrum of the raw spectrum with the x-axis converted into MHz. **48**
Figure 2.19: Screen shots of the data file .ein for the fitting process of the linearized spectrum..... **49**
Figure 2.20: Screen shots of the data file .ein for the fitting process of the linearized spectrum..... **50**

Figure 2.21: Screenshots of the .aus data file showing the input data and iteration data for individual components in the HFS analysis, as well as the fit profile, Cog and hfs constants obtained on the left and right sides of a), respectively. The confidence interval of the fit result is provided in b). **52**
Figure 3.1: The FT spectrum of the observed λ_{air}= 750.912 nm (σ= 13313.46 cm^{-1}) undefined line. **57**
Figure 3.2: Measured 25 GHz OG spectrum with FPI markers with laser wavelength at λ_{air}=750.912 nm (σ=13313.46 cm^{-1})..... **57**
Figure 3.3: Observed fluorescence lines during a 50 nm monochromator scan between 500 nm and 550 nm with fixed laser wavelength at λ_{air}= 750.928 nm (σ=13313.18 cm^{-1}). ($*$: λ_F^-= 536.050 nm) **58**
Figure 3.4: Simultaneously measured LIF and OGS spectra with FPI markers of laser wavelength λ_{air}= 750.916 nm (σ=13313.46 cm^{-1}) with the monochromator set to the fluorescence line at a) λ_F^-= 536.050 nm and b) λ_F= 538.800 nm give the same hfs structure indicating they belong to the energy levels of the laser line. **59**
Figure 3.5: The FT observed spectrum at λ_F=536.000 nm of the measured fluorescence line λ_F^-= 536.050 nm. **59**
Figure 3.6: Experimental LIF spectrum of the line at λ_{air}=750.912 nm (σ= 13313.47 cm^{-1}) measured with the monochromator set at λ_F^-= 536.050 nm with the best-fit curve superposed..... **60**
Figure 3.7: Measured spectral lines in the discovery of the energy level E_{upper}= 31964.93(0.03) cm^{-1}, J= 13/2 (o), with the monochromator fixed at λ_F= 662.831 nm. a) line at σ= 13106.73 cm^{-1} (λ= 762.757 nm), E_{lower}= 18858.19 cm^{-1}, J=13/2, (e) $\longrightarrow E_{upper}$ b) line at σ= 13313.47 cm^{-1} (λ= 750.912 nm), E_{lower}= 18651.53 cm^{-1}, J=15/2, (e) $\longrightarrow E_{upper}$ c) line at σ= 13143.66 cm^{-1} (λ= 760.614 nm, E_{lower}= 18821.25 cm^{-1}, J=11/2, (e) $\longrightarrow E_{upper}$ d) line at σ= 13473.71 cm^{-1} (λ= 741.982 nm), E_{lower}= 18491.21 cm^{-1}, J=11/2, (e) $\longrightarrow E_{upper}$ **61**
Figure 3.8: Illustration of a 20 GHz OG scan in the search for an undefined spectral line. **63**
Figure 3.9: The FT observed spectrum at λ_F^-= 592.900 nm of the measured fluorescence line λ_F= 592.915 nm (σ=16861.15 cm^{-1})..... **63**
Figure 3.10: Simultaneously measured LIF and OGS spectra of λ_{air}= 798.464 nm line with the monochromator set to the fluorescence line at λ_F^-= 592.915 nm. This OGS scan was recorded on a different day, resulting in a noisy spectrum when compared with the scan in Fig.3.8. ..... **64**
Figure 3.11: Experimental LIF spectrum of the line at λ_{air}=798.468 nm (σ= 12520.54 cm^{-1}) measured with the monochromator set at λ_F^-= 592.915 nm with the best-fit curve superposed..... **65**
Figure 3.12: FT spectrum observed positive fluorescence line at λ_F=683.629 nm arising from the transition of the new discovered energy level E_{upper}= 40077.43 cm^{-1}. **66**

Figure 3.13: Measured spectral lines in the discovery of the energy level E_{upper} = 40077.35 (0.08) cm^{-1}, J= 11/2 (o), with the monochromator fixed at λ_F=683.629 nm. a) line at σ= 12437.11 cm^{-1} (λ= 803.824 nm), E_{lower}= 27640.05 cm^{-1}, J=11/2, (e) $\longrightarrow E_{upper}$ b) line at σ= 12520.54 cm^{-1} (λ= 798.468 nm), E_{lower}= 27556.90 cm^{-1}, J=9/2, (e) $\longrightarrow E_{upper}$ c) line at σ= 12936.16 cm^{-1} (λ= 772.815 nm), E_{lower}= 27141.28 cm^{-1}, J=13/2, (e) $\longrightarrow E_{upper}$ d) line at σ= 13130.00 cm^{-1} (λ= 761.405 nm), E_{lower}= 26947.33 cm^{-1}, J=13/2, (e) $\longrightarrow E_{upper}$ **66**

Figure 3.14: Simultaneously measured LIF and OGS spectra of λ_{air}= 798.468 nm line with the monochromator set to the fluorescence line at λ_F= 683.629 nm. The highlighted extra peak observed in the OG spectrum at σ= 12520.73 cm^{-1} indicates a possible new starting point in the search for a new fine structure energy level..... **67**

Figure 3.15: Measured spectral lines (25 GHz) in the discovery of the energy level E_{upper} = 36859.56(0.03) cm^{-1}, J= 11/2 (o), with the monochromator fixed at λ_F=546.455 nm. a) line at σ= 12913.39 cm^{-1} (λ= 774.177 nm), E_{lower}= 23946.16 cm^{-1}, J=11/2, (e) $\longrightarrow E_{upper}$ b) line at σ= 12998.32 cm^{-1} (λ= 769.119 nm), E_{lower}= 23861.17 cm^{-1}, J=9/2, (e) $\longrightarrow E_{upper}$ **69**

Figure 3.16: Measured spectral lines in the discovery of the energy level E_{upper} = 40165.71(0.07) cm^{-1}, J= 13/2 (o), with the monochromator fixed at λ_F=684.995 nm and λ_F^-=464.165 nm, shown respectively in a) and b). a) line at σ= 13024.48 cm^{-1} (λ= 767.574 nm), E_{lower}= 27141.28 cm^{-1}, J=13/2, (e) $\longrightarrow E_{upper}$ b) line at σ= 13207.93 cm^{-1} (λ= 756.912 nm), E_{lower}= 26957.70 cm^{-1}, J=15/2, (e) $\longrightarrow E_{upper}$ **70**

Figure 3.17: Measured spectral lines in the discovery of the energy level E_{upper} = 39653.44(0.04) cm^{-1}, J= 13/2 (e), with the monochromator fixed at λ_F=480.962 nm. a) line at σ= 12003.87 cm^{-1} (λ= 832.836 nm), E_{lower}= 27649.51 cm^{-1}, J=15/2, (o) $\longrightarrow E_{upper}$ b) line at σ= 12730.98 cm^{-1} (λ= 756.912 nm), E_{lower}= 26922.40 cm^{-1}, J=15/2, (o) $\longrightarrow E_{upper}$ **71**

Figure 3.18: Measured spectral lines in the discovery of the energy level E_{upper} = 42407.40(0.1) cm^{-1}, J= 17/2 (e), with the monochromator fixed at λ_F^-=555.311 nm for line a) and λ_F=475.406 nm for line b). a) line at σ= 12714.58 cm^{-1} (λ= 786.282 nm), E_{lower}= 29692.67 cm^{-1}, J=19/2, (o) $\longrightarrow E_{upper}$ b) line at σ= 12964.23 cm^{-1} (λ= 771.141 nm), E_{lower}= 29443.09 cm^{-1}, J=17/2, (o) $\longrightarrow E_{upper}$ **71**

Figure 3.19: Measured spectral line in the discovery of the energy level E_{upper} = 36954.20(0.04) cm^{-1}, J= 13/2 (o), with the monochromator fixed at λ_F=406.139 nm. c) shows the visually combined line spectrum of measured spectra a) and b) at σ= 12998.50 cm^{-1} (λ= 769.108 nm), E_{lower}= 23955.68 cm^{-1}, J=13/2, (e) $\longrightarrow E_{upper}$ **72**

Figure 3.20: Measured spectral lines in the discovery of the energy level E_{upper} = 42337.80(0.07) cm^{-1}, J= 17/2 (e), with the monochromator fixed at λ_F=548.617 nm for lines a) and b) and λ_F^-=475.695 nm for line e). e) shows the visually combined measured spectra of c) and d). a) line at σ= 12503.75 cm^{-1} (λ= 799.540 nm), E_{lower}= 29834.05 cm^{-1}, J=15/2, (o) $\longrightarrow$ E_{upper} b) line at σ= 12806.54 cm^{-1} (λ= 780.636 nm), E_{lower}= 29531.25 cm^{-1}, J=17/2, (o) $\longrightarrow$ E_{upper} e) line at σ= 12894.77 cm^{-1} (λ= 775.295 nm), E_{lower}= 29443.09 cm^{-1}, J=17/2, (o) $\longrightarrow$ E_{upper} **73**

Figure 3.21: Measured spectral line in the discovery of the energy level E_{lower}= 27113.28(0.02) cm^{-1}, J= 11/2 (e), with the monochromator fixed at λ_F=683.629 nm. line at σ= 12964.07 cm^{-1} (λ= 771.151 nm), E_{upper}= 40077.35 cm^{-1}, J=11/2, (o) $\longrightarrow$ E_{lower} **74**

Figure 3.22: Measured spectral line in the discovery of the energy level E_{upper}= 31062.22(0.02) cm^{-1}, J= 11/2 (o), with the monochromator fixed at λ_F^-=586.026 nm. line at σ= 14002.85 cm^{-1} (λ= 713.943 nm), E_{lower}= 17059.35 cm^{-1}, J=13/2, (e) $\longrightarrow$ E_{upper} **75**

Figure 3.23: Measured spectral line in the discovery of the energy level E_{upper} = 32663.47(0.04) cm^{-1}, J= 11/2 (o), with the monochromator fixed at λ_F=492.015 nm. c) shows the visually combined line spectrum of the measured spectra a) and b). c) line at σ= 13842.15 cm^{-1} (λ= 722.232 nm), E_{lower}= 18821.25 cm^{-1}, J=11/2, (e) $\longrightarrow$ E_{upper} **76**

Figure 3.24: Measured spectral line in the discovery of the energy level E_{upper} = 37774.72(0.05) cm^{-1}, J= 11/2 (o), with the monochromator fixed at λ_F^-=404.081 nm): Line at σ= 13034.14 cm^{-1} (λ= 786.282 nm), E_{lower}= 24740.52 cm^{-1}, J=13/2, (e) $\longrightarrow$ E_{upper} **77**

Figure 3.25: Measured spectral lines in the discovery of the energy level E_{upper} = 37776.32(0.04) cm^{-1}, J= 13/2 (o), with the monochromator fixed at λ_F^-=404.081 nm for line a) and λ_F^-=416.300 nm for line b). a) line at σ= 13035.77 cm^{-1} (λ= 766.099 nm), E_{lower}= 24740.52 cm^{-1}, J=13/2, (e) $\longrightarrow$ E_{upper} b) line at σ= 13762.17 cm^{-1} (λ= 726.429 nm), E_{lower}= 24014.22 cm^{-1}, J=13/2, (e) $\longrightarrow$ E_{upper} **78**

Figure 3.26: Measured spectral line in the discovery of the energy level E_{upper} = 38048.24(0.03) cm^{-1}, J= 11/2 (o), with the monochromator fixed separately at λ_F^-=416.303 nm and λ_F=476.309 nm, where both gave the same hfs. line at σ= 14034.05 cm^{-1} (λ= 712.356 nm), E_{lower}= 24014.22 cm^{-1}, J=13/2, (e) $\longrightarrow$ E_{upper} **79**

Figure 3.27: Measured spectral line in the discovery of the energy level E_{upper} = 38087.78(0.06) cm^{-1}, J= 15/2 (o), with the monochromator fixed at λ_F^-=405.392 nm. line at σ= 13426.96 cm^{-1} (λ= 744.565 nm), E_{lower}= 24660.80 cm^{-1}, J=15/2, (e) $\longrightarrow$ E_{upper} **80**

Figure 3.28: Measured spectral lines in the discovery of the energy level E_{upper} = 42770.41(0.04) cm^{-1}, J= 15/2 (e), with the monochromator fixed at λ_F= 550.034 nm for line a) and λ_F^-=475.700 nm for line b). a) line at σ= 13239.15 cm^{-1} (λ= 755.128 nm), E_{lower}= 29531.25 cm^{-1}, J=17/2, (o) $\longrightarrow$ E_{upper} b) line at σ= 13327.37 cm^{-1} (λ= 750.129 nm), E_{lower}= 29443.09 cm^{-1}, J=17/2, (o) $\longrightarrow$ E_{upper} **81**

Figure 3.29: Measured spectral line in the discovery of the energy level E_{upper} = 37734.93(0.02) cm^{-1}, J= 19/2 (e), with the monochromator fixed at λ_F=573.926 nm. Line at σ= 13849.21 cm^{-1} (λ= 721.864 nm), E_{lower}= 23885.74 cm^{-1}, J=17/2, (o) $\longrightarrow E_{upper}$ **84**

Figure 3.30: Measured spectral line in the discovery of the energy level E_{upper} = 38665.37(0.08) cm^{-1}, J= 13/2 (e), with the monochromator fixed at λ_F^-= 410.380 nm. Line at σ= 14307.48 cm^{-1} (λ= 698.742 nm), E_{lower}= 24357.92 cm^{-1}, J=15/2, (o) $\longrightarrow E_{upper}$. **85**

Figure 3.31: Measured spectral lines in the discovery of the energy level E_{upper} = 38077.21(0.04) cm^{-1}, J= 13/2 (o), with the monochromator fixed at λ_F^-=405.393 nm. c) shows the visually combined line spectrum of a) and b) at σ= 13416.45 cm^{-1} (λ= 745.148 nm), E_{lower}= 24660.80 cm^{-1}, J=15/2, (e) $\longrightarrow E_{upper}$ **86**

Figure 3.32: Measured spectral lines in the discovery of the energy level E_{upper} = 38257.19(0.05) cm^{-1}, J= 19/2 (o), with the monochromator fixed at λ_F^-= 410.383 nm and λ_F^-= 501.883 nm for line a) and b), respectively. Both lines were measured in two parts; a) and b) show the visually combined spectra. a) line at σ= 13896.34 cm^{-1} (λ= 719.416 nm), E_{lower}= 24360.81 cm^{-1}, J=17/2, (e) $\longrightarrow E_{upper}$ b) line at σ= 13993.18 cm^{-1} (λ= 714.437 nm), E_{lower}= 24263.96 cm^{-1}, J=17/2, (e) $\longrightarrow E_{upper}$ **87**

Figure 3.33: Experimental LIF spectrum of the line at λ_{air}= 702.106 nm (σ=14238.94 cm^{-1}) measured with λ_F = 561.360 nm and best-fit curve superposed. **95**

Figure 3.34: Experimental LIF spectrum of the line at λ_{air}= 702.191 nm (σ=14237.22 cm^{-1}) measured with λ_F = 462.800 nm and best-fit curve superposed. **96**

Figure 3.35: Experimental LIF spectrum of the line at λ_{air}= 705.143 nm (σ= 14177.59 cm^{-1}) measured with the monochromator adjusted to λ_F^-= 410.700 nm and best-fit curve superposed. **97**

Figure 3.36: Theoretical fit (blue line) of the line at λ_{air}= 705.143 nm of the FT observed spectrum (red line) using the hfs simulation program. a) Fit with the hfs constants of the upper energy determined from this study. b) Theoretical fit (blue line) of the line at λ_{air}= 705.143 nm with the upper energy level A and B constants from [20]. **98**

Figure 3.37: Experimental LIF spectrum of the line at λ_{air}= 707.196 nm (σ=14136.45 cm^{-1}) measured with the monochromator adjusted to λ_F = 509.188 nm and best-fit curve superposed. **99**

Figure 3.38: Experimental LIF spectrum of the line at λ_{air}= 719.821 nm (σ=13888.51 cm^{-1}) measured with the monochromator adjusted to λ_F = 390.080 nm and best-fit curve superposed. **100**

Figure 3.39: Experimental LIF spectrum of the line at λ_{air}= 724.179 nm (σ= 13804.93 cm^{-1}) measured with the monochromator adjusted to λ_F = 462.800 nm and best-fit curve superposed. **101**

Figure 3.40: Experimental LIF spectrum of the line at λ_{air}= 725.056 nm (σ=13788.22 cm^{-1}) measured with the monochromator adjusted to λ_F = 564.811 nm and best-fit curve superposed. **102**

Figure 3.41: Experimental LIF spectrum of the line at λ_{air}= 736.079 nm (σ=13581.75 cm^{-1}) measured with the monochromator adjusted to λ_F = 570.695 nm and best-fit curve superposed. **103**

INVESTIGATION OF FINE AND HYPERFINE STRUCTURE ENERGY LEVELS OF HOLMIUM I USING LASER SPECTROSCOPIC TECHNIQUES

SUMMARY

The fundamentals of atomic physics are based on theoretical and experimental studies throughout history. Atomic physics focuses mainly on the structure of atoms, their interactions with each other, and their interactions with photons. The interaction of photons with matter is widely used in experimental studies to understand the properties of atoms and obtain information about their energy levels and the dynamics of excited atoms.

In atoms, the orbital and spin motion of the electron around the nucleus creates an internal magnetic field that interacts with the electron's magnetic moment and orients its spin. This interaction is known as the spin-orbit interaction and causes fine structure (fs) splitting of the energy levels in the atom. The interaction of electromagnetic multiple nuclear moments with the electric and magnetic field produced by spinning and orbiting electrons around the nucleus gives rise to a further splitting, namely hyperfine structure splitting (hfs) of the fine structure levels.

Photons can be absorbed or emitted by their interaction with atoms. Absorption takes the atom from a lower to a higher energy level, whereas emission occurs spontaneously or is induced from a higher to a lower energy level by releasing radiation. The study of absorption or emission of light by matter is known as 'Spectroscopy'.

With the development of laser technology, coherent light sources, such as lasers, have been used in spectroscopic studies due to their high intensity, extremely narrow linewidth, good focusing properties, and enhanced sensitivity in measurement techniques. The spectral line occurring from emission or absorption can be measured using laser spectroscopic methods for further analysis. The use of lasers in spectroscopic studies gave rise to different techniques such as Laser-Absorption Spectroscopy, Optoacoustic Spectroscopy, Optogalvanic Spectroscopy (OGS), Cavity-Ringdown Spectroscopy, Laser Induced Fluorescence (LIF) Spectroscopy, Ionization Spectroscopy and Saturation Spectroscopy.

This dissertation aimed to experimentally discover new even and odd parity fine structure energy levels of atomic Holmium in the 690-830 nm wavelength range using Laser Induced Fluorescence spectroscopy (LIFS) and Optagalvanic spectroscopy (OGS) methods simultaneously. Free and excited Holmium atoms were generated in a liquid nitrogen-cooled hollow-cathode lamp. The corresponding magnetic dipole (A) and electric quadrupole (B) hyperfine structure constants were also determined. To confirm the existence and precisely determine the energy values of the new energy levels, we analyzed lines from previously recorded Fourier Transform (FT) spectra.

In total, 16 new energy levels have been discovered, comprising five with even parity and 11 with odd parity. Data on the hyperfine structure of these new levels, as well as additional hyperfine structure data for three known levels of even parity obtained from existing literature, have been presented for the first time.

The findings of this dissertation will be available as a resource in the National Institute of Standards and Technology (NIST) Atomic and Molecular Database. This will help establish a crucial infrastructure for other scientific pursuits, especially in the fields of astrophysics.

HOLMİYUM I'İN İNCE VE AŞIRI İNCE YAPI ENERJİ SEVİYELERİNİN LASER SPEKTROSKOPİK YÖNTEMLERLE İNCELENMESİ

ÖZET

Atom fiziğinin temelleri, tarih boyunca yapılan teorik ve deneysel çalışmalara dayanmaktadır. Atom fiziği temel olarak atomların yapısı, birbiriyle ve fotonlarla olan etkileşimlerine odaklanır. Deneysel çalışmalarda fotonlar, atomların özelliklerini anlamak, uyarılmış atomların dinamikleri ve enerji seviyeleri hakkında bilgi edinmek için yaygın olarak kullanılmaktadır.

Fotonlar atomlarla etkileşimleri sonucu soğrulur (absorbe edilir), yayılır (emisyona uğrarlar) veya saçılmaya uğrarlar. Absorpsiyon, atomu düşük bir enerji seviyesinden yüksek bir enerji seviyesine çıkartırken, kendiliğinden veya indüklenmiş emisyon sonucunda atom uyarılmış seviyeden daha düşük bir enerji seviyesine iner. Işığın madde ile etkileşimi sonucunda absorbe edilmesi, emisyona uğraması ya da saçılması olaylarının incelenmesi "Spektroskopi" olarak bilinir.

Laser teknolojisinin gelişmesiyle birlikte, koherent ışık kaynağı olan laserler, yüksek şiddete, son derece dar çizgi genişliklerine ve iyi odaklama özelliklerine sahip olmalarından dolayı hassas ölçüm tekniklerinin söz konusu olduğu spektroskopik çalışmalarda kullanılmaktadır.

Atomlarda elektronun çekirdek etrafındaki yörünge ve spin hareketi, elektronun manyetik momentiyle etkileşime giren ve spinini yönlendiren bir iç manyetik alan yaratır. Bu etkileşim, spin-yörünge etkileşimi olarak bilinir ve atomdaki enerji seviyelerinde ince yapı (fs) yarılmalarına neden olur. Atomun elektrik ve manyetik nükleer momentlerinin, çekirdek etrafındaki elektronların spin ve yörünge hareketleri sonucunda üretilen elektrik ve manyetik alanla etkileşime girmesi sonucunda ince yapı seviyelerinde aşırı ince yapı yarılması (hfs) olarak adlandırılan daha fazla yarılmaya neden olur.

Emisyon ya da absorpsiyon sonucu oluşan spektral çizgiler laser spektroskopik yöntemler kullanarak ölçülebilir ve farklı analiz teknikleri ile incelenebilir. Laserlerin spektroskopik çalışmalarda kullanılması, Laser-Absorpsiyon Spektroskopisi, Optoakustik Spektroskopi, Optogalvanik Spektroskopi (OGS), Kavite Ring-Down Spektroskopisi, Laserle İndüklenen Floresans (LIF) Spektroskopisi, İyonizasyon Spektroskopisi ve Satürasyon Spektroskopisi gibi farklı tekniklerin ortaya çıkmasına neden olmuştur.

Bu tezin amacı, Laserle İndüklenen Floresans spektroskopisi (LIFS) ve Optagalvanik spektroskopi (OGS) yöntemlerini simultane kullanarak 690-830 nm dalgaboyu aralığında atomik holmiyumun çift ve tek pariteli yeni ince yapı enerji seviyelerini keşfetmek ve bu seviyelere ait manyetik dipol (A) ve elektrik kuadrupol (B) aşırı ince yapı sabitlerini belirlemektir.

LIF metodunda, laser ışığının frekansı incelenen atomun enerji geçişlerine ayarlanır, böylelikle atomlar laser dalgaboyunun alt enerji seviyesinden (E_i) bir üst enerji seviyesine (E_k) uyarılır. Uyarılma sonucunda seviyeler arasındaki geçişte seviyelerin nüfus yoğunlukları değişir. Uyarılmış atom, floresans ışığı olarak bilinen ışığı yayarak, kendiliğinden (veya çarpışma sonucunda) düşük enerjili seviyeyelere iner. Dedekte edilen floresans çizgileri bize laser uyarma çizgisinin enerji seviyeleri hakkında bilgi verir. Floresans sinyalleri, atomun üst ve alt enerji seviyelerinden 3 farklı şekilde meydana gelebilir ve *Pozitif*, *Negatif* ve *Çarpışma Etkileşimi* floresansı olarak gruplandırılabilir.

Pozitif Floresans laser uyarılma çizgisinin üst enerji seviyesinden meydana gelen floresans yayılımları olarak tanımlanır. *Negatif Floresans* ise, laser uyarılma çizgisinin alt enerji seviyesinden daha düşük enerji seviyelerine meydana gelen floresans yayılımlarıdır. *Çarpışmalı Etkileşimde* ise, uyarılmış seviyedeki atom enerjisini yakınındaki, neredeyse aynı enerji seviyesine sahip başka bir atoma aktarır. Bu enerji seviyesinden olan yayılımlar pozitif floresans olarak dedekte edilebilir. Çarpışmalı etkileşim ile ortaya çıkan floresans yayılımlarının meydana gelme olasılığı düşük basınçlı deşarjlarda daha düşüktür.

Deneysel ölçümlerde, laser tarama aralığında bazen birden fazla seviye eş zamanlı olarak uyarılır. LIF metoduyla yapılan spektroskopik ölçümlerde monokromatör, laser uyarma frekansında en güçlü çizgi spektrumunu veren floresans sinyalin dalgaboyuna ayarlanır. Bu yöntem ile spektrometreye giren olası birden fazla seviyenin uyarılmasından kaynaklı karışmış çizgi spektrumlarının önüne geçilmiş olur. Böylece her bir çizginin aşırı ince yapı spektrumları kaydedilebilir ve analiz programlarıyla analiz edilebilir.

Laser uyarılma çizgisinde pozitif floresans gözlendiyse ve uyarılan seviyelerinden bir tanesi biliniyorsa, floresans çizgisi ve laser uyarılma frekansının dalga sayıları matematiksel olarak toplanarak bilinmeyen enerji seviyesi değeri bulunabilir.

Her iki enerji seviyesinin tanımsız olması durumunda, negatif floresansın varlığı kolaylık sağlamaktadır. Negatif floresans ile laser uyarılma çizgisinin alt enerji seviyesi tanımlanır ve laser çizgisinin uyarılma frekansına eklenerek üst enerji seviyesi bulunabilir.

Negatif floresansın yokluğunda ise, pozitif floresans kullanarak spektral çizgi LIFS metodu ile ölçülür. Hfs analiz programına üst ve alt enerji seviyesinin tahmini J, A ve B değerleri girilerek fit işlemi yapılır. İşlem sonucunda iyi sonuç veren J, A ve B aşırı ince yapı sabiti değerleri elde edilir. Bulunan değerler, literatürde mevcut enerji seviyeleri ile karşılaştırılır. Laser çizgisine karşılık gelen alt ya da üst enerji seviyesinden (ve onlara ait J ile A ve B değerleri) bir tanesi ile örtüşen bir seviye bulunursa bilinmeyen enerji seviyesine ulaşılabilir. Az ayrışmış spektrumlarda ise analiz işlemi her zaman iyi bir sonuç vermez, bu durumda enerji seviyesinin bulunması başarısız olur.

LIF yöntemiyle simültane kullanılan OGS metodunda laser gaz deşarj ortamına gönderilir, frekansı atom ve iyonların enerji geçişine tekabül ettiğinde alt ve üst enerji seviyelerinin nüfus yoğunluklarında belirgin bir değişime neden olur. Enerji seviyelerindeki farklı iyonizasyon olasılıkları nedeniyle nüfus yoğunluğundaki değişim, iyon ve serbest elektron sayılarında değişime ve deşarj akımında (ΔI)

değişikliğe neden olur. Bu değişim bir balast direnci (R) boyunca bir voltaj değişikliği ($\Delta V = R \cdot \Delta I$) olarak gözlemlenebilir. Laserin şiddeti laser kesici (chopper) ile kesildiğinde, lock-in amplifikatör yardımıyla doğrudan ölçülebilen bir AC voltajı elde edilir. Laser uyarım frekansında alt ve üst enerji seviyelerine bağlı olarak pozitif ve negatif optogalvanik sinyalleri gözlenir.

LIFS yöntemini uygulamak için, laser çizgisinin üst veya alt enerji seviyelerinden oluşan floresans çizgilerinin dalgaboylarını bilmek gerekir. LIFS yönteminde kullanılan ve literatürde tanımlı olan floresans çizgilerinin yokluğunda, OGS metodu yardımıyla uyarılma çizgisine ait olan floresanslar bulunabilir. Bilinmeyen enerji seviyelerin keşfinde OGS yol gösterici görev alır. LIFS ve OGS yöntemlerinin simültane kullanılması bu nedenle önem kazanmaktadır.

LIFS ve OGS yöntemleri ile incelenen serbest ve uyarılmış holmiyum atomları laboratuvar yapımı içi boş saydam cam malzemeden yapılmış bir katot lamba içerisinde üretilmiştir. İçi boş katot lambası, katot, anot ve asal gazdan oluşmaktadır. Lambanın merkezine yerleştirilmiş katot, içi oyuk bakır silindir içerisine tabaka şeklinde kaplanmış yaklaşık 0.125 mm'lik ince bir holmiyum levhadan oluşmaktadır. Alüminyumdan yapılan anotlar, seramik tutucular ile lambanın merkezine yerleştirilen silindir katotun her iki ucuna, lambanın dışından akım uygulayabilecek düzenekte tutturulur. Lamba içerisindeki hava vakum pompasıyla 10^{-7} mbar'a kadar boşaltılır ve içerisine 1-1,5 Torr (1.5-2 mbar) basınca sahip asal gaz pompalanır. Bu çalışmada asal gaz olarak neon (Ne) kullanılmıştır. Basınç altında asal gaz atomları birbiriyle çarpışarak iyonize olur. Güç kaynağına bağlandıktan sonra anot ile katot arasında 60 mA civarında akım uygulanır. Pozitif yüke sahip iyonize atomlar elekrik alan altında hızlanır, kinetik enerjiye sahip olur ve katota çarparak silindir katot içerisine yerleştirilmiş holmiyum levhasından atom kopartır. Asal gaz ile çarpışan holmiyum atomları üst enerji seviyelerine uyarılır, ya da iyonize olabilir. Katot lambası içerisinde asal gaz, serbest, uyarılmış ve iyonize olmuş holmiyum atomlarının olduğu sıcak bir plazma ortamı oluşur. Plazma ortamında Doppler çizgi genişleme etkisini azaltmak amacıyla katot lambası deney süresince sıvı azot ile soğutulur. Ayrıca, sıvı azot holmiyum atomlarının laser ışınının katot içerisinden geçtiği yol üzerinde yoğuşmasını da sağlamaktadır.

Bu çalışma sonucunda, çift pariteli 5 ve tek pariteli 11 seviye olmak üzere toplam 16 yeni ince yapı enerji seviyesi keşfedildi. Bulunan yeni seviyeler için aşırı ince yapı sabitleri, buna ek olarak literatürden bilinen üç çift pariteli ince yapı enerji seviyesi için aşırı ince yapı sabitleri ilk kez bu çalışmada sunulmuştur.

Yeni enerji seviyelerini hassas olarak belirlemek için daha önce Ne ve Ar asal gazlarıyla 300-850 nm aralığında ölçülmüş FT spektrumu analiz edilmiştir. Bu spektrumun olduğu analiz programı daha önce ölçülen Ho çizgilerinin bir listesi, ince yapı enerji seviyelerinin bir listesi ve literatürden bunlara karşılık gelen A ve B sabitlerini içermektedir. Analiz programı, laser dalgaboyu aralığındaki tanımsız çizgi spektrumlarının görüntülenmesini ve bilinmeyen enerji seviyelerinin tespit edilmesini sağlar.

İkinci bir analiz programı ile LIFS ve OGS yöntemleri ile ölçülen spektral çizgilerin analizi yapılır. Bu program, ölçülen aşırı ince yapı (hfs) spektrumu üzerinde en küçük

kareler yöntemini kullanarak, spektrumlar teorik spektrum ile fit edilir ve çizginin ağırlık merkezi ve A ve B hfs sabitleri hassas bir şekilde bulunur.

Bu çalışma sonucunda elde edilen ince yapı enerji seviyeleri, Ulusal Standartlar ve Teknoloji Enstitüsü (NIST) Atomik ve Moleküler Veritabanı'nda bir kaynak olarak erişilebilir olacaktır.

Astrofizik alanındaki çalışmalar için bir alt yapı oluşturacak olan ince ve aşırı ince yapı çalışmaları, kozmik radyasyonun tanımlanmasında, güneş ve yıldız atmosferlerinin bolluk oranlarının analizinde, güneş ve yıldız yapılarının tanımlanması ve galaksimizin oluşumu ve kimyasal evrimi ile ilgili çalışmalarda katkı sağlayacaktır. Ayrıca, yıldızlardaki ağır elementlerin nükleosentezini incelemek için holmiyum gibi nadir toprak elementlerinin verilerine ihtiyaç vardır. Bununla birlikte, yakın zamanda elde edilen yüksek çözünürlüklü yıldız spektrumları, atomik çizgi veri tabanının hala eksik olduğunu göstermiştir. Bu nedenle, herhangi bir nötr veya iyonik atom spektrumunun ve nadir toprak elementlerinin aşırı ince yapılarının atomik ve iyonik çizgi veritabanına katkısı önemli bir rol oynamaktadır.

1. INTRODUCTION

1.1 Purpose of Thesis

The objective of this study was to experimentally discover new even and odd parity fine structure energy levels of atomic Holmium within the wavelength range of 690-830 nm using Laser Induced Fluorescence spectroscopy (LIFS) and Optogalvanic spectroscopy (OGS) methods simultaneously. Additionally, the study aimed to determine their corresponding magnetic dipole (A) and electric quadrupole (B) hyperfine structure constants.

The first chapter of this dissertation provides a fundamental overview of the Holmium atom, including the importance of the element, with a literature review covering the subject matter of this thesis. In the other upcoming chapters, a general theoretical background on fs and hfs formation in atoms, a brief summary of laser spectroscopic methods and the methods applied in this study, a detailed schematic view and images of the experimental setup, information on the apparatus and programs used for measuring and analyzing the spectra and the outcomes of this study are provided, respectively.

1.2 The Holmium Element

Accurate experimental data on the structure of complex atoms are in great demand in physics, especially in astrophysics. Atoms with more than one open valence electron shell in an excited state, such as transition metals, are called complex atoms. Lanthanides and actinides, atoms with open f electron shells, exhibit the highest complexity. The degree of complexity increases with the angular quantum number of the valence electron.

Holmium (Ho) is one of the 17 elements of the rare earth metal family of the lanthanide series, with an atomic number of 67 and atomic weight of 164.93 g/mol (Table 1.1) [1]. Ho has only one stable isotope in its natural state with a 100 % isotopic

abundance ($^{165}_{67}$Ho (Ho I)) and a relatively high nuclear spin I=7/2, a large nuclear magnetic dipole moment value μ= 4.17(3) μ_N [2] and a high electric quadrupole moment between Q= 2.7 and 3.6 barn. The neutral isotope Ho I has a ground state configuration of [Xe] $4f^{11}6s^2$, an open $4f$ shell, causing the atom to have considerably complex spectra with dense electronic levels, which makes it a good candidate for investigating and classifying new energy levels of fine and hyperfine structures.

Z (Atomic Number)	67
A (Atomic Weight)	164.93 g/mol
Electron Groundstate Configuration and Term	[Xe] $4f^{11}6s^2$; $^4I^o_{15/2}$
Ionization Energy of the Groundstate	48567 cm^{-1} (6.0215 eV)
Nuclear Spin (I)	7/2
Magnetic Dipole Moment	4.17(3) μ_N
Electric Qudrupole Moment	2.7-3.6 barn
Melting Point	1472 ^{o}C
Boiling Point	2700 ^{o}C

Table 1.1 : Chemical and physical properties of atomic Holmium.

Identification and classification of cosmic radiation with spectroscopic studies provide information on abundance ratios of solar and stellar atmospheres and stellar structures [3]–[6], galaxy formation, and chemical evolution [7]–[9]. For abundance analysis, the atomic line database is an important component. In addition, accurate data on rare-earth elements are required to study the nucleosynthesis of heavy elements in stars [10]–[12]. Recent astrophysics studies highlight that hyperfine structure data in the line database are still incomplete and contain significant inaccuracies [13]–[16]. Thus, the contribution of any accurate neutral or ionic spectra and their hyperfine structure of rare-earth elements to the atomic and ionic line database plays a key role.

The accuracy of the experimental data plays a significant role in improving theoretical calculations and semi-empirical atomic structure analysis.

1.3 Literature Review

Since 1977, many groups have conducted experimental and theoretical studies on the element Ho using different methods. The first of these was conducted by Wyart et al. [17]. A total of 1462 transitions in the range of 2493-12344 cm^{-1} were investigated in this study using Fourier transform (FT) spectroscopy. 913 of the 1462 were classified as 144 odd and 116 even levels of Ho I. Among those, 111 energy levels with odd parity and 116 energy levels with even parity were determined. Burghardt et al. [18] found the hfs constants of the ground level of Ho I and the g_j factor of some electronic levels by the Atomic Beam Magnetic Resonance (ABMR) in 1982. The following year, Childs et al. [19] discovered three new energy levels of Ho I using both the Laser-Induced Fluorescence (LIF) and Laser-rf double resonance methods. They also determined the hfs constants of these levels and four new spectral transitions involving these levels. In 1992, Reddy et al. [20] classified new spectral transitions in the spectrum of Ho I using the OGS method and determined the magnetic dipole moment A and the electric quadrupole moment B through the analysis of the hyperfine structure of the energy levels associated with these transitions. Smirnov [21] classified 107 spectral lines of Ho I and 26 of Ho II in 1992. In 1997, Kröger et al. [22] conducted a theoretical study in the visible region on the $4f^{10}5d6s6p$ and $4f^{10}5d^26s$ configurations of Ho I and determined their hfs constants. In 1999, E. A. Den Hartog et al. [23] measured the lifetime of energy levels from the Ho I spectra in the range of 17 000-41 000 cm^{-1} and the Ho II spectra in the range of 20 000-38 000 cm^{-1} obtained by time-resolved LIF method. In 2003, [24] calculated the transition probabilities of 321 spectral transitions among 73 energy levels in the 345–1080 nm spectral range by analyzing the Ho I spectrum recorded using the FTS method. In 2004, Lawler et al. [25] used the FT spectrometer for improved energy levels and hyperfine structure constants for a selected set of Ho II levels. They also measured the branching fractions for the strong blue-UV lines originating from these levels. The outcomes of these new laboratory measurements were used to enhance Ho abundance calculations in the Sun and three metal-poor Galactic halo giant stars. In 2005, Sansonetti and Martin [26] conducted a study providing data on the energy levels of all atoms with atomic numbers between 1

and 99, including Holmium. The study also included information on the wavelengths, intensities, and transition probabilities of possible transitions between these energy levels. Gurell et al. [27] recorded spectra of Ho II emitted by hollow-cathode lamps using the ultraviolet FT spectrometer in 2009. They measured 303 lines in these spectra and used them to determine energies and hyperfine structure constants of 100 levels. Among these, 41 energy levels and hyperfine structure constants have not been reported previously for 83 levels. In 2013, Smirnov measured excited cross-section values for 102 spectral transitions of the Holmium atom when it was excited with electrons with an energy of 50 eV. Using known energy levels, Smirnov classified Ho I lines in the ultraviolet and visible regions. The findings were published in [21]. In 2017, N. Al-Labady et al. [28] studied the FT spectra of a Ho hollow cathode discharge lamp in the UV region. They classified 71 lines of atomic Holmium for the first time based on the known energy levels of Ho I and assigned 402 spectral lines to Ho I. The continuation of this work was carried forward in 2017 by Gö. Başar et al. [29]. They applied the identical method in the same region, primarily concentrating on the ionic lines of Holmium. They identified 97 lines of Ho II and 9 lines of Ho III. Of these, 6 lines of Ho II had not been previously classified or listed in the literature. Additionally, 215 lines in Ho II have been assigned but were not classified due to unknown energy levels.

Stefanska and Furmann (2018) reported experimental results on the hyperfine structure of holmium I (Ho I) using the laser-induced fluorescence (LIF) method in the visible region. They determined (A) and (B) for 61 odd parity levels, of which 40 were measured for the first time [30].

Following this study, Stefanska et al. (2018) investigated the hyperfine structure (hfs) for the even-parity level system of Ho I. They determined the constants A and B for 24 levels of even parity, 14 of which were reported for the first time. In addition, they conducted a parametric study based on data obtained from the literature [31]. Later in the same year, Stefanska et al. [32] presented new experimental findings regarding the hyperfine structure of holmium. They proposed possibilities for studying variations in the constant α in Ho I. As a result, five new odd-parity electronic levels were identified, and their corresponding hyperfine structure constants A and B were also determined.

Furmann et al. (2018) [33] analyzed 73 spectral lines of Ho I and investigated 21 new odd parity electronic levels with previously unknown energies, identified as upper levels. Hyperfine structure (hfs) constants were also identified from the obtained data.

In 2019, Özdalgıç et al. [34] conducted a study on the spectrum of Ho I, focusing on the sıngly (Ho II) and doubly ionized ionic lines of Holmium (Ho III) within the visible range using FT spectroscopy. The study was expanded [35] to include an analysis of Ho I in the visible range, resulting in the detection of 4 193 spectral lines. Of these, 2 862 were assigned to Ho I, and 2 417 of the assigned lines had not previously been listed in the literature.

In 2019, Elantkowska et al. conducted a theoretical study on the fine and hyperfine structures of the odd-parity level system in Ho I. This study was significant as it performed multi-configuration calculations for both the fine and hyperfine structures for the first time, incorporating second-order perturbation theory [36].

In 2019, Özdalgıç et al. continued their systematic analysis of the atomic hyperfine structure of holmium (Ho) using Fourier Transform (FT) spectroscopy in the visible range. They relied on high-resolution FT spectra from their previous research. The study involved the analysis of 164 spectral lines. Hyperfine structure constants for 43 energy levels were published for the first time. Additionally, for 42 previously known hyperfine structure constants, the accuracy was improved and verified [37]. In 2020, Gö. Başar et al. [38] studied the hyperfine structure of Ho I using two separate methods: Laser Induced Fluorescence (LIF) and Optical Grid (OG) spectroscopy, within the wavelength range of 780-830 nm. They analyzed a total of 42 spectral lines. The researchers determined the magnetic dipole and electric quadrupole hyperfine structure constants, denoted A and B, respectively, for 23 levels of even parity and 25 levels of odd parity. Notably, eight hyperfine structure constants were published for the first time in this study. Additionally, they identified a new energy level that aligns with semi-empirical fine structure calculations.

In 2021 Chomski et al. [39] published Landé-g_J factors of Ho I for some measured electronic levels. The measurements were performed with the use of the Zeeman effect of the hyperfine structure. The effect was observed with LIF detection using

the laser spectroscopy method in a hollow cathode discharge lamp placed in a constant magnetic field. In this study, they have investigated 69 spectral lines of Ho in the 490 nm – 670 nm spectral region. They determined Landé-g_J factors for 15 odd and 18 even parity configurations of Ho I levels for the first time. A year later, in 2022, Chomsky et al. [40] had two more publications on Ho. The first was a continuation of the Landé g_J study, where they used the same method to examine 33 spectral lines of Ho I in the 488 nm- 677 nm wavelength range. They presented the results of Landé g_J factors measurements for 18 electronic levels, 13 of which were published for the first time. In the second publication by Chomsky et al. in 2023 [41], 79 spectral lines of Ho I were obtained in the 485 nm-535 nm wavelength range by the LIF method and 27 previously unknown electronic energy levels were defined for the first time. Additionally, hyperfine structure constants were found for 23 odd parity and 11 even parity energy levels. The values found for 31 levels were presented for the first time in their study. In this study 32 new energy levels were found, although it was stated that 5 of them required further verification. The five levels that require verification, as stated in [41], were analyzed by [42](2023). This study confirmed two of the five levels with high certainty through LIF spectroscopy measurements and selected lines from FT spectra. For the remaining three levels, though the lines were identified in the FT spectrum, they were weak or obscured by other lines, resulting in the inability to verify them with high precision.

The most recent publication on holmium was by Furmann et al. (2024). Their study investigated the hyperfine structure of more than 100 spectral lines of the holmium atom. The research involved laser excitation using a hollow cathode and detection through laser-induced fluorescence (LIF) [43].

1.4 Summary of Theoretical Background

The generation and detection of fluorescence light involves the interaction between light (i.e. electromagnetic waves) and the atom. At the end of the 19^{th} century, it became clear that the laws of classical physics did not apply to studies in the field of spectroscopy. After the introduction of quantum mechanics, it was possible to apply quantitative approaches to atomic and molecular systems. The Schrödinger equation describes atomic and molecular systems, including both the particle and wave properties of light. This chapter briefly discusses the interaction Hamiltonian of an atomic system and the background theory of fine and hyperfine structures of an atom.

1.4.1 Application of quantum mechanics on atoms

In a conservative system, the total energy of a particle in classical physics is given as:

$$E = T + V \tag{1.1}$$

T and V represent the kinetic energy and potential energy of a moving particle, respectively. For a particle of mass m and velocity $v = \frac{dx}{dt}$ moving along the x axis in a potential field defined as $V(x)$, we can express the kinetic energy as follows:

$$T = \frac{1}{2}m(\frac{dx}{dt})^2 \tag{1.2}$$

The total mechanical energy can be rewritten as follows:

$$E = \frac{1}{2}m(\frac{dx}{dt})^2 + V(x) = \frac{p^2}{2m} + V(x) \tag{1.3}$$

In 1923, after being introduced to quantum mechanics, Louis de Broglie concluded that it was possible to assign a wavelength to a mass. This solved the problem of the electron moving as a body on a circular or elliptical path and could be represented as a wave moving around the nucleus. The wave has to travel on a closed path around the nucleus in such a way that the phases close properly. If there is a phase jump during the revolution and the path does not close in the correct phase, the wave can cancel itself out through interference. The required quantization of the wave corresponds exactly to the quantization of the electron energy proposed by Niels Bohr. Erwin Schrödinger

completed and unified de Broglie's ideas and published his wave mechanics in 1926. In 1.3, p denotes the particle's momentum. Changing p with the operator $-i\hbar\frac{\partial}{\partial x}$ and multiplying 1.3 by the wave function $\Psi(x,t) = Ae^{i(kx-\omega t)}$ we obtain the time-dependent Schrödinger wave equation for free particles in a force field, which is the case for atoms.

$$E\Psi(x,t) = -\frac{\hbar^2}{2m}\frac{\partial^2}{\partial x^2}\,\Psi(x,t) + V(x)\Psi(x,t) \tag{1.4}$$

In the study of atomic and molecular systems, the distance of electrons from the nucleus exhibits a radial dependence of the wave functions. In three dimensions and in the case of one-electron atoms the time-dependent Schrödinger equation can be rewritten using the central field approximation by replacing E with the operator $i\hbar\frac{\partial}{\partial t}$, the wave function with $\Psi(r,t) = exp(-iEt/\hbar)\Psi(r)$, the potential field with radial dependence $V(r)$ and using the Laplacian operator $\nabla^2 = \frac{\partial^2}{\partial x^2} + \frac{\partial^2}{\partial y^2} + \frac{\partial^2}{\partial z^2}$ as follows:

$$i\hbar\frac{\partial}{\partial t}\Psi(r,t) = -\frac{\hbar^2}{2m}\nabla^2\,\Psi(r,t) + V(r)\Psi(r,t) \tag{1.5}$$

or

$$E\Psi(r,t) = \mathscr{H}\Psi(r,t) \tag{1.6}$$

$$\mathscr{H} = -\frac{\hbar^2}{2m}\nabla^2 + V(r) \tag{1.7}$$

where $\mathscr{H}$ is called the Hamiltonian operator and represents the total energy of the system.

To obtain the interaction Hamiltonian, the Laplacian operator must be converted additionally to spherical coordinates;

$$\nabla^2 \equiv \frac{1}{r^2}\frac{\partial}{\partial r}\left(r^2\frac{\partial}{\partial r}\right) + \frac{1}{r^2 sin\theta}\frac{\partial}{\partial\theta}\left(sin\theta\frac{\partial}{\partial\theta}\right) + \frac{1}{r^2 sin^2\theta}\frac{\partial^2}{\partial\phi^2} \tag{1.8}$$

Inserting 1.8 into 1.7, the Schrödinger equation with a partially differentiated Laplacian operator becomes as follows.

$$-\frac{\hbar^2}{2m}\left[\frac{\partial^2}{\partial r^2} + \frac{2}{r}\frac{\partial}{\partial r} + \frac{1}{r^2}\left(\frac{\partial^2}{\partial\theta^2} + \frac{1}{tan\theta}\frac{\partial}{\partial\theta} + \frac{1}{sin^2\theta}\frac{\partial^2}{\partial\phi^2}\right)\right]\Psi + V(r)\Psi = E\Psi \tag{1.9}$$

The term in the inner parentheses of the left-hand side of Eq. 1.9 is equal to $-\frac{L^2}{\hbar^2}$, where L^2 is the square of the angular momentum operator.

The Schrödinger equation can be rewritten in the following form.

$$E\Psi = \left[-\frac{\hbar^2}{2m}\left(\frac{\partial^2}{\partial r^2} + \frac{2}{r}\frac{\partial}{\partial r} - \frac{L^2}{r^2\hbar^2}\right) + V(r)\right]\Psi \tag{1.10}$$

For a one-electron system, the Schrödinger equation can be solved by variable separation, where the wave function can be separated into the radial dependence of the interaction potential $V(r)$ (which in this case is the Coulomb potential) and the angular part associated with the angular momentum as $\Psi(r,\theta,\phi) = R(r)Y_l^m(\theta,\phi)$. The resultant radial equation and angular equations are given respectively in Eq. 1.11 and Eq. 1.12.

$$\frac{1}{R(r)}\frac{\partial}{\partial r}\left(r^2\frac{\partial}{\partial r}\right)R(r) - \frac{2mr^2}{\hbar^2}\left[V(r) - E\right] = l(l+1) \tag{1.11}$$

$$\frac{1}{Y_l^m(\theta,\phi)sin\theta}\frac{\partial}{\partial\theta}\left(sin\theta\frac{\partial}{\partial\theta}\right)Y_l^m(\theta,\phi) + \frac{1}{Y_l^m(\theta,\phi)sin^2\theta}\frac{\partial^2}{\partial\phi^2}Y_l^m(\theta,\phi) = -l(l+1) \tag{1.12}$$

The solution of the eigenvalues of the radial equation leads to the eigenenergies of the one-electron system as follows.

$$E_n = -\frac{\hbar^2}{2\mu a_0^2 n^2} = -\frac{13.6\ eV}{n^2} \tag{1.13}$$

where a_0 is the Bohr radius ($a_0 = \frac{\hbar^2}{\mu e^2} = 0.529\ \mathring{A}$) μ represents the reduced mass ($\mu = \frac{m_e M}{m_e + M}$, where m_e and M denote the mass of the electron and nucleus, respectively) and n the principle quantum number. The principal quantum number defines the energy and can only have positive integers from 1 to ∞.

The solution of the angular equation is obtained by splitting the equation into azimuthal and polar angle equations, where the solution of the azimuthal equations leads to exponentials ($e^{im\phi}$) including the magnetic moment quantum number m, while the solutions of the polar angle equations lead to Legendre polynomials with the orbital angular momentum quantum number l and the magnetic moment quantum number m.

$$Y_l^m(\theta,\phi) = (-1)^m \sqrt{\frac{(2l+1)(l-m)!}{4\pi(l+m)!}} P_l^m(cos\theta) e^{im\phi} \qquad m \geq 0 \qquad (1.14)$$

The quantum number of orbital angular momentum $\overrightarrow{l}$, $|l| = \sqrt{l(l+1)}\hbar$, can have values from 0 to (n-1), with corresponding orbitals $s, p, d, f, ..$, while the quantum number of the corresponding magnetic moment, which is denoted with m_l, can have integer values from $-l$ to l.

In addition to the orbital angular momentum, the spin motion of the electron causes an intrinsic angular momentum called the electron spin angular momentum or spin $\overrightarrow{s}$, $|s| = \sqrt{s(s+1)}\hbar$, where the corresponding quantum number is denoted with m_s and can have only two values $+\frac{1}{2}$ and $-\frac{1}{2}$ indicating the spin states of the electron, namely spin-up and spin-down, respectively.

In summary, the state of the electron in an atom can be defined by four quantum numbers, n, l, m_l, m_s. According to Pauli's exclusion principle, no two electrons can have the same set of four quantum numbers. The degeneracy of an energy state is given by the expression $2(2l+1)$, where $2l+1$ are the possible values of the orbital magnetic quantum number m_l for a given orbital quantum number l, and the factor "2" contribution comes from the possible spin quantum states $m_s = \pm 1/2$ in an orbital state, which doubles the degeneracy.

Furthermore, the sum of the orbital and spin angular momentum vectors gives rise to the total angular quantum number, denoted with $\overrightarrow{j}$, $|j| = \sqrt{j(j+1)}\hbar$, with possible values from $|l-s|$ to $(l+s)$.

In many-electron systems, the letter indication of vectors and quantum numbers is replaced with capital letters as given below.

Orbital angular momentum: $\overrightarrow{L} = \sum_{i=1}^{N} \overrightarrow{l_i}$

Spin angular momentum: $\overrightarrow{S} = \sum_{i=1}^{N} \overrightarrow{s_i}$

Total angular momentum: $\overrightarrow{J} = \overrightarrow{L} + \overrightarrow{S}$

1.4.2 *LS* and *JJ* couplings in atoms and their properties

The spin and orbital angular momentum of electrons can be organized in different ways to give different values of total angular momentum. The coupling of the total angular momentum is mainly classified according to the dominance of either the spin-orbit interaction or the electrostatic Coulomb interaction between the electrons. LS coupling occurs when the mutual interaction between the outer electrons is greater than the interaction of the spin and orbital moment of each of the electrons. In this case, the vector coupling scheme shown in Fig.1.1 a) applies, where the spin angular momenta of the individual electrons combine to give the total spin angular momentum $\overrightarrow{S}$ and similarly the orbital angular momenta of the electrons combine to give the total angular momentum $\overrightarrow{L}$ and interact to give the total angular momentum $\overrightarrow{J} = \overrightarrow{L} + \overrightarrow{S}$, known as the LS or Russel Saunders coupling.

However, in the case where the spin and orbital interaction dominate the interaction between the outer electrons, *JJ* coupling occurs and the coupling scheme in Fig.1.1 b) applies. The angular and spin orbital momentum of single electrons combine to form the resultant angular momentum, $j_i = l_i + s_i$. The resultant angular momentum of different electrons combines to form the total angular momentum of the atom, $\overrightarrow{J} = \sum_i \overrightarrow{j_i}$.

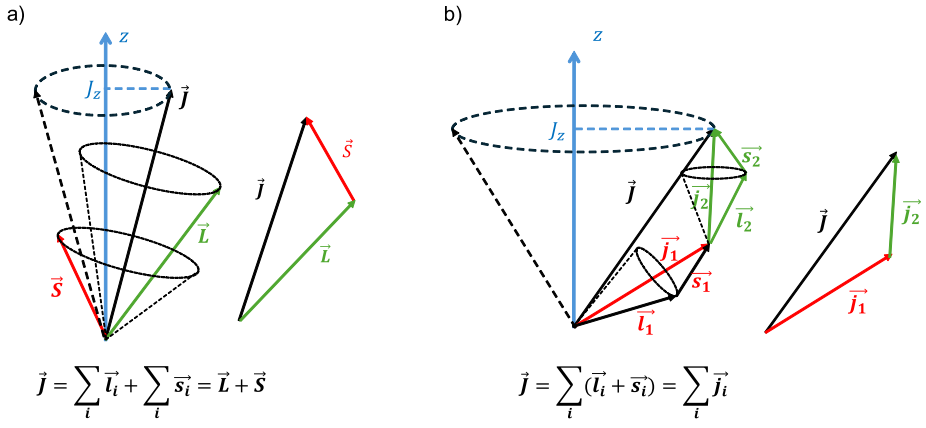


Figure 1.1 : Illustration of a) *LS* and b) *JJ* vector coupling for a two-electron atom.

In light atoms, i.e., atoms with low atomic numbers, *LS* coupling is more common, whereas in heavy atoms, *JJ* coupling is more common. However, for a heavy atom,

both couplings are applicable, since the dominance of the coupling changes for high- or low-lying energy states and with the number of optically active electrons in orbitals (i.e. open orbitals) [44,45]. In atomic Ho I, both couplings are applicable, as one can observe the term symbols of lower and higher energy levels provided in [46].

1.4.3 *JI* coupling in atoms and their properties

The nucleus has a spin quantum number indicated with $\overrightarrow{I}$, $|I| = \hbar\sqrt{I(I+1)}$, with possible integral or half-integral values, depending on the number and arrangement of protons and neutrons in the nucleus.

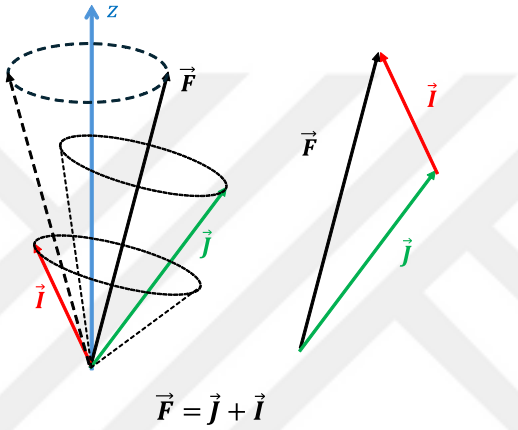


Figure 1.2 : Illustration of *JI* vector coupling.

In the *JI* coupling, also known as hfs coupling, the total angular momentum of the electrons $\overrightarrow{J}$ and the nucleus $\overrightarrow{I}$ couples to form a new total angular momentum $\overrightarrow{F}$, as shown in Fig.1.2. $\overrightarrow{F} = \overrightarrow{J} + \overrightarrow{J}$, $|\mathbf{F}| = \hbar\sqrt{F(F+1)}$, with possible values $F = |I-J|$, $|I-J|+1$, ..., $I+J$ [47].

1.4.4 Term symbol of an energy state

In atomic physics, the term symbol gives information about the quantum numbers of an electronic state of an atom. The symbol for lighter atoms or elements belonging to the first-row transition metals, such as holmium, where the *LS* coupling occurs, is given below, while for the *JJ* coupling it is much more complex ($(j_1, j_2, j_3, ...)_J$ [48]).

$$^{2S+1}L_J^{(P)}$$

The "P" in the upper right corner of the term symbol denotes the parity of the state and refers to the behaviour of the wave function upon reflection of the spherical coordinates $\Psi(r,\pi-\theta,\pi+\phi)=(-1)^{\sum_i l_i}\Psi(r,\theta,\phi)$. The parity is even or odd if $\sum_i l_i$ is even or odd, which is denoted as (e) and (o) respectively [49]. Thus, for a given electronic configuration, the parity can be found by summing the angular momenta for each electron in the open orbital.

As an example, the term symbol of the ground state of Ho I, [Xe] $4f^{11}6s^2$ can be found accordingly; $S=1/2+1/2+1/2=3/2$; $L=\sum_i m_l=1+2+3=6$ which refers to the I orbit, $J=|L-S|,...|L+S|=9/2,11/2,13/2,15/2$, where $J=15/2$ according to Hund's rule we choose the highest J value for more than half-filled shells and $P=(-1)^{33}$ leading to a term symbol ${}^4I^{(o)}{}_{15/2}$.

1.4.5 Fine structure

The orbital motion of the electron around the nucleus generates an internal magnetic field ($B_l=\frac{Ze\mu_0}{4\pi r^3 m_0}l$) that interacts with the magnetic spin moment ($\mu_s=-g_s\frac{e}{2m_0}s$) generated by the intrinsic spin motion of the electron, resulting in an additional magnetic energy, as shown in Fig.1.3.

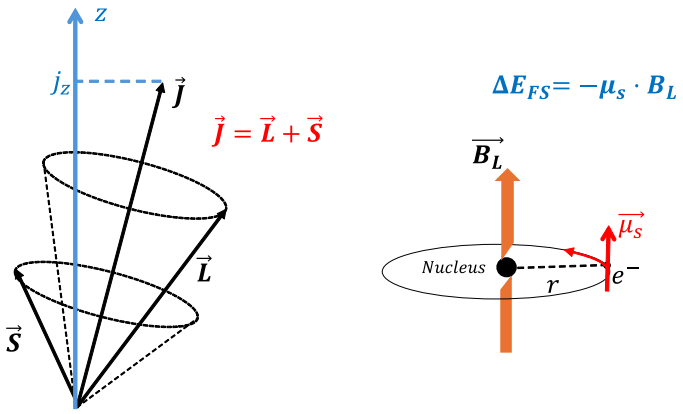


Figure 1.3 : LS coupling and the interaction energy of fine structure splitting (ΔE_{FS}).

This additional energy, $\Delta E_{FS}=-\mu_s\cdot B_L$, results in the splitting of the energy levels. This is illustrated in the vector model in the corresponding figure as the precession of $\overrightarrow{L}$ and $\overrightarrow{S}$ around $\overrightarrow{J}$ [50].

1.4.6 Hyperfine structure

The hyperfine structure (hfs) of atomic energy levels arises from the interaction between the electromagnetic multipole moments of the nucleus and the electric and magnetic fields generated by the motion and spin of the surrounding electrons [51].

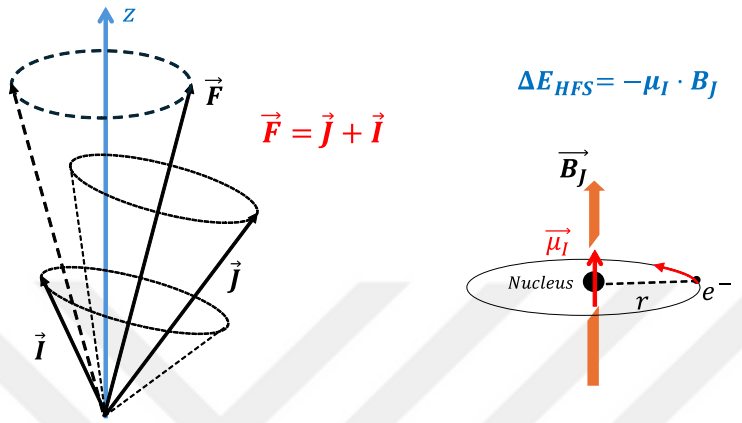


Figure 1.4 : *JI* coupling and the interaction energy of hyperfine structure splitting (ΔE_{HFS}).

This interaction, as illustrated in Fig. 1.4, leads to a further splitting of the fine structure energy levels due to the contribution of the magnetic potential energy, $\Delta E_{HFS} = -\mu_I \cdot B_J$, where $\mu_I = g_I \mu_N \frac{I}{\hbar}$ is the nuclear magnetic moment and B_J the magnetic field of the electrons at the nucleus. This is illustrated in the vector model of the corresponding figure (Fig.1.4) as the precession of $\overrightarrow{J}$ and $\overrightarrow{I}$ around $\overrightarrow{F}$. The additional hfs energy arising from the magnetic dipole interaction can be rewritten using the corresponding substitution given in Eq.1.15.

$$\begin{aligned} \Delta E_{HFS} &= -\mu_I \cdot B_J \cos(I,J) \\ &= g_I \mu_N \sqrt{I(I+1)} B_J \cos(I,J) \end{aligned} \tag{1.15}$$

The reversed sign in the second row of the formulation is a consequence of the fact that the vectors B_J and J are antiparallel. According to the law of cosines, the last term of Eq.1.15 can be written as,

$$\cos(I,J) = \frac{F(F+1) - I(I+1) - J(J+1)}{2\sqrt{I(I+1)J(J+1)}} \tag{1.16}$$

Substitution of Eq.1.16 into Eq.1.15 leads to the magnetic dipole interaction term of the hfs energy given in Eq. 1.18:

$$\Delta E_{HFS} = \frac{g_I \mu_N B_J}{2\sqrt{J(J+1)}} [F(F+1) - I(I+1) - J(J+1)] \tag{1.17}$$

or with $A = \frac{g_I \mu_N B_J}{\sqrt{J(J+1)}}$ the magnetic dipole constant hfs, and with the Casimir factor constant $C = F(F+1) - I(I+1) - J(J+1)$ defined as:

$$\Delta E_{HFS} = \frac{A}{2} [F(F+1) - I(I+1) - J(J+1)] = A\frac{C}{2} \tag{1.18}$$

So far, the primary contributor to the hfs splitting was considered, namely, the interaction between the nuclear magnetic dipole moment and the magnetic field of the electrons.

The electric quadrupole interaction also has an effect on the hfs in atoms. The contribution of the interaction between the electric quadrupole moment of the nucleus and the electric field produced by the electrons is only evident in atoms with $I \geq 1$ and $J \geq 1$, corresponding to the non-spherical charge distribution of the atom [47,50]. This interaction leads to asymmetric spacing, resulting in a shift in hfs energy levels.

$$\Delta E_{HFS} = B \cdot \frac{\frac{3}{4}C(C+1) - I(I+1)J(J+1)}{2I(2I-1)J(2J-1)} \tag{1.19}$$

The additional energy is given in Eq.1.19, where $B = eQ\left\langle \frac{\partial^2 V}{\partial z^2} \right\rangle$, (Q: electric quadrupole moment) is the electric quadrupole hfs constant. The derivation of the electric quadrupole hyperfine energy shift is not presented in this study. More details on the subject can be found in [52].

1.4.7 Hamiltonian of many electron system

The Schrödinger equation describes the quantum behavior of a system comprising many interacting electrons and nuclei. Therefore, the interaction Hamiltonian must be modified to account for their interactions with each other. Unlike a single-electron system, the equation becomes very complex and cannot be solved in full. Therefore, some assumptions and approximations must be introduced to find a solution.

The total interaction Hamiltonian for a many-electron system, with fine and hyperfine structure terms, can be expressed as follows:

$$H_{int} = H_{NR} + H_{FS} + H_{HFS} \tag{1.20}$$

The full version of 1.20 is given in 1.21, with the abbreviated terms given below.

H_{NR}: Non-Relativistic interaction term.

H_{FS}: Fine structure term.

H_{HFS}: Hyperfine structure term.

T_e: Kinetic energy of the electrons.

V_{eN}: Coulomb potential between the electrons and the nucleus.

Vee: Coulomb potential between the electrons.

MV: Mass-Velocity Correction term for the Kinetic Energy for relativistic speeds.

$Darwin$: Correction term due to the jittery motion of the electrons near the nucleus (non-zero only in s-orbitals).

SO: Spin-Orbit interaction term.

MD: Magnetic Dipole interaction term.

EQ: Electric Quadrupole interaction term.

$$\left.\begin{aligned} H_{int} = \sum_{i=1}^{N} \underbrace{\left(-\frac{\hbar^2}{2m}\nabla_i^2}_{\mathrm{T}_e} \underbrace{- \frac{Ze^2}{(4\pi\varepsilon_0) r_{ij}} \right)}_{\mathrm{V}_{eN}} + \underbrace{\sum_{j>i=1}^{N} \frac{e^2}{(4\pi\varepsilon_0) r_{ij}}}_{\mathrm{V}_{ee}} \end{aligned}\right\} \mathrm{H}_{NR}$$

$$\left.\begin{aligned} \underbrace{\underbrace{-\sum_{i=1}^{N} \frac{p_i^4}{8m^3c^2}}_{\mathrm{MV}} + \underbrace{\sum_{i=1}^{N} \frac{\hbar^2}{8m^2c^2}\nabla^2 V(r_i)}_{\mathrm{Darwin}}}_{\text{Relativisic Corrections}} + \underbrace{\sum_{i=1}^{N} \xi(r_i) L_i \cdot S_i}_{\mathrm{SO}} \end{aligned}\right\} \mathrm{H}_{FS}$$

$$\left.\begin{aligned} + \underbrace{\frac{A}{2}\left[F(F+1) - I(I+1) - J(J+1)\right]}_{\mathrm{MD}} + \underbrace{\frac{B}{4} \cdot \frac{3C(C+1) - 4I(I+1)J(J+1)}{2I(2I-1)J(2J-1)}}_{\mathrm{EQ}} \end{aligned}\right\} \mathrm{H}_{HFS} \tag{1.21}$$

1.4.8 HFS splitting and selection rules

In this section, the hfs splitting of the fs energy levels will be considered. The electronic energy level of an atom is split into fine-structure energy levels as a result of spin-orbit interaction. The interaction between the nuclear electromagnetic multipole moment and the electric and magnetic fields produced by the electrons causes a further splitting of the fine structure energy levels.

The energy level of the hfs levels can be written as follows, where the expressions of the terms α and β are given within Eq.1.22 and are known as the Casimir formula.

$$E_{HFS} = E_J + A\,\frac{C}{2} + B\cdot\frac{\frac{3}{4}C(C+1) - I(I+1)J(J+1)}{2I(2I-1)J(2J-1)} = E_J + A\alpha + B\beta \qquad (1.22)$$

The hfs energy levels are indicated with the letter F with possible values $|J-I| \leq F \leq J+I$, resulting in
$2I+1$ number of energy levels for $I \leq J$ and
$2J+1$ number of energies for $I > J$.

The spacing of the hfs energy levels is given by the 'Interval Rule', $F \rightarrow F-1 = A\cdot F$.

Allowed transitions between hfs energy levels are given with the selection rule stated below.

- Only transitions between energy levels with different parity are allowed.
- Transitions with $\Delta J = 0, \pm 1$ are allowed, while transitions with $J_{upper} = 0 \rightarrow J_{lower} = 0$ are forbidden.
- Transitions with $\Delta F = 0, \pm 1$ are allowed, while transitions with $F_{upper} = 0 \rightarrow F_{lower} = 0$ are forbidden.

The following equations in Eq.1.23 can be used to calculate the hyperfine structure splitting frequency of the upper and lower levels.

$$\nu_{F_{upper}} = \nu_{J_{upper}} + A_{upper}\alpha_{upper} + B_{upper}\beta_{upper}$$

$$\nu_{F_{lower}} = \nu_{J_{lower}} + A_{lower}\alpha_{lower} + B_{lower}\beta_{lower} \tag{1.23}$$

$$\tag{1.24}$$

Similarly, the frequency of the transition or for each hfs component $\nu_{F_u - F_l}$ spectral line can be found with the Eq.1.25.

$$\nu_{F_u - F_l} = \nu_{F_{upper}} - \nu_{F_{lower}} \tag{1.25}$$

A schematic illustration of the allowed hfs transitions is given in Fig.1.5. The energy spacing between the fine structure levels (FS) typically ranges from 100 to 1000 cm^{-1}, while the separation between hyperfine levels is on the order of 0.1-1 cm^{-1}.

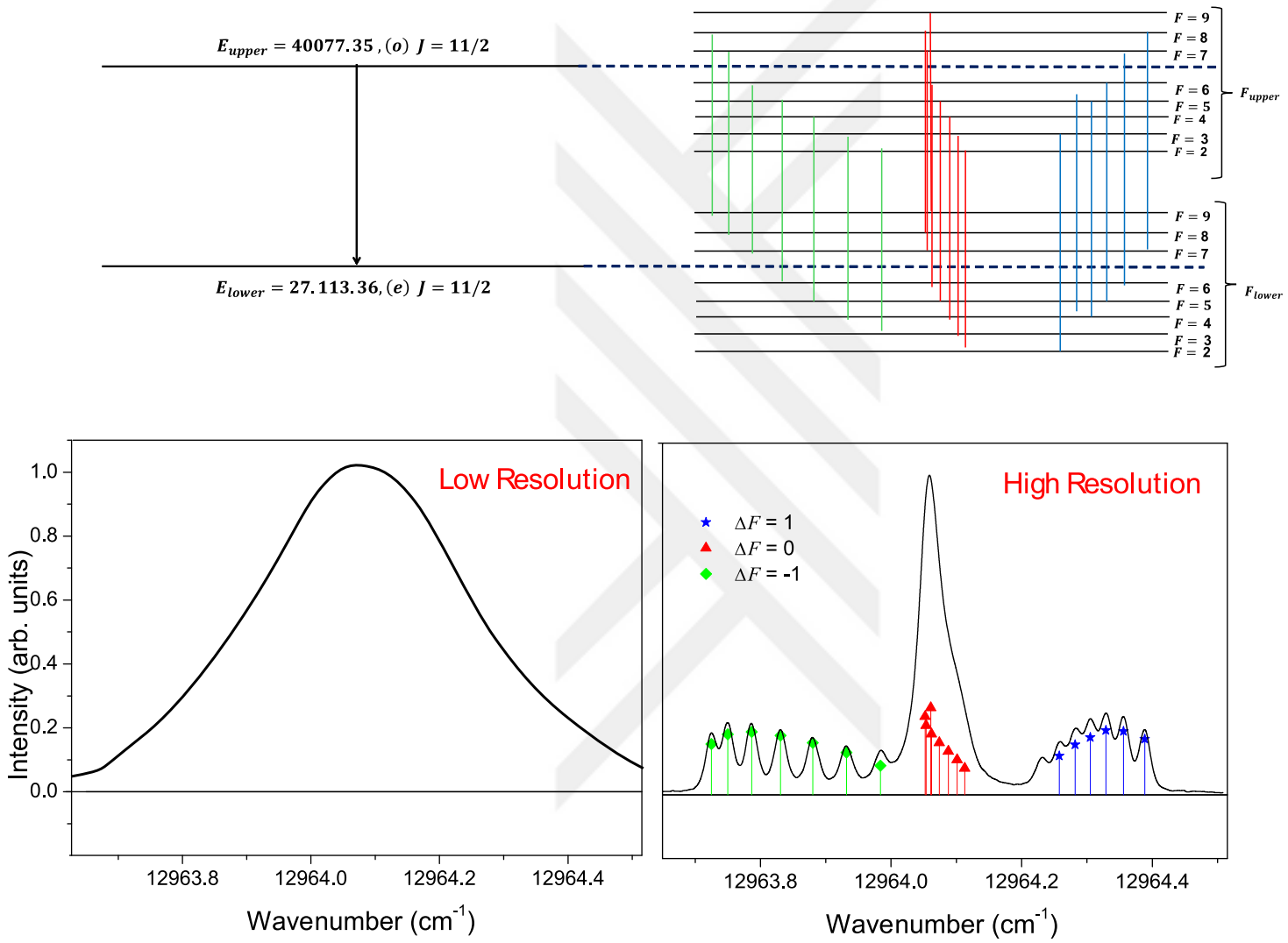


Figure 1.5 : Transition and energy level spacing comparison of fs and hfs of a spectral line at $\sigma = 12964.07$ cm^{-1} ($\lambda = 771.151$ nm).

2. EXPERIMENTAL METHODS AND TECHNIQUES

Advances in laser technology have widened the range of techniques available for spectroscopic investigations, improving both resolution and sensitivity. However, even with high resolution instruments, line broadening must be considered for the accuracy of measurements. This section provides information on the mechanism of line broadening and a brief overview of some laser spectroscopic techniques where line broadening can be minimized. Before discussing line broadening mechanisms, it is necessary to mention the lifetime of the excited state since the intensity of the spectral lines depends on the population density and the transition probability, which are directly related to the lifetime of the excited state. Atoms in an excited state can spontaneously decay to a lower state by emitting a photon, a process called fluorescence. The atom will further decay to the ground state if the lower-energy state is above the ground state again by emitting a photon or collision-induced transition. The emission probability of fluorescence decay of a transition $\langle i| \rightarrow \langle k|$ is given by the Einstein coefficient A_{ik}. The emission rate of the state $\langle i|$ with N_i atoms to the state $\langle k|$ is $dN_i = -A_{ij}N_i\,dt$. The total emission rate of E_i in all possible states, where $A_i = \sum_k A_{ik}$ can be written as

$$dN_i = -A_i N_i\,dt \tag{2.1}$$

Integrating Eq.2.1 yields the time-dependent population density of the state $\langle i|$ as given below.

$$N_i(t) = N_i(0)e^{-A_i t} \tag{2.2}$$

As can be deduced from Eq.2.2, the population density of the energy state decreases exponentially from its initial value $N_i(0)$ at $t = 0$. The time at which the initial population density decreases to $1/e$ is given by τ_i, the mean lifetime of E_i, as shown in Fig.2.1.

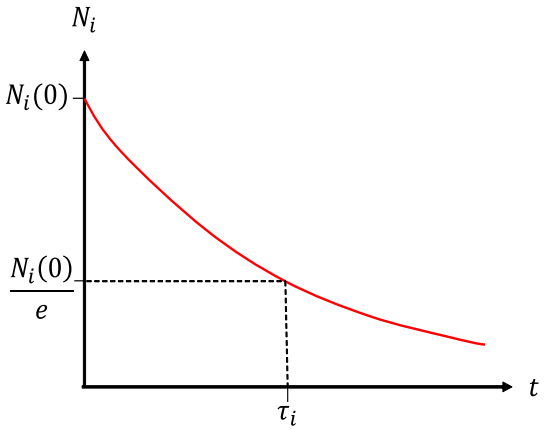


Figure 2.1 : Decay curve of the population density N_i of E_i with τ_i.

The lifetime τ_i is defined by the probability $(P_i(t))$ that the atom undergoes a spontaneous transition between t and $t+dt$ as shown below.

$$\langle t_i \rangle = \int_0^\infty t P_i(t) dt = \int_0^\infty t A_i e^{-A_i t} dt = \frac{1}{A_i} = \tau_i \tag{2.3}$$

2.1 Broadening of Spectral Lines

Spectral lines of emitted or absorbed light from a transition between different energy levels ($\Delta E = h\nu_0 = E_2 - E_1$) are not exactly monochromatic. Instead, they have an intensity distribution around the central frequency of the corresponding transition ($\nu_0 = \frac{E_2 - E_1}{h}$). The intensity line profile with half-width $\delta\nu = |\nu_2 - \nu_1|$ for which $I(\nu_1) = I(\nu_2) = \frac{I_o}{2}$ is known as the full width at half maxima (FWHM) as shown in Fig. 2.2 [50]. The spectral regions within and outside the half-width of the line are called the kernel and the wing, respectively. The FWHM depends on the lifetime of the energy levels involved in the transition, the temperature, and the pressure of the atomic or molecular medium.

Line broadening is divided into homogeneous and inhomogeneous line broadening. In the homogeneous line broadening, the absorption and emission probability of light for a frequency corresponding to a transition $E_i \longrightarrow E_f$ is the same for all atoms in a medium. Homogeneous line broadening results in a Lorentzian profile of the emission or absorption frequency distribution profile. Examples of homogeneous line broadening are natural and collisional broadening. In contrast, inhomogeneous line

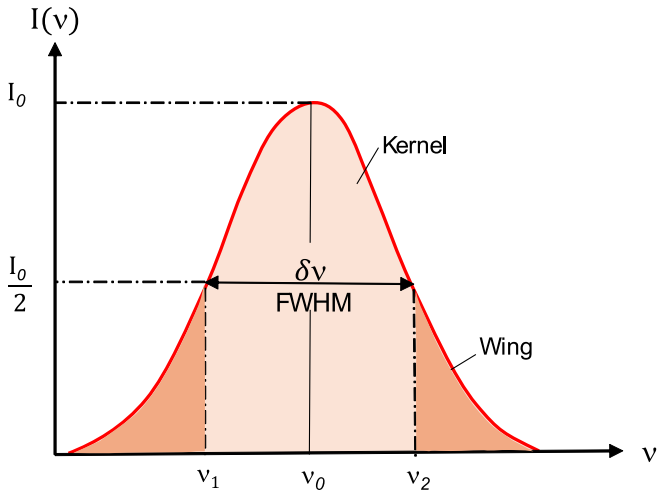


Figure 2.2 : Spectral line profile.

broadening occurs when the atoms in a medium do not have the same absorption or emission probabilities. Inhomogeneous broadening results in a Gaussian profile of the emission or absorption frequency distribution. An example of inhomogeneous broadening is Doppler broadening.

2.1.1 Natural line broadening

Natural broadening is defined in both classical and quantum mechanical terms. In the quantum mechanical picture, Heisenberg's uncertainty principle $\Delta E \Delta t \sim \hbar$ states that finding an atom in a particular state, which is related to the lifetime of that state($\tau = \Delta t$), is inversely proportional to the energy spread of the atom and causes a broadening of the spectral line of the corresponding transition. A schematic illustration of the natural line broadening is shown in Figure 2.3. [50] [53].

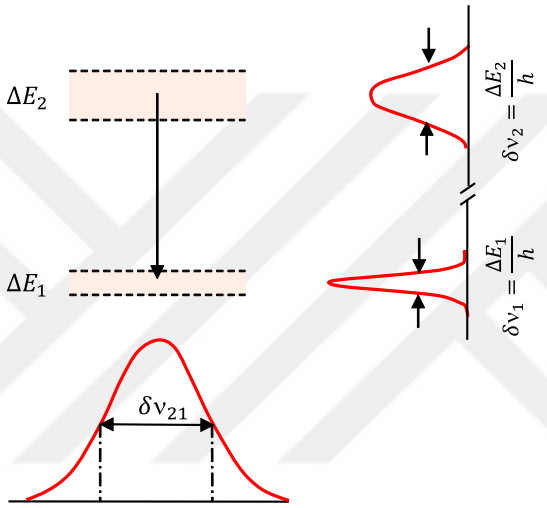


Figure 2.3 : Natural line broadening of a transition caused by the lifetime of the energy states ΔE_1 and ΔE_2.

In the classical picture, a spectral line distribution of a transition can be described using the damped harmonic oscillator model since the excited atom will radiate its energy in a damped manner. According to this model, the electron of the excited atom is described with a frequency ω, mass m, restoring force constant k and a damping constant γ. The time-dependent oscillation amplitude of the electron can be obtained from the following equation of motion, where $\omega_0 = \sqrt{\frac{k}{m}}$.

$$\ddot{x} + \gamma\dot{x} + {\omega_0}^2 x = 0 \tag{2.4}$$

The solution of Eq. 2.4 with the initial values $x(0) = x_0$ and $\dot{x}(0) = 0$ is :

$$x(t) = x_0 e^{-(\gamma/2)t}[\cos\omega t + (\gamma/2\omega)\sin\omega t] \tag{2.5}$$

where the damped oscillation frequency of the electron $\omega = \sqrt{\omega_0{}^2 - (\gamma/2)^2}$ is slightly lower than ω_0, likewise for most excited atoms the assumption $\gamma \ll \omega_0$ is true and therefore we can neglect the second term in Eq. 2.5 and set $\omega \simeq \omega_0$, the solution for real atoms can be obtained as follows:

$$x(t) = x_0 e^{-(\gamma/2)t}\cos\omega_0 t \tag{2.6}$$

Since the amplitude of the oscillation decreases with time, as shown in Fig.2.4 a), we can conclude that the frequency of the emitted light is no longer monochromatic [50] [53]. Instead, the intensity distribution of the spectral line is a normalized Lorentzian profile, which can be mathematically solved by a Fourier transformation of Eq.2.6. The normalized Lorentzian profile of the natural broadening is given in Eq.2.7, which can be derived from the integration of the Fourier transform; more details can be found in textbooks.

$$L(\omega - \omega_0) = \frac{\gamma/2\pi}{(\omega - \omega_0)^2 + (\gamma/2)^2} \tag{2.7}$$

An illustration of the Lorentzian line profile is shown in Fig.2.4 b) [54] [53]. The FWHM of the line profile $\delta\omega_n = \gamma \Rightarrow \delta\nu = \gamma/2\pi$ is called the natural line width, caused by the spontaneous emission of the atom without any external influence, and cannot be reduced by any spectroscopic method. The natural line broadening is in the range of 0.1-100 MHz for stable levels.

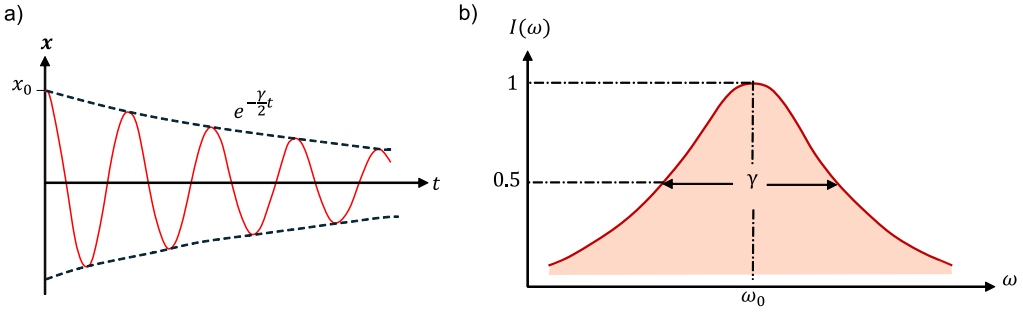


Figure 2.4 : Natural line width a) Damped oscillation and b) Lorentzian line profile.

2.1.2 Doppler broadening

The Doppler broadening of the spectral line is caused by the Doppler effect, which refers to the change or shift in the wavelength or frequency of the signal due to the relative motion between the source and the observer. In a dense gaseous medium, the shift is caused by the thermal motion of the emitting atoms or molecules. As the source signal moves toward the observer, a decrease in wavelengths of the emitted light (or increase in frequency) causes a blue shift; as the source signal moves away from the observer, an increase in wavelength (or decrease in frequency) results in a red shift of the emitted signal. The frequency shift of the emitted signal due to motion relative to the observer differs from the emitted signal of an atom at rest (ω_o) by $\omega = \omega_0(1 \pm \frac{v}{c})$ as illustrated in Fig. 2.5 a).

For a gas in thermal equilibrium at temperature T, the number of atoms (N) with a velocity between v and $v+dv$ moving in the direction of the observer is given by the Boltzmann distribution;

$$n(v)dv = \frac{N}{v_p\sqrt{\pi}} exp^{-(v/v_p)^2} dv = N\left(\frac{m}{2\pi k_B T}\right)^{1/2} exp\left(-\frac{mv^2}{2k_B T}\right)dv \tag{2.8}$$

where k_B is the Boltzmann constant, $v_p = (2k_B T/m)^{1/2}$ is the most probable velocity of the atoms, and m is the atomic mass.

Since velocity v is associated with the frequency shift $dv = (c/\omega_0)d\omega$, the intensity distribution of the observed Doppler line profile is given by

$$I(\omega) = I_0 exp\left(-\frac{(\omega-\omega_0)^2}{\omega_0 v_p}\right) \tag{2.9}$$

which shows a Gaussian line profile symmetric at the center frequency (ω_o) with a FWHM, as illustrated in Fig. 2.5 b) [50] [53].

The Doppler width of a spectral line is proportional to the frequency and the temperature as follows.

$$\delta\omega_D = \frac{\omega_0}{c}\left(\frac{8kTln2}{m}\right)^{1/2} \tag{2.10}$$

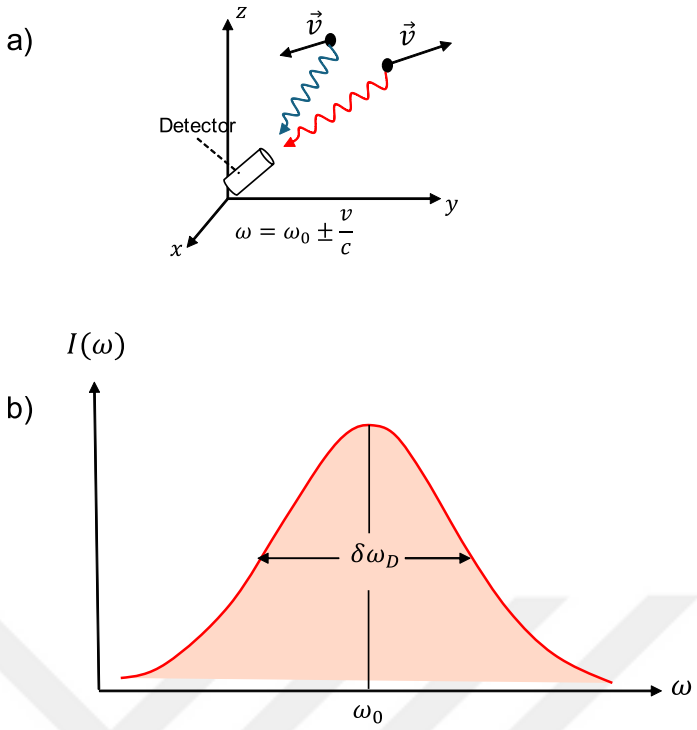


Figure 2.5 : Doppler broadening. a) Doppler effect b) Gaussian line profile.

Inserting Eq. 2.10 into Eq. 2.9 and using the numeric value $1/(4ln2) = 0.36$, the Gaussian line profile of the Doppler broadening can be rewritten in the following form,

$$I(\omega) = I_0 exp\left(-\frac{(\omega - \omega_0)^2}{0.36\ \delta\omega_D{}^2} \right) \tag{2.11}$$

In comparison, the Doppler broadening of the spectral lines is much larger than the natural broadening. Doppler broadening is also more significant in visible and UV regions. A comparison of the Lorentzian line profiles of Natural broadening and the Gaussian line profile of Doppler broadening is illustrated in Fig. 2.6 [54].

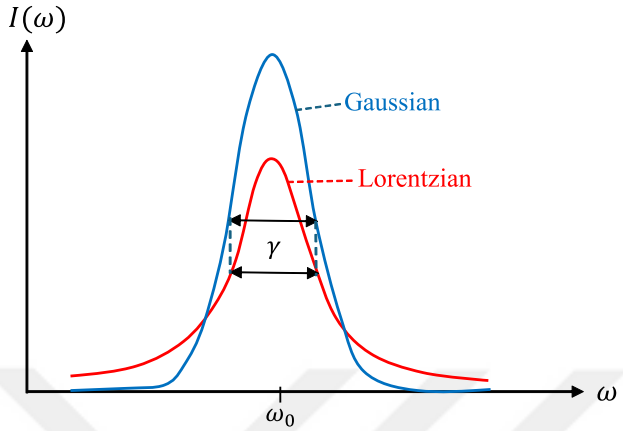


Figure 2.6 : Comparison of Gaussian and Lorentzian line profiles with the same FWHM.

For high-resolution spectroscopy, as can be deduced from Eq.2.10, Doppler broadening can be reduced by lowering the temperature of the medium.

2.1.3 Saturation/Power broadening

Saturation broadening is a specific type of broadening that occurs when the intensity of the incoming light source is high enough to cause stimulated absorption to increase until the populations of the lower and upper energy states approach equilibrium, leading to a point where the absorption is "saturated". This effect reduces further absorption at certain frequencies, causing a broadening of the spectral line, as illustrated in Fig.2.7. [55]. Saturation broadening is also known as power broadening. In a gaseous medium, Saturation/Power broadening can also interact with Doppler broadening and modify the spectral line.

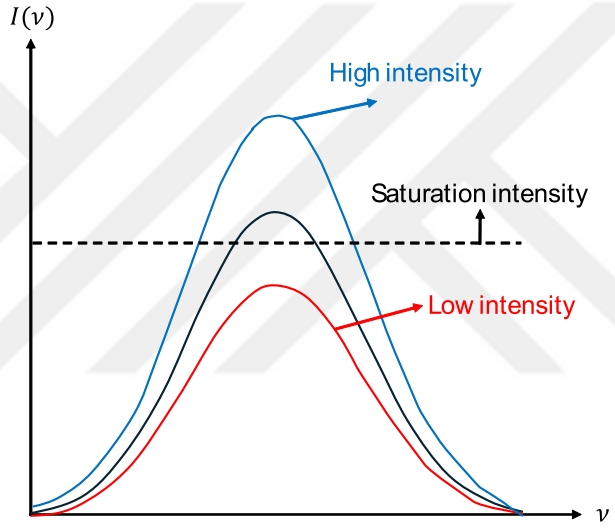


Figure 2.7 : Saturation broadening with increasing intensity of the light source.

2.1.4 Collisional/Pressure broadening

Collisional broadening occurs when neighboring atoms, ions, or molecules collide in a high-density medium, such as a gas discharge or plasma. It is also known as pressure broadening since the number of collisions per second increases with increasing pressure. Short-range interactions can be categorized primarily into elastic and inelastic collisions. They both influence the broadening of spectral lines in different ways. Elastic collisions occur when two particles collide and exchange momentum without changing their internal energy states and separate after the collision time. The velocity of the emitting particle changes as a result of momentum transfer, which causes a random shift of the spectral line due to the Doppler effect. Elastic collisions are, therefore, often referred to as phase perturbing collisions. Inelastic collisions occur when two particles collide, where either one or both of the particles' internal energy states change, reducing the lifetime of the excited states and leading to line broadening, according to the energy-time uncertainty principle, as already discussed in natural line broadening Sect. 2.1.1. Inelastic collisions are often referred to as quenching collisions because they reduce the number of atoms in the excited state and quench the intensity of the emitted fluorescence line.

In summary, both elastic and inelastic collisions contribute to the broadening of a spectral line with a Lorentzian distribution; elastic collisions additionally cause a shift in the center of the spectral line, as illustrated in Fig. 2.8 [50].

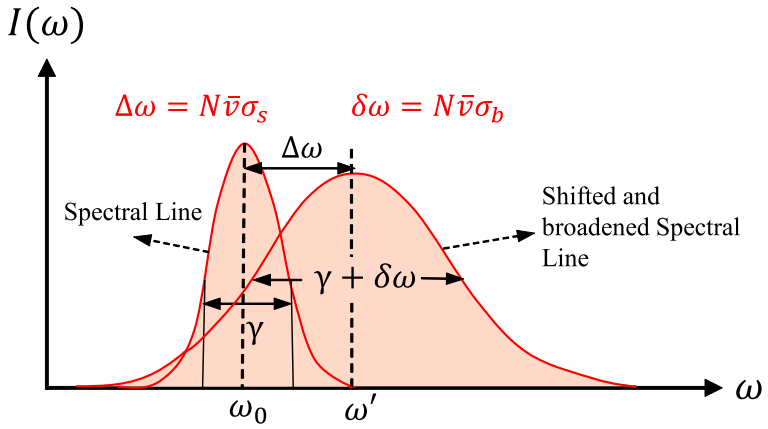


Figure 2.8 : Collision-induced shift and broadening of a spectral line.

Line shift $\Delta\omega$ and line broadening $\delta\omega$ are determined by $\bar{v}$ the mean relative velocity and N the number of densities of the colliding particles and the cross sections of broadening and shifting σ_s and σ_b, respectively.

2.1.5 Combined line profile: Voigt profile

In spectroscopic studies, multiple broadening mechanisms affect the observed line shape and must be taken into account for accurate analysis, especially in studies where the contributions of natural, Doppler and collisional broadening must be considered separately. Voigt line profile is the combined intensity profile of the Lorentzian and Gaussian line profiles as illustrated in Fig.2.9 [50] [54].

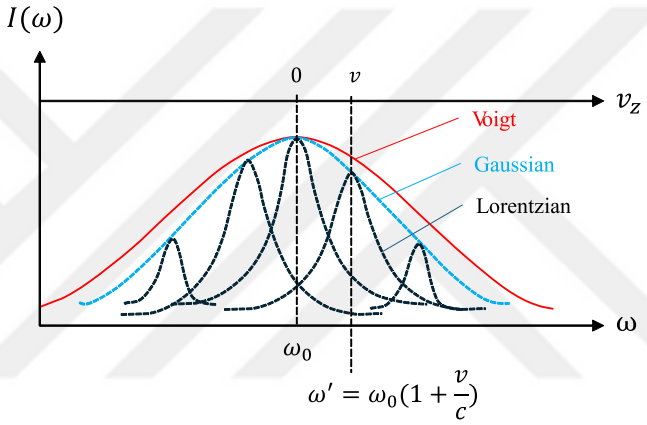


Figure 2.9 : Voigt profile of a spectral line formed by the combination of the Lorentzian and Gaussian line profiles.

The Voigt profile plays an important role in fine- and hyperfine-structure studies and in stellar atmosphere studies to separate the contributions of different broadening effects in spectroscopic measurements, where pressure and temperature information of the layers can be derived from Voigt profile modeling of the spectra.

2.2 Basis of the Experiment

To investigate the even- and odd-parity fine-structure energy levels of Ho I and to determine their corresponding hfs constants, laser-induced fluorescence spectroscopy and laser optogalvanic spectroscopy methods were used simultaneously. This section introduces the hollow cathode used to generate the metal vapor or plasma medium of the holmium atom, explains the experimental basis of the measurement methods employed, and briefly describes the programs used to analyze the measured data.

The experimental study of this dissertation was conducted at the Laser Spectroscopy Research Laboratory in the Department of Atomic and Molecular Physics at Istanbul University.

2.2.1 Hollow cathode discharge lamp

For metals to be excited and investigated spectroscopically, they must be in a gaseous state. In this study, a hollow cathode (HC) discharge lamp was used to create a plasma medium of holmium (Ho), which was then spectroscopically investigated simultaneously with laser-induced fluorescence and optogalvanic spectroscopy methods. Fig.2.10 shows an illustration of a cross section of the hollow cathode discharge lamp used in this study. To operate, gas discharge lamps must first be evacuated, and then filled with a noble gas at a filling pressure of less than one hundredth of the atmospheric pressure. In our experiment, the hollow cathode was filled with neon (Ne) at a pressure between 1 and 1.5 Torr and operated with a discharge current of 60 mA.

When high voltage is applied between the cathode and the anode, the Ne atoms ionized by collisions are accelerated by the potential difference. Positive ions hit the cathode and sputter Ho atoms upon impact from the HC. This vaporizes the Ho metal into the gaseous phase and simultaneously excites the free atom, creating the plasma medium consisting of free electrons, ionized atoms, and neutral atoms. With higher discharge currents, the spectra of these sputtered atoms become more and more prominent. The

kinetic energy of the particles increases with the current, allowing us to investigate high-lying energy levels.

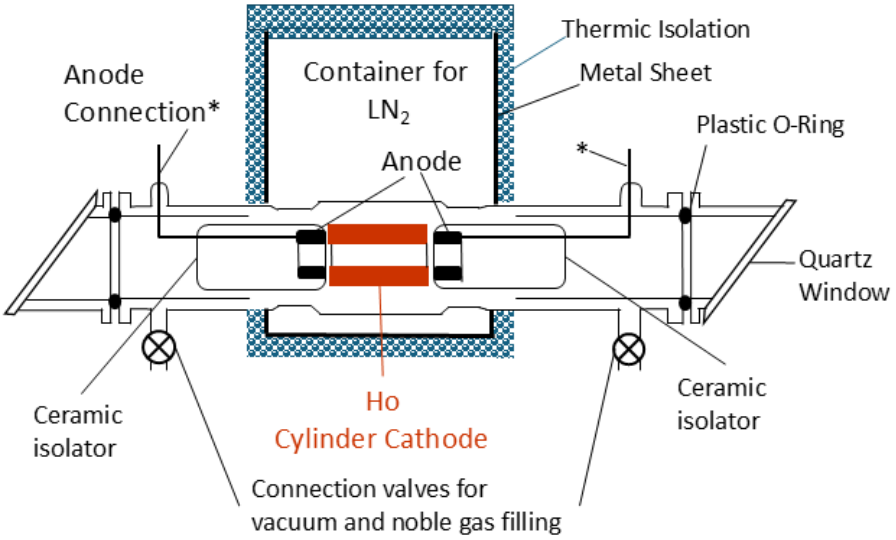


Figure 2.10 : Cross section of an HC discharge lamp.

2.2.2 Optogalvanic spectroscopy

Optogalvanic spectroscopy (OGS) is a simple and suitable spectroscopic technique used in gas discharges. When the laser beam passes through the gaseous discharge volume and the laser frequency is tuned to an optical transition of the atom or ion, a significant change in the population densities of the lower and excited states occurs. Because of the varying ionization probabilities of each level, changes in the population at different energy levels will result in variations in the number of ions and free electrons. This will result in either an increase or a decrease in the conductivity of the discharge volume, known as the optogalvanic effect (OGE). This technique does not require any monochromator or detector for the investigation of the spectra, since the discharge itself acts like a detector. The OGE can be observed as a voltage change ($\Delta V = R\Delta I$) across a ballast resistor.

The experimental setup of our OGS is shown in Fig.2.11. The hollow-cathode discharge tube is irradiated by a tunable Ti-Sa laser, which is constant in intensity, is periodically switched on and off with a mechanical chopper. This modulation ensures that only the voltage signals correlated with resonant laser-induced transitions are detected, effectively suppressing background and non-resonant contributions.

The applied ignition voltage of the hollow cathode is typically hundreds of volts, while the voltage change to be measured is in the millivolt range, so a lock-in amplifier must be employed. Both negative and positive signals can be observed, depending on the levels involved. [50,56]. More information and an overview of the OGS and its applications can be found in [57].

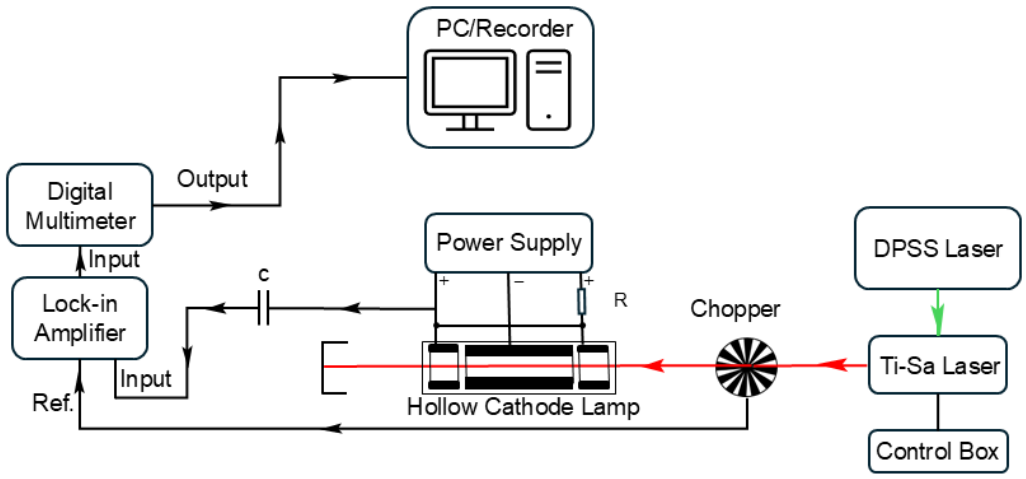


Figure 2.11 : Experimental setup of Optogalvanic Spectroscopy.

2.2.3 Laser induced fluorescence spectroscopy

Laser-induced fluorescence (LIF) spectroscopy is a highly sensitive technique used to investigate the energy level structures of atoms. In this method, laser light is directed through the plasma generated within a hollow cathode gas discharge lamp. Atomic excitation occurs when the laser wavelength is tuned to the energy difference between the lower and upper states, as outlined in Sec.2.2.2. The change in population density causes the atoms to emit light known as fluorescence as they return to lower energy states via spontaneous or collisional deexcitation. Fluorescence signal detection of the transition from the upper and lower levels provides information on the energy levels of the laser line.

In laser-induced fluorescence spectroscopy, the fluorescence signals are categorized as either direct or indirect. Direct fluorescence arises from one of the two energy levels involved in the laser-induced transition and can be categorized as either positive-phase or negative-phase. Positive-phase fluorescence originates from the upper level of the laser-excited transition, where the population density increases because of the

absorption of laser light. In contrast, negative-phase fluorescence originates from the lower level, where population density decreases as a result of the same absorption process. Indirect fluorescence signals do not arise directly from the laser-excited transition, since the laser transition and the resulting fluorescence emission do not share a common energy level. Instead, the change in population density caused by the laser excitation is transferred through collisions within the plasma from the levels involved in the laser transition to other nearby levels, which almost have the same energy. Collisional coupling is known to be less likely to occur at low-pressure discharges.

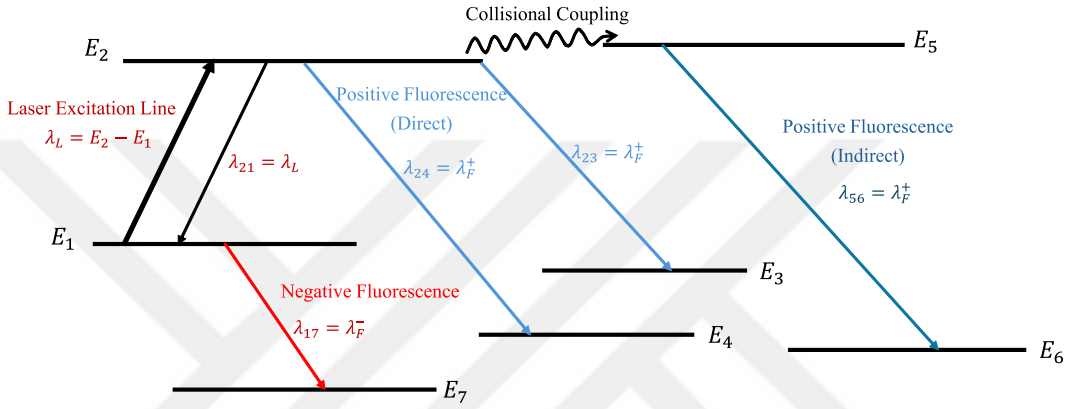


Figure 2.12 : Energy level diagram with possible fluorescence channels for LIF.

Fig.2.12 provides a schematic representation of the possible fluorescence channels in LIF. While collisional coupling is shown only for the upper level of the laser transition, it should be noted that such coupling can also occur from the lower level.

The experimental setup of our LIF spectroscopy is shown in Fig.2.13. As mentioned in previous Sect.2.2.2, the laser is intensity modulated prior to the entrance of the HC discharge lamp to suppress non-resonant contributions that might increase background noise or cause non-resonant transition contributions.

The laser is sent through a holed mirror (HM) (a plane mirror with a hole in the center) into the transparent HC discharge lamp. The small hole, precisely matched to the diameter of the laser beam and drilled at a 45^0 angle relative to the mirror surface, allows the laser beam to pass through the mirror without obstruction. The divergent emission from the hollow cathode lamp is efficiently separated from the laser beam by the same mirror, which is positioned at 45^0 to the optical axis, with negligible

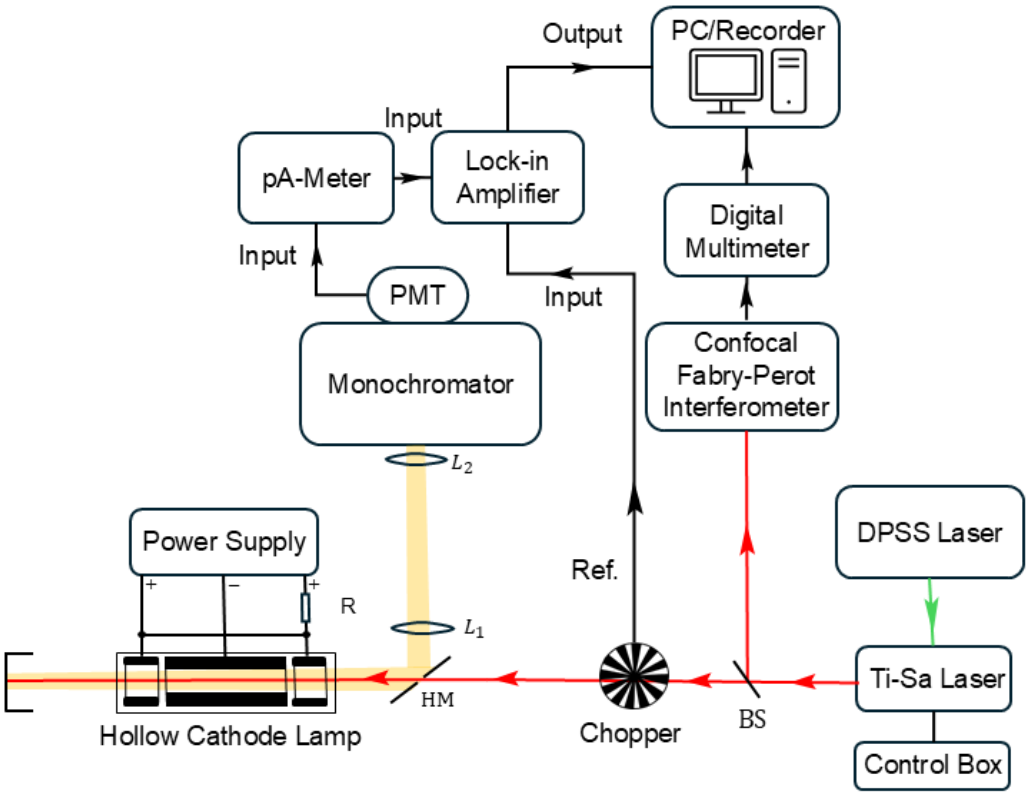


Figure 2.13 : Experimental setup of Laser-Induced Spectroscopy.

losses. Because all fluorescence signals can occur simultaneously in the plasma, directly measuring the fluorescence light with a photomultiplier is not practical. The emitted light is therefore collimated by a lens (L) and subsequently focused on the monochromator entrance slit by a second lens before it is sent to a photomultiplier. The monochromator separates the spectrum into single spectral lines, which can then be measured by a photomultiplier, which is installed on the exit side of the monochromator. The measured photocurrent signal is sent to a picoammeter and converted into a voltage, which is then fed into the input of a lock-in amplifier.

The LIFS method is a sensitive and selective spectroscopic method, since by fixing the monochromator to the fluorescence lines occurring from either of the two levels involved in the laser transition, unwanted fluorescence light from the plasma medium is eliminated and the signal-to-noise ratio is enhanced. This also prevents the spectral line under investigation from overlapping or blending with other line spectra [58,59]. The line spectra of the laser transition are obtained with the fixed monochromator by scanning the laser in a 20-35 GHz range.

2.2.4 Experimental setup of the study

The study combines both the OG and the LIF spectroscopic methods in the investigation of the fine structure energy levels of atomic Ho. Both methods were performed simultaneously to improve the detection sensitivity. The experimental setup of this study is illustrated in Fig.2.14.

A custom-built transparent HC discharge lamp was used to generate the plasma medium of Ho. The lamp consisted of a cylindrical copper cathode, 20 mm in length with an inner diameter of 3 mm, into which a 0.125 mm thick holmium foil of 99.9 % purity was inserted. The discharge was operated with neon as buffer gas at a pressure of approximately 1-1,5 Torr (1–2 mbar) and maintained with a stable current of 60 mA. To reduce Doppler broadening and improve spectral resolution, the central part of the hollow cathode was cooled with liquid nitrogen throughout the measurements.

The excitation of Ho atoms was achieved using a tunable, continuous wave (cw), single-mode titanium-sapphire (Ti:Sa) laser system (Coherent MBR 110, maximum output 4 W), pumped by a diode pumped solid-state (DPSS) laser (Coherent Verdi V-18, 532 nm, 18 W). The laser system provided coverage in the wavelength range of 690 to 835 nm. This was achieved using two sets of mirrors, one covering 680–750 nm and the other covering 750–850 nm. To prevent saturation broadening and maintain consistent power during scanning, the laser output was attenuated to approximately 1.8 W.

A small portion of the laser beam was separated by a beam splitter (BS_1) and directed to a wavemeter (Highfinesse WS6 200, accuracy $\pm$200 MHz), which simultaneously adjusts precisely the transition wavelength of the atomic line and allows us to record the initial wavelength of the scan. Another beam splitter (BS_2) directed the laser beam to a laboratory-built temperature-stabilized confocal Fabry-Perot interferometer (FPI) with a free spectral range (FSR) of 299.001(8) MHz, which was used for relative frequency calibration. The laser beam was modulated with a mechanical chopper operating around 1 kHz to facilitate lock-in detection. For OGS detection, the laser-induced change in discharge voltage was measured across a ballast resistor. For LIFS, light from the plasma inside the hollow cathode lamp is coupled to a McPherson 607

monochromator equipped with a Hamamatsu R928 photomultiplier via mirrors and lenses.

Using the optogalvanic spectroscopy (OGS) method with lock-in detection, the spectra are recorded over a scan range of 30 GHz to obtain all possible transitions. There may be one, two, or even more transitions corresponding to different energy-level pairs in the scan region. The LIFS method is applied to resolve the closely lying transitions. Firstly, in the OG spectra, an isolated peak was observed and chosen to fix the laser wavelength. Keeping the laser wavelength fixed, the monochromator was scanned in the range of 370 nm- 850 nm, excluding the region of the excitation laser wavelength ($\pm$25 nm) to record the fluorescence line spectra using the lock-in technique, which distinguishes the laser-induced signal from the emission signal. All fluorescence lines from the levels involved are identified and recorded.

The laser wavelength was then continuously scanned over a range of 20 to 35 GHz and the spectral line was measured while keeping the monochromator wavelength fixed on the identified fluorescence lines for high-resolution measurement with the LIFS method. To ensure statistical reliability, each spectral line of interest was measured at least five times under the same experimental conditions. Data analysis was performed on the spectral line measured with the LIFS method to determine the hfs constants A and B of the corresponding fine-structure energy levels. The "Fitter" analysis program is used in analyzing the hfs spectra, as explained in Sect.2.2.5.

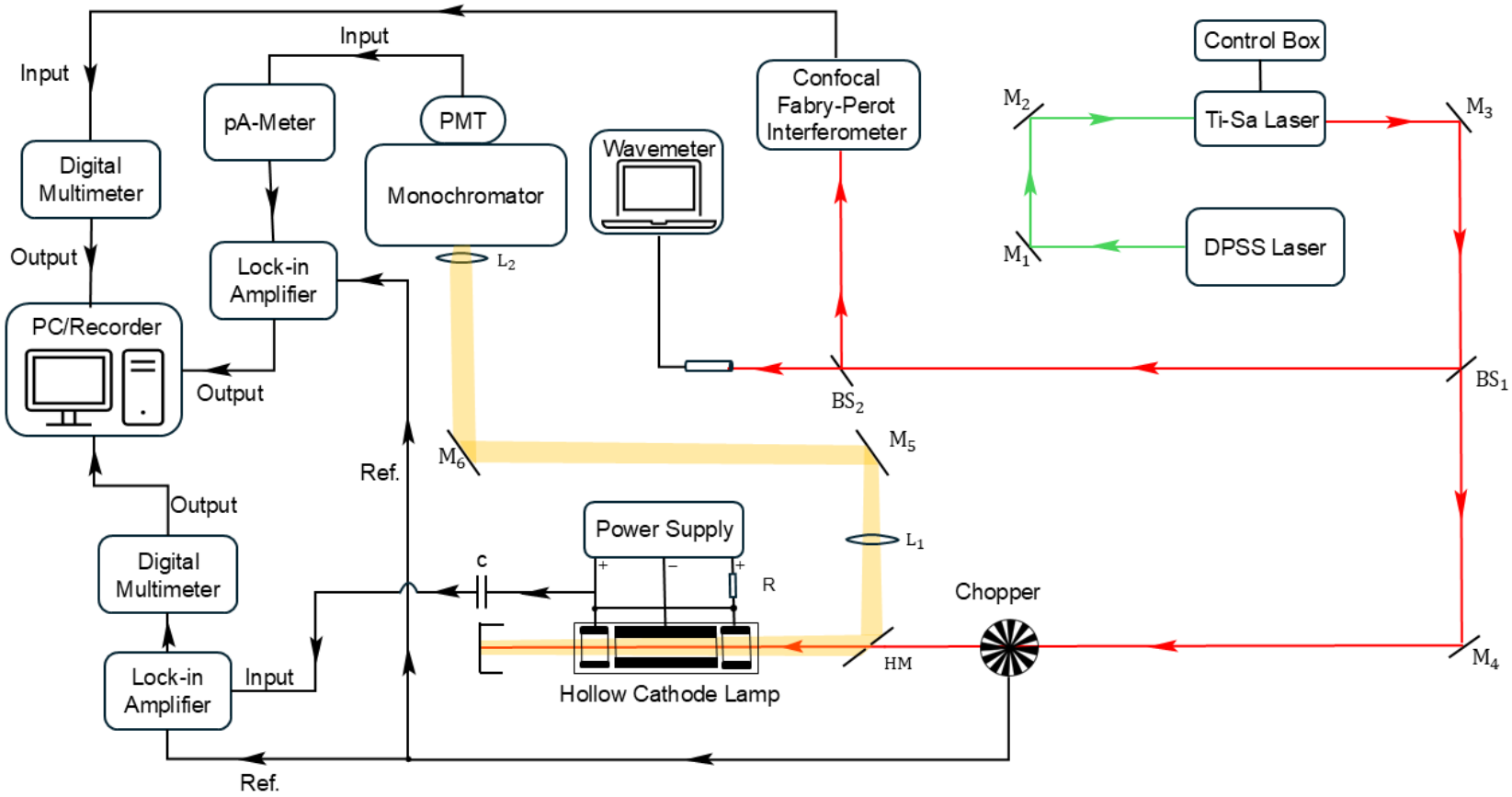


Figure 2.14 : Experimental setup of the combined LIF and OG spectroscopy method.

2.2.5 Data analysis programs

During this study, two different analysis programs were used. The Elements classification program was used to manage data related to the identification and classification of spectral lines. The Fitter HFS analysis program was used to fit the appropriate theoretical mathematical distribution function to the measured spectral lines to determine the hfs constant values of the lower and upper energy levels.

2.2.5.1 Elements program

The computer program 'Elements' is used [60,61] to analyze all defined and undefined spectral lines of holmium in the literature and to determine the unknown energy levels of the measured spectral line.

The program uses the measured FT spectra of the holmium atom and converts the data into a wavelength(Å)-dependent change in intensity function. The FT spectra (320 nm- 1750 nm) embedded in the program were measured by our research group at the Laser Center of the University of Latvia in Riga with two noble gases, Ar and Ne. Two noble gases were used as buffer gases to observe the spectra belonging to the holmium atom. The SNRs of both spectra were already calibrated by [62]. The program reads both spectra simultaneously. The wavelength axis for both spectra, Ho-Ar and Ho-Ne, is equivalent, so that the two spectra overlap completely, resulting in the spectral line of Ho being observed at the same wavelength for both spectra.

For the program to run properly, the following input data are needed;

- Level.dat file contains all known atomic and ionic fine structure energy levels of holmium, their corresponding quantum number J, parity and hfs constants, A and B (if available), together with reference information if available. The list of energy levels in the input data file, including the energy levels discovered and published from this study [63], is given in Table A.1 in the appendix.

- wHo.dat file of atomic and ionic holmium, containing the spectral lines defined in the literature in terms of wavelengths. This file can be considered a dynamic

file since it serves as both an input and an output file. The input file is created by writing known transitions between energy levels from the literature. As the program runs, new data are written into the output file. The file contains and provides the information listed below.

1. The wavelength of the transition in (Å), i.e. the cog of the spectral line.
2. The SNR of the spectral line observed in the FT spectra with Ar and Ne and the SNR of the spectral line from the literature, if available.
3. If the line is classified, the upper and lower energy levels (cm^{-1}), their quantum number J, parity, A and B hfs constants (MHz), together with reference information if available.
4. Information on which atom or ionic state (Ho I, Ho II or Ho II) the transition from the energy level belongs to.

The interface of the program consists mainly of two windows, as shown in Figs.2.15 a) and b). The window indicated as a) is the main window of the program and consists of three sections, and b) contains the superimposed FT spectra of Ho measured with Ar (blue) and Ne (red). Both windows are actively used simultaneously during the search and classification of spectral lines.

Right Section of Window a) The right section displays a graphical overview of the hf structures of all theoretically possible transitions calculated. If the hfs constants of the calculated level pairs are unknown, the display remains blank. The difference between the cog of the spectral line and the proposed transition is provided in the left corner of the displayed possible hfs. The smaller the difference in number, the greater the probability that the defined line is c orrect. Due to the limitation value set by us, only values below 0.35 in wavelength difference are displayed among the possible lines. Fig.2.15 a) shows the main window with the classification of the line at $\lambda = 7509.12$ Å as an example as a result of this study.

Middle Section of Window a) The middle section of the window contains a list of all theoretically possible suggestions of spectral lines, considering the energy difference



Figure 2.15 : Classification window of the Elements program, with examined line at $\lambda = 7509.12$ Å.

of the level pairs that match the cog of the examined spectral line, within the selection rules.

Left Section of Window a)

This section of the main window displays the wavelength and wavenumber of the cog of the spectral line observed from the FT spectrum.

The spectral line in the right section is selected and transferred to the left window. If the lower or upper energy levels of the hfs are unknown, the simulation program is used to obtain an experimental spectrum, which provides an approximate value for the hfs constants. The simulation program is explained in further text. The line is then defined and transferred to the left window. In this example, the second theoretical spectrum at the upper right of window a) is consistent with the experimental FT spectrum, and has been defined in the left section of window a).

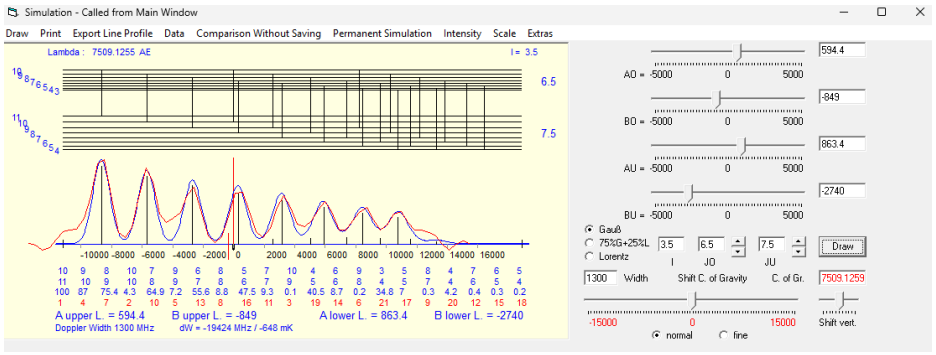
Window b) This window consists of the FT spectra. The buttons on the left side of the FT spectra allow the user to examine and navigate through the FT spectrum, where one can intensity-wise increase/ decrease or expand (zoom in) or shrink (zoom out) the

viewed FT spectra. To move along the spectrum, the Left and Right buttons increase or decrease the wavelength, respectively.

The left Section of Window a) remains blank if a line observed in the FT spectrum is not defined in the literature. The transition wavelength of the observed line is entered in the main window using the button 'Insert Line' (indicated with a red ellipse in the figure). The program calculates all level pairs for possible matches in the transition corresponding to the cog of the examined line. If the suggested hfs of the calculated matches the observed spectral line, which is checked with the simulation program in the Elements program, the line is then saved to the program by the button 'Select for Entry' (indicated with a black ellipse in the figure). The simulation program in the classification program can be reached directly from the simulation button indicated with a purple ellipse in the main window of the program. The simulation program for the line at $\lambda = 7509.12$ Å is shown in Figs.2.16. Fig.2.16 a) shows a good simulation example with good overlap of theoretical and experimental spectra, red and blue, respectively. b) gives an example of a poor fit result with simply altering the A constant of the lower energy level.

If the fine structure energy levels of the lower and/or upper spectral line under investigation are unknown, or if these levels are known but the associated magnetic dipole (A) and electric quadrupole (B) hyperfine structure constants are unknown, the simulation program included in the classification program can be used to determine approximate values for A and B that yield spectra similar to those obtained by LIF spectroscopy.

a)



b)

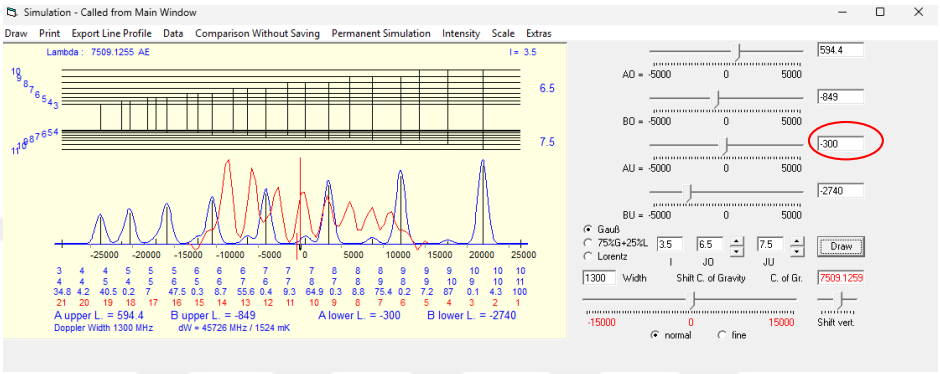


Figure 2.16 : Simulation of the line at λ= 7509.12 Å using the simulation program, where the red spectrum shows the experimental spectral line and blue the theoretical fit. a) and b) illustrate a good and bad fit, respectively, due to altered *B* hfs value.

2.2.5.2 Fitter program

The Fitter program [64] is a specialized software tool to analyze the measured hyperfine structure of a spectral line with theoretical models (fitting) to precisely determine the hyperfine structure constants *A* and *B* and the cog of the examined spectral line, which was developed by the research group in Germany at the University of the Bundeswehr Hamburg and was later used in many spectroscopic studies, including our research group.

The program is based on the least squares method to fit the optimal mathematical model (e.g., Voigt profile) to the experimental data by adjusting the width, intensity, cog and hfs constants of the spectral line. The Voigt profile is a convolution of Lorentzian and Gaussian profiles, which allows for realistic modeling of the line shape, where partially resolved hfs components or blended spectral lines are present.

The program calculates the frequency of transition of each HFS component with its HFS constants using the following relation. Here, the subscripts are abbreviations in German: o-oben means 'upper' and u-unten means 'lower'.

$$\nu = \nu_{cog} + \alpha.A_o + \beta_o \cdot B_o - \alpha_u \cdot A_u - \beta_u \cdot B_u \tag{2.12}$$

Here, α and β are the so-called Casimir factors for the upper and lower energy levels, and ν_{cog} is the frequency of the investigated spectral lines.

The program uses non-linear least squares methods (Eq.2.13) to minimize the square deviation between the experimental and model intensity of a given frequency using a parametrized function $I_{model}(\nu_i; \overrightarrow{p})$ [64], where $\overrightarrow{p}$ is defined as the vector of A, B, line width, center position, and intensity parameters to be fitted.

$$S(\overrightarrow{p}) = \sum_{i}^{N} [I_{measured_i}(\nu_i) - I_{model}(\nu_i; \overrightarrow{p})]^2 \tag{2.13}$$

During a spectral scan, the wavelength change of the laser is nonlinear, while the Fitter program needs the recorded spectra to be uniformly spaced, i.e., linearly spaced in terms of frequency, to perform the least squares method on the line spectra. The nonlinear spectra are calibrated using a simultaneously recorded FPI signal as shown in our experimental setup in Fig.2.14. The frequency data of the spectra were calibrated with the linearization program within the Fitter. This program linearizes the spectrum using the start and end wavelengths of the laser scan and the FSR of the FPI. In this method, the frequency values (in MHz) corresponding to each data point are calculated, and the number of data points on the horizontal axis of the spectrum is converted to a frequency value.

The Fitter program relies on text-based input files to run. The required input files include the measured experimental data, model parameters, and constraints for the fitting process and are given as follows.

- '.mes' file (measurement file): Contains the line spectrum experimentally measured (frequency vs. intensity).

- '.par' file (parameter file): The metadata of the .mes file, containing the start frequency, number of data points, and step size between data points of the recorded line spectrum.

- '.lin' file (linearized spectra): The file contains a one-column text file listing the wavenumber (cm^{-1}) or frequency (MHz) value that matches the number of points in the.mes file and conforms to the spacing shown in the.par file.

- '.ein' file (eingabe/input file): The file contains the main control data for the fitting procedure to be applied, namely the number of components for each spectral transition of the hfs structure ($\Delta F = 0, \pm 1$), initial estimates for the parameters and the fixed and variable parameters for each spectral transition.

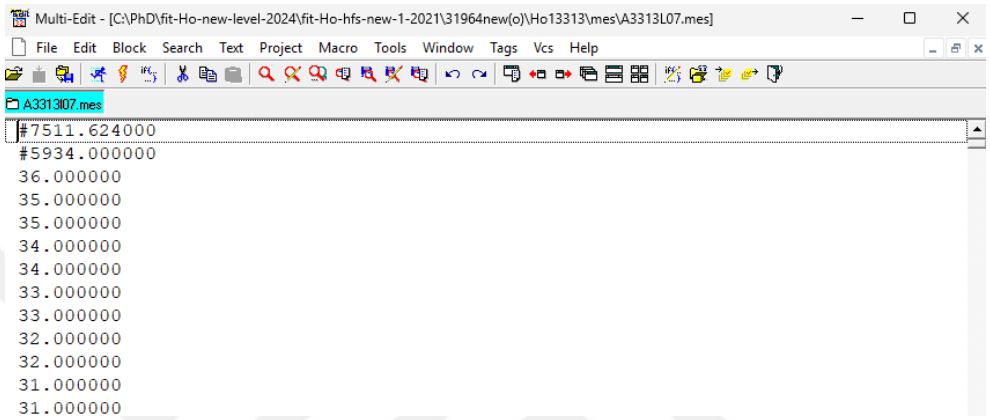
  The fixed parameters in the file ".ein" are the isotope number of the examined element, the isotopic ratio, the nuclear spin, and the J values of the lower and upper fine structure energy levels of the spectral line to be fitted. These parameters are kept fixed during the fit process.

  The variable parameters of the file ".ein" are the cog, the hfs constants A and B of the lower and upper fs energy levels, the saturation intensity, the line width, and the FWHM of the Voigt profile with Gaussian and Lorentzian contribution ratio (Theta= Gaussian/Voigt) of the spectral line. Screenshots of the data files .mes and .par are given Fig.2.17, measured and linearized spectrum in Fig.2.18.

  A screenshot of the file ".ein" is shown in Fig.2.19. Each variable parameter is labeled with the number as '0' or '1', indicating that the variable parameter is to be fixed (0) or set free for the fitting process (Fixed (0) or Fitted (1)). For a known and classified level of a spectral line, the corresponding hfs constants from the literature are kept fixed by labeling the hfs constants with the number '0'.

  The fitted spectrum of the linearized spectrum is shown in Fig.2.20.

a)



b)

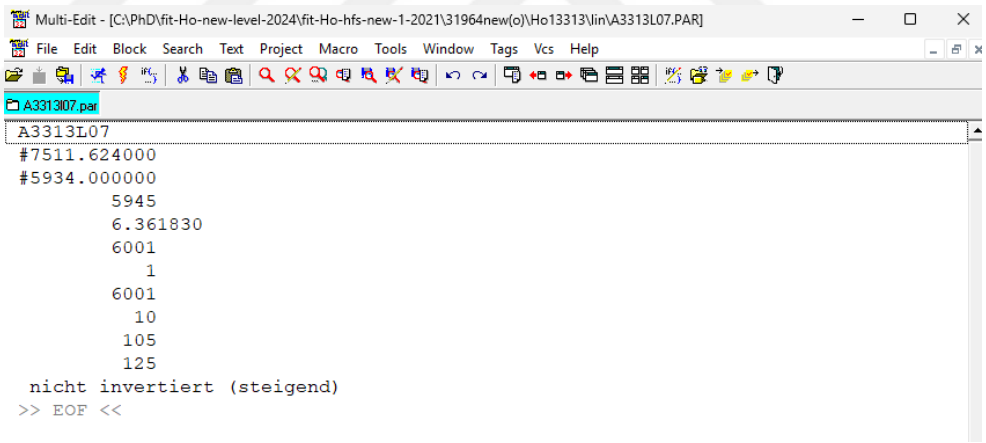


Figure 2.17 : Screen shots of the data files .mes and .par, respectively.

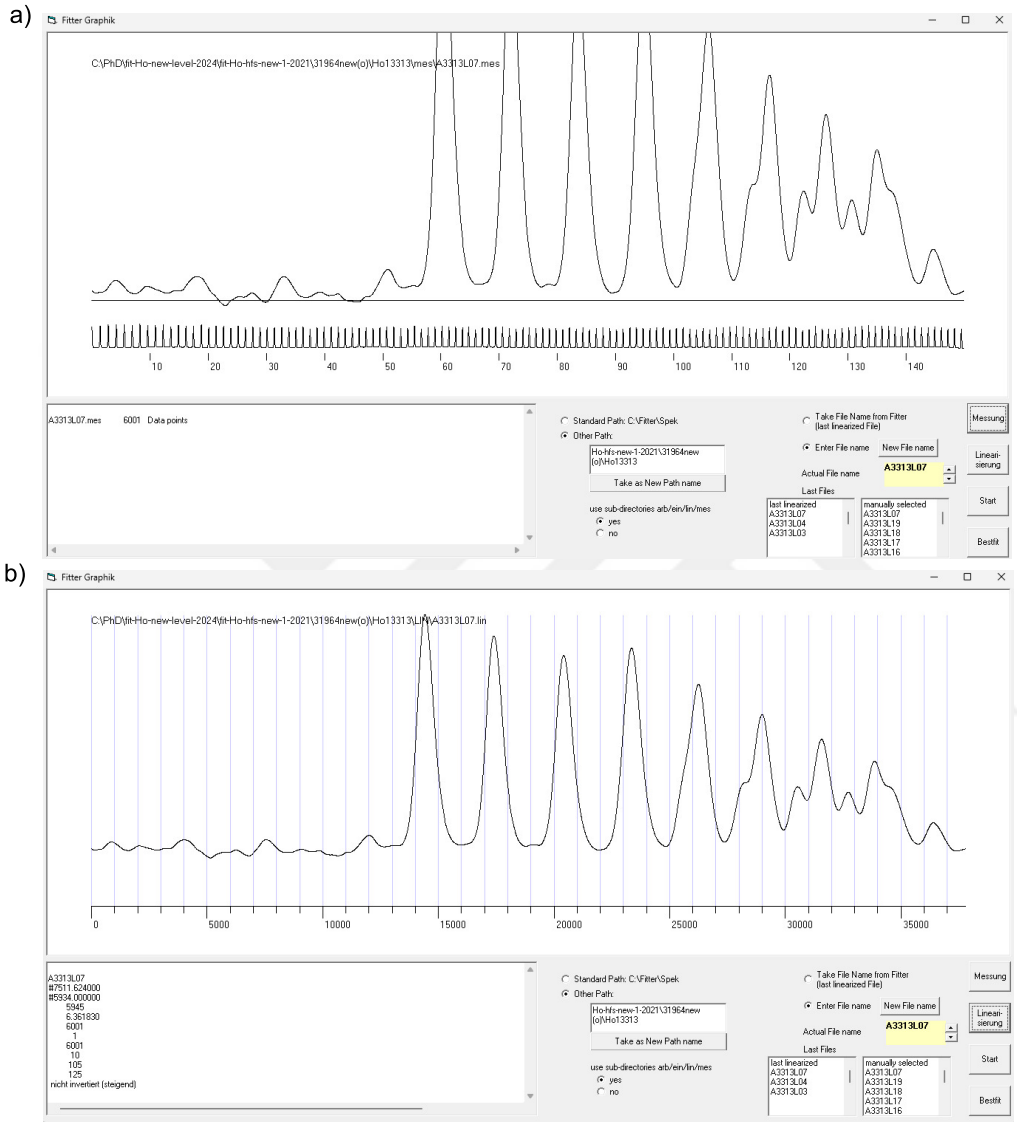


Figure 2.18 : Screen shots of the data files .mes and .lin, respectively. The raw spectrum from the LIFS measurement is given in a). Linearized spectrum of the raw spectrum with the x-axis converted into MHz.

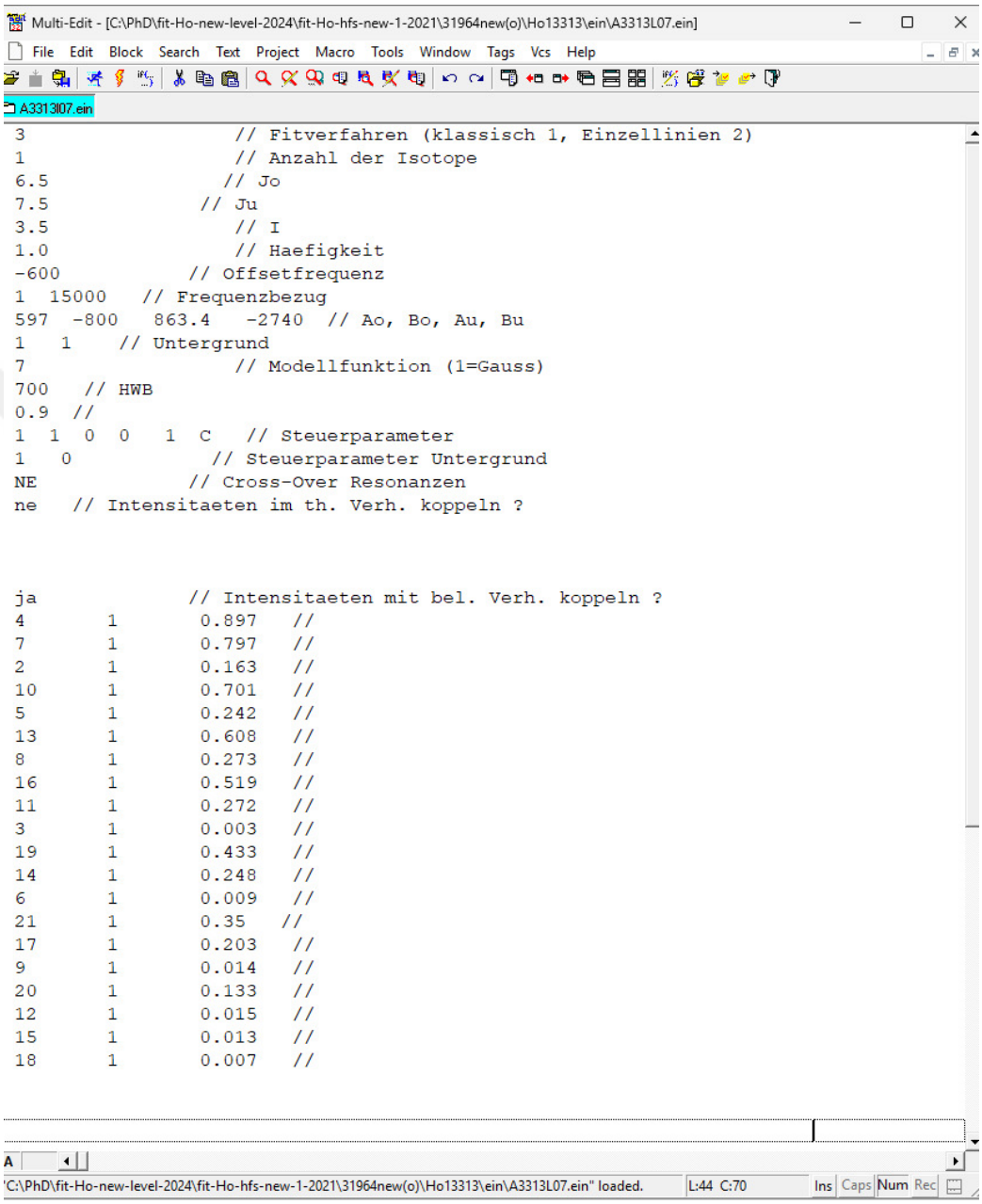


Figure 2.19 : Screen shots of the data file .ein for the fitting process of the linearized spectrum.

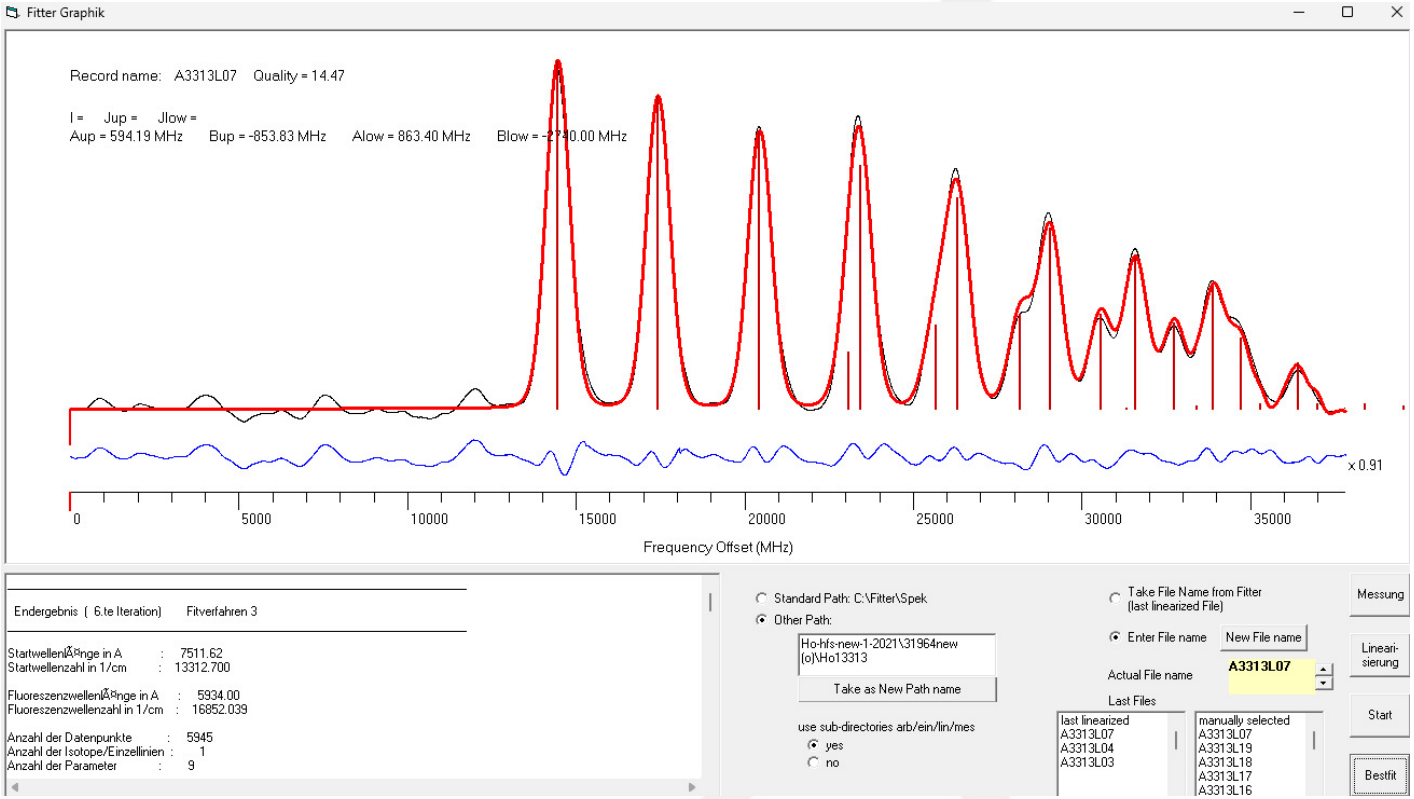
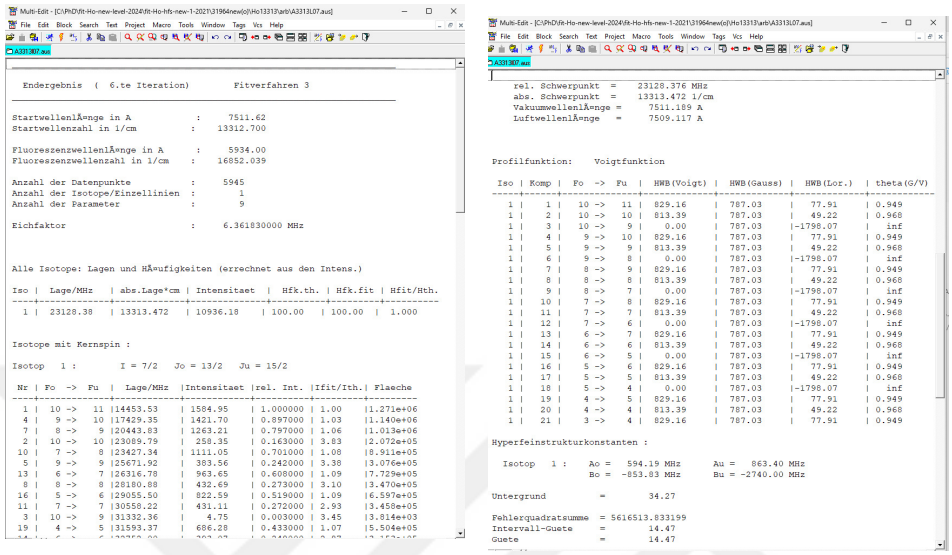


Figure 2.20 : Screen shots of the data file .ein for the fitting process of the linearized spectrum.

- 'arb' file (arbeit/work file): This folder is the output folder of the Fitter program. The file contents of the fit-created subdata files are '.aus'(ausgabe/output), '.bf' (bestfit), '.bw' (berechnete Werte/ calculated values), and '.stw'(schrittweise datei/ the stepwise or iteration log of the least-squares fitting process.

The sub data file '.aus'(ausgabe/output) contains the main output data which contain the results from the hfs analysis, the hfs constants of the fine structure energy levels, the cog, the line widths, and the voigt ratio (Gaussian/Lorentzian) of the spectral line and the confidence interval of the obtained values. A screenshot of the data file '.aus'(ausgabe/output) is given in Fig.2.21.

a)



b)

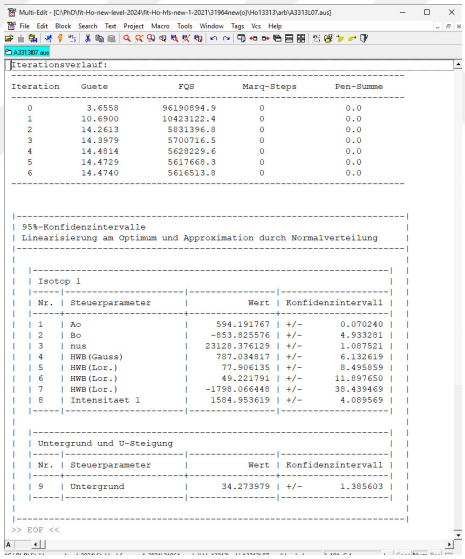


Figure 2.21 : Screenshots of the .aus data file showing the input data and iteration data for individual components in the HFS analysis, as well as the fit profile, Cog and hfs constants obtained on the left and right sides of a), respectively. The confidence interval of the fit result is provided in b).

3. EXPERIMENTAL RESULTS

The aim of this thesis was to discover fine structure energy levels of atomic holmium (Ho I) using laser induced fluorescence spectroscopy (LIFS) and optogalvanic spectroscopy (OGS) in the wavelength range of 690 nm to 830 nm, and to determine the corresponding new magnetic dipole and electric quadrupole hyperfine structure constants, A and B, respectively. The wavelength range under investigation was experimentally covered in two parts by changing the mirror setup of the laser. First, the 750 nm to 830 nm region was examined, and later the 690 nm to 780 nm region.

A total of 20 new energy levels were discovered in the two regions studied: eight in the first wavelength region (750 nm- 830 nm) and 12 in the second (690 nm-780 nm). Their corresponding A and B constants were also determined. Four of the 20 discovered energy levels were published more quickly by the research group in Poland at the Poznan University of Technology [41,43], leaving us with 16 new discovered energy levels for the publication of the results of this dissertation study.

The list of spectral lines measured in the discovery of new energy levels using the LIFS method is summarized in Table 3.3. $\sigma(\mathrm{cm}^{-1})$, the center of gravity (cog) of the spectral lines is obtained from the hfs analysis. Each spectral line was measured at least five times. The mean value of all measurements of the spectral line was considered for accuracy. The accuracy in determining the cog of the spectral line is relatively dependent on the wavemeter, since the starting wavenumber of a 20-35 GHz scan was recorded from the reading of the wavemeter (absolute accuracy 200 MHz (0.007 cm^{-1}) as explained earlier in Sec.2.2.4. The precision of the calibrated FT spectra was within 0.005 cm^{-1}.

Therefore, the LIFS determined energy level values were confirmed and improved with the FT spectrum to obtain the absolute energy value given in this study using the FT lines. Error analysis of the new discovered energy values was achieved from the theoretically calculated spectral lines in the FT spectrum. The theoretically calculated

possible fluorescence lines from the discovered energy levels were obtained from the Elemente classification program [60,61] as explained in Sec.2.2.4. Table 3.5 lists the lines theoretically calculated that are used to improve the accuracy of the energy levels discovered. The absolute energy level values and errors provided in the results section are taken from Table 3.5. Table 3.6 lists the theoretically calculated lines used to improve the accuracy of the already published four energy levels, which were also discovered in this thesis study. The energy value of the discovered levels with error bars obtained from the hfs analysis of the FT lines, with their corresponding hfs constants, are given in Table 3.1. As a by-product of the new energy levels investigated, the hfs constants for already known energy levels are experimentally obtained and listed in Table 3.4, where the literature values are also provided for comparison.

Hfs constants, A and B, of the new levels were obtained from the hfs analysis [64] of the spectral lines, which were measured at least 5 times using the LIFS method. The experimentally obtained hfs constants given in Table 3.5 are the weighted mean values of the hfs fit results of all the corresponding measurements, using the same methods as given in [38]. The uncertainties of the weighted mean values are calculated with the formula given below.

$$\Delta A_{\mathrm{mean}} = \frac{\sqrt{\sum_i \left[\frac{(\Delta A_{\mathrm{exp},i})^2 + (A_{\mathrm{mean}} - A_{\mathrm{exp},i})^2}{(\Delta A_{\mathrm{Fitter,i}})^4}\right]}}{\sum_i \left[(\Delta A_{\mathrm{Fitter,i}})^2 + (\Delta s_{A,i})^2\right]^{-1}} \tag{3.1}$$

The uncertainties of the hfs constants for A and for B are calculated using the formula as follows;

$$\Delta A_{\mathrm{exp}} = \sqrt{(\Delta A_{\mathrm{Fitter}})^2 + (\Delta s_A)^2 + (\Delta A_{\mathrm{fixed}})^2} \tag{3.2}$$

where in Eqn.3.2 the term $(\Delta A_{\mathrm{Fitter}})$ corresponds to the standard deviation from the fit of the obtained A constant, the term (Δ s_A) is the standard deviation of the mean value obtained from all corresponding measurements, the last term corresponds to the uncertainty of the constant if the value of the hfs constant of the level from the literature was fixed during the hfs analysis, if this is not the case, the contribution of the last term

in the uncertainty calculation is omitted. The same formula applies to the hfs constant B as mentioned.

In addition, for 10 known energy levels from the literature, including unknown A and B constants of two odd parity energy levels, and already known A and B constants of eight energy levels of even and odd parity were determined to contribute to the literature database. The findings of the thesis study are discussed and provided in the following sections.

3.1 Search for New Levels

Two methods were used to discover new energy levels. These two methods will be explained in detail in the following subsections, using two example levels to illustrate the procedure for finding all new energy levels.

3.1.1 Method 1: Discovery with the lines observed in the FT spectra

In this method, the regions of the available FT spectra of holmium corresponding to the wavelength range of our laser were analyzed. The available FT spectra of holmium cover the ultraviolet (UV) range from 317 nm to 400 nm, the visible (VIS) range from 400 nm to 700 nm and the near infrared (NIR) range from 700 nm to 1750 nm. In the search for undefined lines, the VIS and NIR regions within our laser wavelength range were analyzed.

The wavelength of the laser is adjusted to the FT observed line, then a 20-35 GHz OG spectrum was measured. The laser wavelength is then fixed at the most intense and undisturbed peak. The monochromator is then scanned in the 400- 650 nm range in 50 nm steps to record the spectra of the fluorescence lines. The observed fluorescence lines can be measured in positive and negative phases.

LIFS method was performed by adjusting the monochromator to the wavelength of each recorded fluorescence line. This method is used to eliminate the overlap or blending of other line spectra with the measured one. In cases where both positive and negative fluorescence lines are present, the determination of the unknown fine-structure energy level is straightforward if the negative fluorescence line is defined in the

literature, i.e., the energy level value, parity, and the corresponding hfs constants are defined. If the negative line is not defined, or if only positive fluorescence lines are present, hfs data analysis of the measured LIF spectra is required. Data analysis on the LIF measured spectral lines of each fluorescence line was performed with the 'Fitter' program [64]. This program determines the center of gravity of the analyzed line. The upper energy level of the negative fluorescence line corresponds to the lower energy level of the laser line. The sum of the obtained center of gravity of the laser line and the upper energy level of the negative fluorescence line gives us the new energy level, which is the upper level of the laser excitation line. Using the Fitter [64] program, the J value, parity, and hfs constants A and B of the new level are also obtained. From the data analysis performed, the newly found energy value, with its parity, the value J and the constants A and B, is saved to the level file in the Elemente classification program [60,61], which calculates all possible lines occurring from this upper level. This program calculates all theoretically possible spectral lines that could occur within the transition rules from this new energy level. From the calculated spectral lines, those within the laser wavelength range were measured, if measurable, using the LIFS method with the monochromator set to the calculated fluorescence line to confirm the presence of the newly discovered energy level. In the case where the theoretically possible fluorescence lines from the upper or lower energy levels of the laser line are not measurable with the LIFS method, hfs simulation analysis on the FT spectrum of the calculated lines is applied to increase the accuracy of the discovered energy level and hfs constant values.

Discovery of E= 31964.93(0.03) cm^{-1} using Method 1 The discovery of the fine structure energy level, E= 31964.93 cm^{-1}, was achieved using Method 1. The first undefined line observed in our laser wavelength range in the FT spectrum was at λ_{air}= 750.912 nm (σ= 13313.46 cm^{-1}) as shown in Fig.3.1.

The laser wavelength was adjusted to λ_{air}=750.912 nm (σ=13313.46 cm^{-1}), and a 25 GHz wide OG spectrum was measured with FPI markers as shown in Fig.3.2.

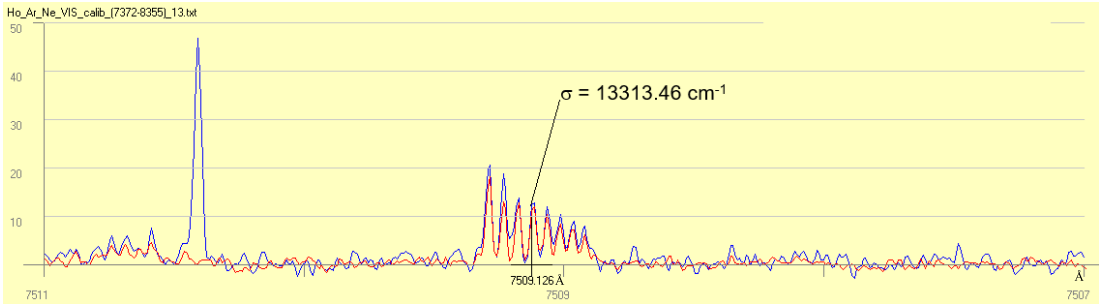


Figure 3.1 : The FT spectrum of the observed λ_{air}= 750.912 nm (σ= 13313.46 cm^{-1}) undefined line.

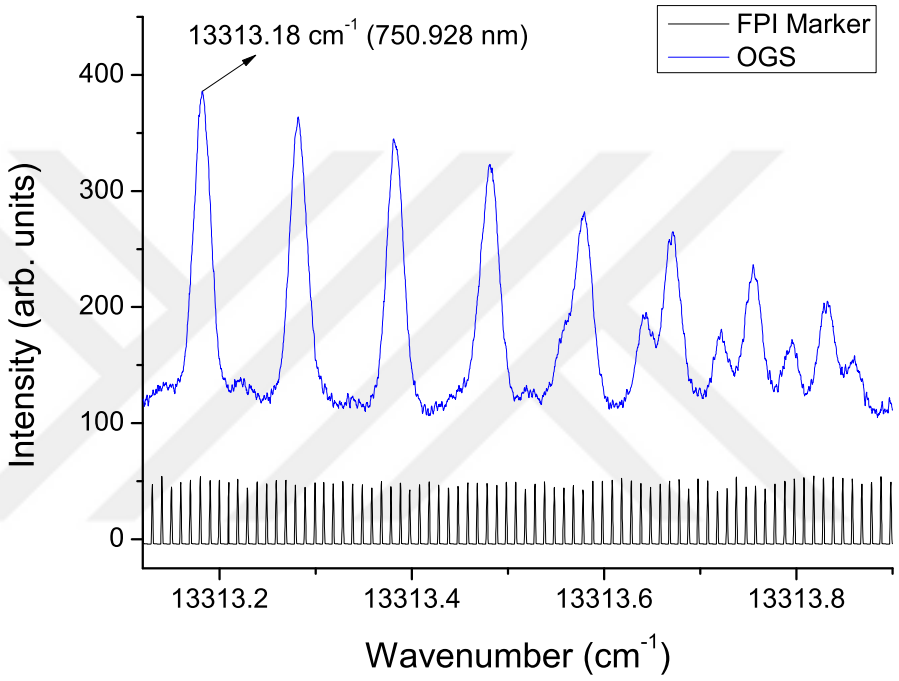


Figure 3.2 : Measured 25 GHz OG spectrum with FPI markers with laser wavelength at λ_{air}=750.912 nm (σ=13313.46 cm^{-1}).

Next, the laser wavelength is fixed at the most intense and undisturbed peak observed in the measured OG spectrum, which in this case was the peak at λ_{air}= 750.928 nm (σ= 13313.18 cm^{-1}) as pointed out in Fig.3.2.

The monochromator was then scanned in the 400- 650 nm range in 50 nm steps and spectra with fluorescence lines were recorded. In the recorded spectrum, fluorescence lines can be observed as negative and positive phases. An illustration of a 50 nm monochromator scan with fixed laser wavelength at λ_{air}=750.928 nm between 500-550 nm is given in Fig.3.3. The positive phase fluorescence lines are formed from the upper energy level of the laser wavelength, whereas the negative phase

fluorescence lines are formed from the lower energy level of the laser wavelengths, as already defined in Sec.2.13. From the whole scan, fluorescence lines were observed

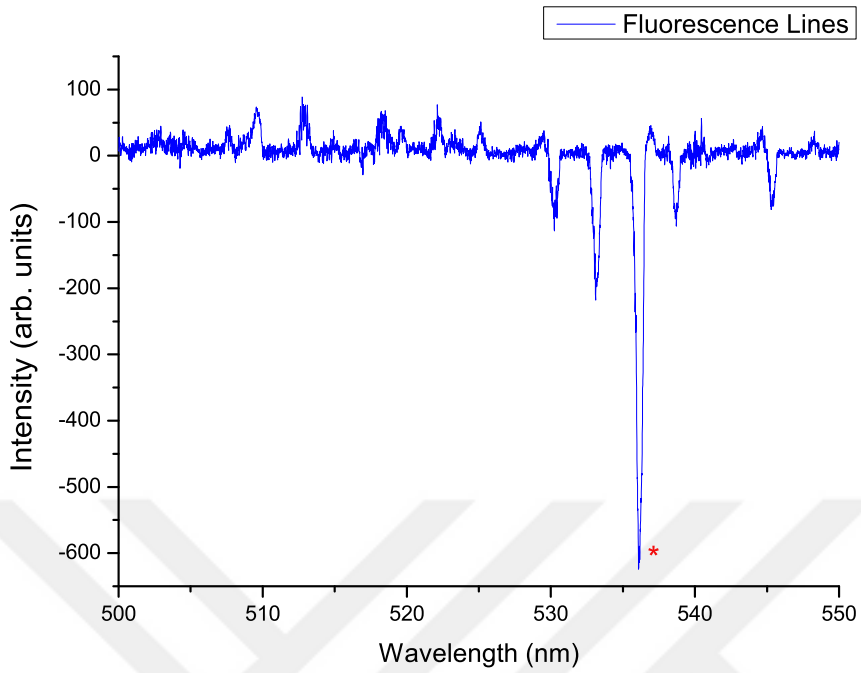


Figure 3.3 : Observed fluorescence lines during a 50 nm monochromator scan between 500 nm and 550 nm with fixed laser wavelength at λ_{air}= 750.928 nm (σ=13313.18 cm^{-1}). ($*$: λ_F^-= 536.050 nm)

at $^*\lambda_F^-$= 536.050 nm, λ_F^-= 586.200 nm, λ_F= 538.800 nm, λ_F= 593.400 nm, λ_F= 426.800 nm, λ_F= 422.500 nm and λ_F= 662.900 nm. Negative fluorescence lines are emphasized with a (-) sign for clarity. The LIF spectrum of the λ_{air}= 750.912 nm (σ=13313.46 cm^{-1}) laser line was measured individually with the monochromator adjusted to each observed fluorescence line. For all measured LIF spectra, the hfs structure showed the same structure. This indicates that the fluorescence lines belong to the energy levels of the laser line rather than to collisions. For illustration, the simultaneously measured LIF and OGS spectra of the λ_{air}= 750.912 nm (σ=13313.46 cm^{-1}) line with the monochromator set to λ_F^-=586.200 nm and λ_F= 538.800 nm are given in Fig.3.4. The spectra were shifted vertically for better comparison.

When searching for the measured fluorescence line λ_F^-= 536.050 nm in the FT spectrum, it was observed that it had a wavelength of λ_F= 536.000 nm as shown in Fig.3.5. The upper and lower energy levels of the λ_F= 536.000 nm line are as follows. E_{upper}= 18651.53 cm^{-1} J=15/2 (e) $\rightarrow$ E_{lower}= 0.0 cm^{-1} J=15/2 (o). We can conclude

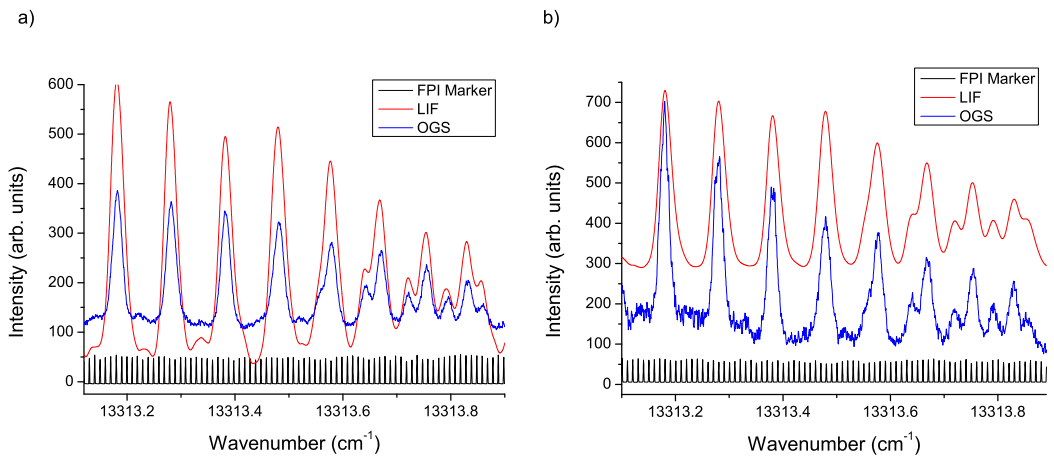


Figure 3.4 : Simultaneously measured LIF and OGS spectra with FPI markers of laser wavelength λ_{air}= 750.916 nm (σ=13313.46 cm^{-1}) with the monochromator set to the fluorescence line at a) λ_F^-= 536.050 nm and b) λ_F= 538.800 nm give the same hfs structure indicating they belong to the energy levels of the laser line.

from here that the lower energy level of the laser line is E_{lower}=18651.53 cm^{-1} with J=15/2(e). On the other hand, this assumption needs further proof. The investigated LIF spectra, shown in Fig.3.4a), of laser line at λ=750.912 nm (σ=13313.46 cm^{-1}) measured with λ_F^-= 536.050 nm was fitted with the hfs analysis program "Fitter" [64].

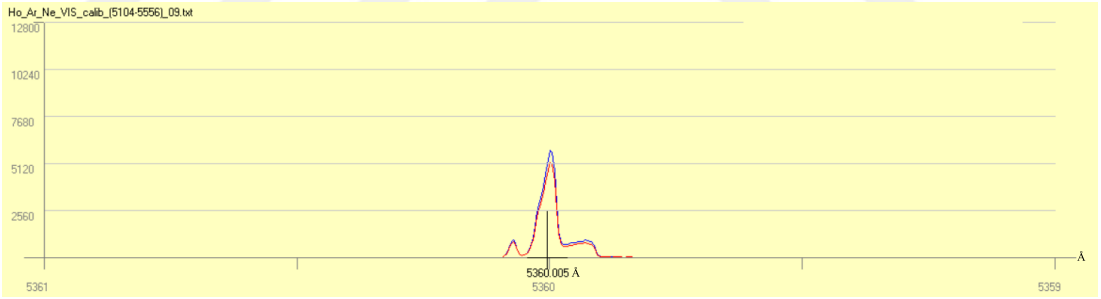


Figure 3.5 : The FT observed spectrum at λ_F=536.000 nm of the measured fluorescence line λ_F^-= 536.050 nm.

During this fit, the values of the hyperfine structure constants A and B of the lower energy level (E_{lower}=18651.53 cm^{-1} J=15/2) were kept fixed at the value given in the literature [38]. In this case, the J values that comply with the transition rules of the upper energy level can be 13/2, 15/2, and 17/2. The spectrum was fitted with each J value. Among these possible J values, the spectrum could only be fitted with J=13/2. From the fit, the center of gravity (cog) and the value of J, its parity, and hfs constants A and B of the laser line are obtained. As a result, it was seen that for the upper energy

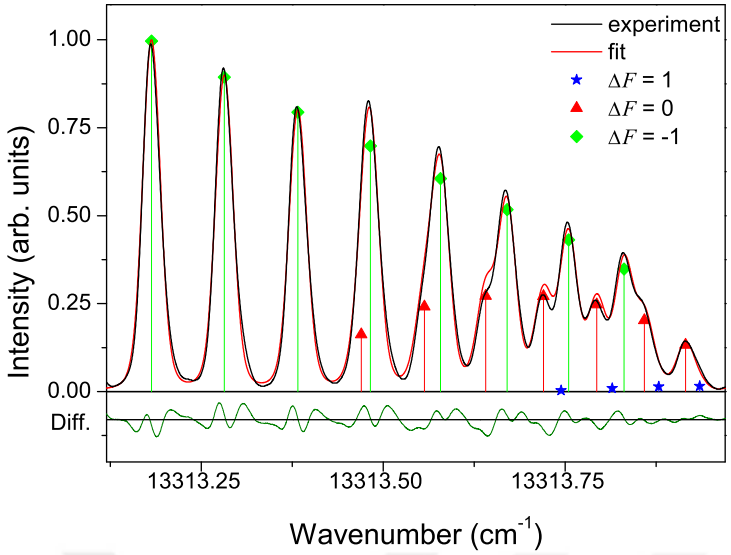


Figure 3.6 : Experimental LIF spectrum of the line at λ_{air}=750.912 nm (σ= 13313.47 cm^{-1}) measured with the monochromator set at λ_F^-= 536.050 nm with the best-fit curve superposed.

level the obtained values were in good agreement with the experimental spectrum, as shown in Fig.3.6

The new upper energy level can be found by simply adding the energy level value of the lower level and the laser line as follows:

E_{upper}= σ+E_{lower}= 13313.46+18651.53= 31964.99 cm^{-1}

To increase the precision of the newly found energy level, the energy level value with its J value, parity, and hfs constants, A and B, is saved to the "level" file, which is the input file of the "Elemente" program [60,61].

This file contains all experimentally known fine-structure energy values, their parity, and A and B values from the literature, if known. Using the 'Elemente' program, all possible spectral lines occurring from this newly found energy level within the transition rules are calculated. The calculated possible fluorescence lines were compared with those detected from the monochromator scan. The line at λ= 662.831 nm was found to coincide with one of the possible calculated lines from the discovered energy level. This means that the other four observed positive fluorescence lines arise from collisional coupling. On the other hand, λ_F= 662.831 nm can be used

in the LIFS measurements for all possible calculated lines arising from the new energy level. Thus, all possible lines within the laser region were measured using the LIFS method with the monochromator set to λ_F= 662.831 nm.

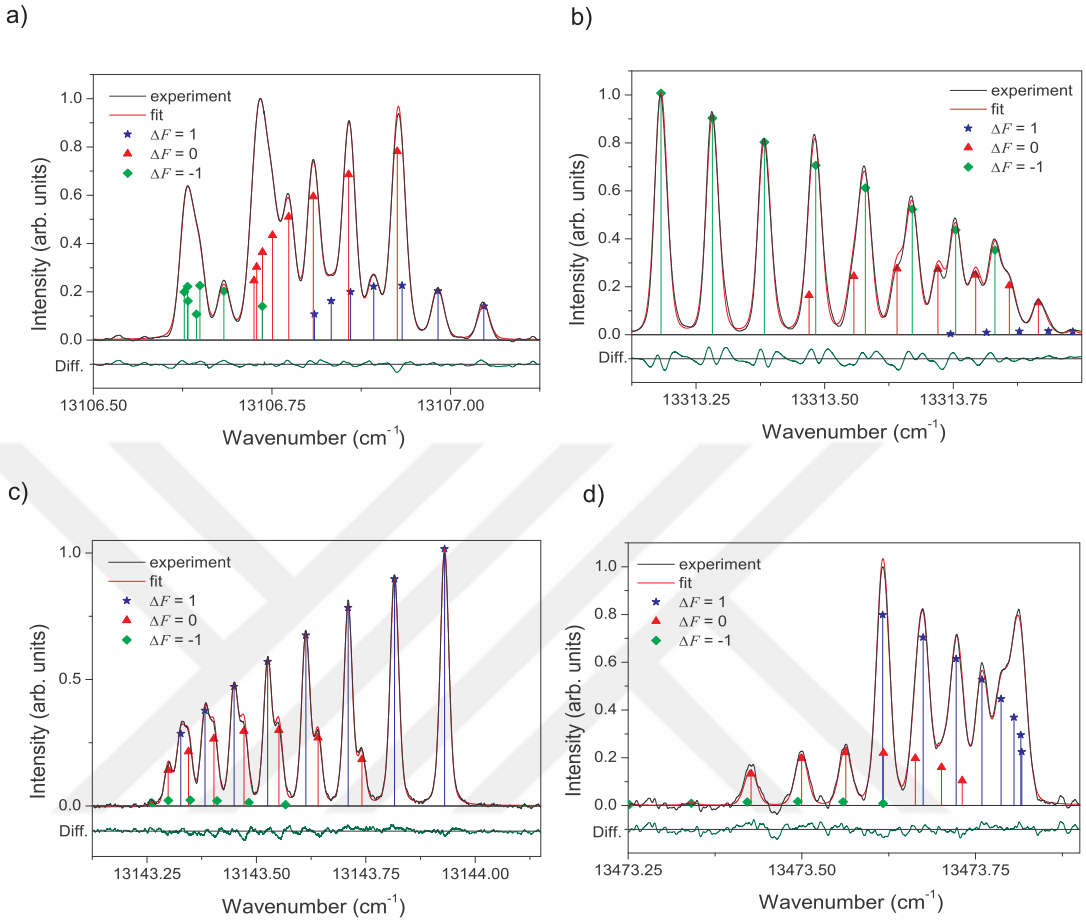


Figure 3.7 : Measured spectral lines in the discovery of the energy level E_{upper}= 31964.93(0.03) cm^{-1}, J= 13/2 (o), with the monochromator fixed at λ_F= 662.831 nm.
a) line at σ= 13106.73 cm^{-1} (λ= 762.757 nm), E_{lower}= 18858.19 cm^{-1}, J=13/2, (e) $\longrightarrow E_{upper}$
b) line at σ= 13313.47 cm^{-1} (λ= 750.912 nm), E_{lower}= 18651.53 cm^{-1}, J=15/2, (e) $\longrightarrow E_{upper}$
c) line at σ= 13143.66 cm^{-1} (λ= 760.614 nm, E_{lower}= 18821.25 cm^{-1}, J=11/2, (e) $\longrightarrow E_{upper}$
d) line at σ= 13473.71 cm^{-1} (λ= 741.982 nm), E_{lower}= 18491.21 cm^{-1}, J=11/2, (e) $\longrightarrow E_{upper}$

Among the many calculated lines from the newly discovered energy level, only the hfs spectra of the lines at λ= 762.757 nm, λ= 760.614 nm, and λ= 741.982 nm could be measured. The line at λ= 741.982 nm was measured after the mirror setup was changed to cover the second laser region, the wavelength range between 690 nm and 780 nm. The weighted mean value of the new energy level and the corresponding hfs constants from all four measured lines were found as:

E_{upper} **= 31964.93(0.03) cm^{-1},** J**= 13/2 (o),** A**=594.4(0.5),** B**= -849(28)**.

Fig.3.7 shows the experimental LIF spectra and the analyzed hfs best-fit curve superposed of the four spectral lines that were used to discover the new energy level. The residuals between the experiment and the fit are given in the lower parts of each spectrum in the hfs analysis.

3.1.2 Method 2: Using systematic OG scans

In this method, an OG scan was performed with 20 GHz scan widths in the laser wavelength range to search for undefined lines. The wavelength of the laser is then adjusted and fixed at the wavelength of the most intense and undisturbed peak observed in the measured OG spectrum, or to the extra maxima observed within the OG spectrum, which do not belong to the line under investigation.

The monochromator was then scanned in the 400- 650 nm range in 50 nm steps and spectra with fluorescence lines were recorded. From here on, the same steps as in the FT observed lines guided methods are applied.

Discovery of E**= 40077.35(0.08) cm^{-1} using Method 2**

The discovery of the energy level E= 40077.35 cm^{-1} is an example of how energy levels are found using Method 2, by performing systematic OG scans within our laser wavelength range. Therefore, the discovery of other energy levels using the same method will not be presented in further detail for each energy level; only the results will be given. In the systematic search with OGS for undefined lines, an OG scan in the laser wavelength range with scan widths of 20 GHz was performed, as shown in Fig.3.8.

The laser wavelength was adjusted and fixed at the wavelength of the most intense and undisturbed peak observed in the measured OG spectrum, which in this case was the peak at λ_{air}= 798.464 nm (σ= 12520.61 cm^{-1}) as pointed out in Fig.3.10.

The monochromator was then scanned in the 400- 650 nm range in 50 nm steps and spectra with fluorescence lines were recorded. From the monochromator scan, a negative phase fluorescence line was recorded at λ_F^- = 592.900 nm. From here on, the same steps as in the FT observed lines guided methods were applied. The

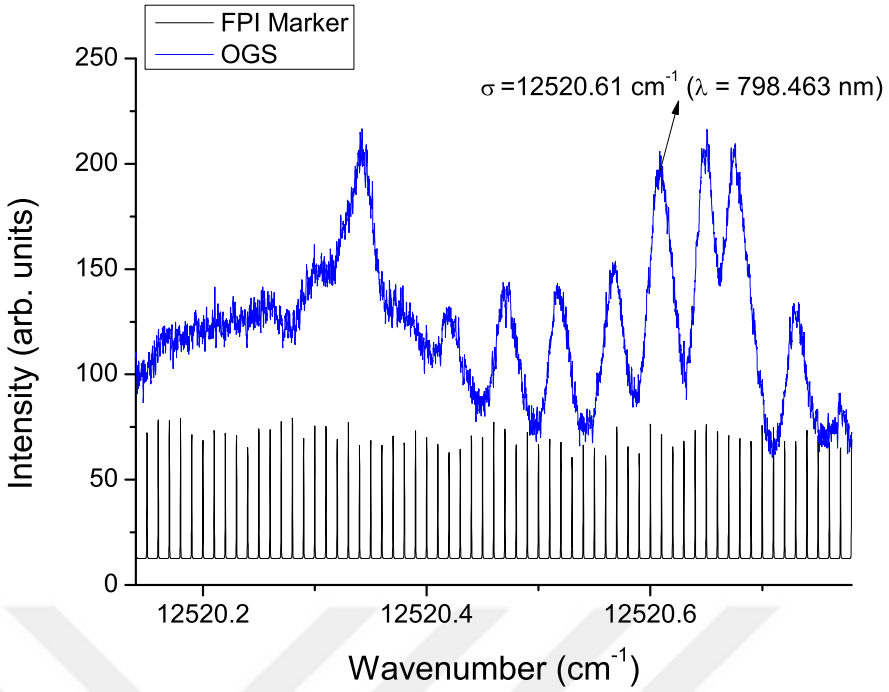


Figure 3.8 : Illustration of a 20 GHz OG scan in the search for an undefined spectral line.

measured fluorescence line λ_F^-= 592.900 nm was searched in the FT spectrum, and it was observed that it had a wavelength of λ_F= 592.915 nm as shown in Fig.3.9 and was defined in [19].

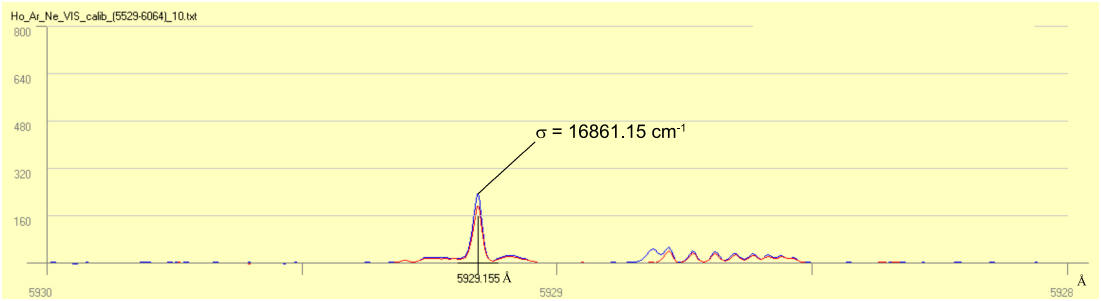


Figure 3.9 : The FT observed spectrum at λ_F^-= 592.900 nm of the measured fluorescence line λ_F= 592.915 nm (σ=16861.15 cm^{-1}).

The line at λ_F^-= 592.915 nm occurs from the transition between the following energy levels. E_{upper}= 27556.90 cm^{-1} J=9/2 (e) $\rightarrow$ E_{lower}= 10695.75 cm^{-1} J=9/2 (o). From the observed negative fluorescence line λ_F^-= 592.915 nm, we can conclude that E = 27556.90 cm^{-1}, J=9/2, (e) corresponds to the lower energy level of the laser excitation line λ_{air}= 798.464 nm.

The LIF spectrum of the laser line at λ_{air}= 798.468 nm was measured with the monochromator set to the fluorescence line at λ_F^-= 592.915 nm as shown in Fig.3.10.

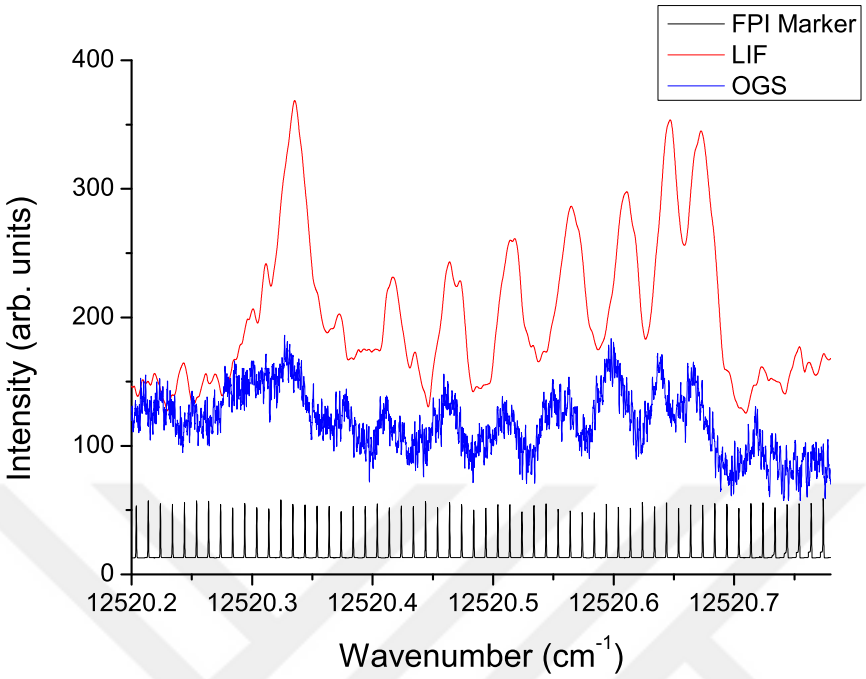


Figure 3.10 : Simultaneously measured LIF and OGS spectra of λ_{air}= 798.464 nm line with the monochromator set to the fluorescence line at λ_F^-= 592.915 nm. This OGS scan was recorded on a different day, resulting in a noisy spectrum when compared with the scan in Fig.3.8.

Hfs analysis of the LIF spectrum of the laser line was performed with the Fitter program [64]. During this fit, the values of the hyperfine structure constants A and B of the lower energy level (E_{lower}= 27556.90 cm^{-1} J=9/2 (e)) were fixed at the value given in the literature [19]. In this case, the J values that comply with the transition rules of the upper energy level can be 7/2, 9/2, and 11/2. The spectrum was fitted with each J value. Among these possible J values, the spectrum could only be fitted with J=11/2. The theoretical and experimental LIF spectrum of the line λ_{air}= 798.464 nm is shown in Fig.3.11. From the fit, the center of gravity (cog), the value of J, its parity, and the hfs constants A and B of the laser line are obtained. As a result, it was seen that for the upper energy level the obtained values were in good agreement with the experimental spectrum, as can be seen in Fig.3.11.

The new upper energy level can be found by simply adding the energy level value of the lower level and the laser line as follows:

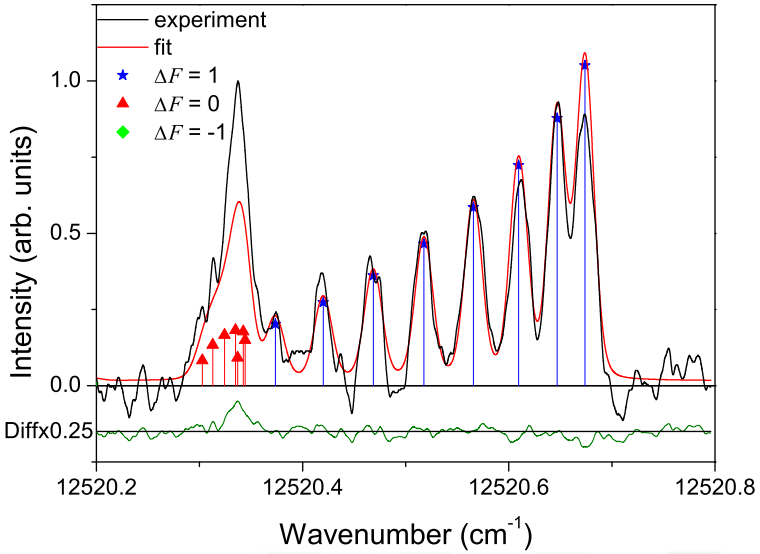


Figure 3.11 : Experimental LIF spectrum of the line at λ_{air}=798.468 nm (σ= 12520.54 cm^{-1}) measured with the monochromator set at λ_F^-= 592.915 nm with the best-fit curve superposed.

E_{upper}= σ+E_{lower}= 12520.53 cm^{-1} + 27556.90 cm^{-1}= 40077.43 cm^{-1}

For precision, the line at σ= 12520.54 cm^{-1}(or λ= 798.468 nm) is measured at least five times. Likewise, for each LIF measurement, the hfs analysis is applied. From the statistical mean of the values obtained, the hfs constants of the energy level are found as: E_{upper}= 40077.43 cm^{-1}, J=11/2 (o), A=1143.9 (0.6), B= -645 (21).

To increase the precision of the newly found energy level, the energy level value with its J value, parity, and hfs constants, A and B, is also saved for this method to the "level" file, which is the input file of the "Elemente" program [60,61] to calculate all possible lines arising from the new energy level. Among the possible lines calculated, the lines that could be measured with the LIFS method were at λ_{air}= 803.824 nm, 772.815 nm and 761.405 nm. All three lines could be measured with the same positive fluorescence line at λ_F=683.629 nm, which could also be observed in the FT spectrum as shown in Fig.3.12

The weighted mean value of the new energy level and the corresponding hfs constants from all four measured lines were found as:

E_{upper}= 40077.35 (0.08) cm^{-1}, J= 11/2 (o), A= 51143.8(0.5), B= -635(10).

Fig.3.13 shows the experimental LIF spectrum and the analyzed hfs best-fit curve

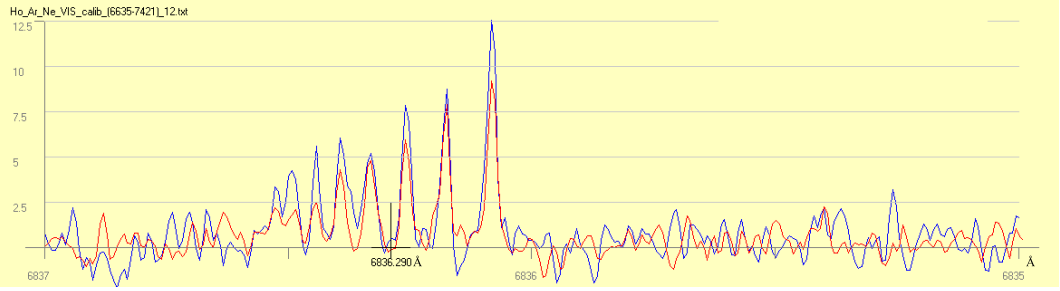


Figure 3.12 : FT spectrum observed positive fluorescence line at λ_F=683.629 nm arising from the transition of the new discovered energy level E_{upper}= 40077.43 cm^{-1}.

superposed of all four spectral lines that were used to discover the new energy level. The residuals between the experiment and the fit are given in the lower parts of each spectrum in the hfs analysis.

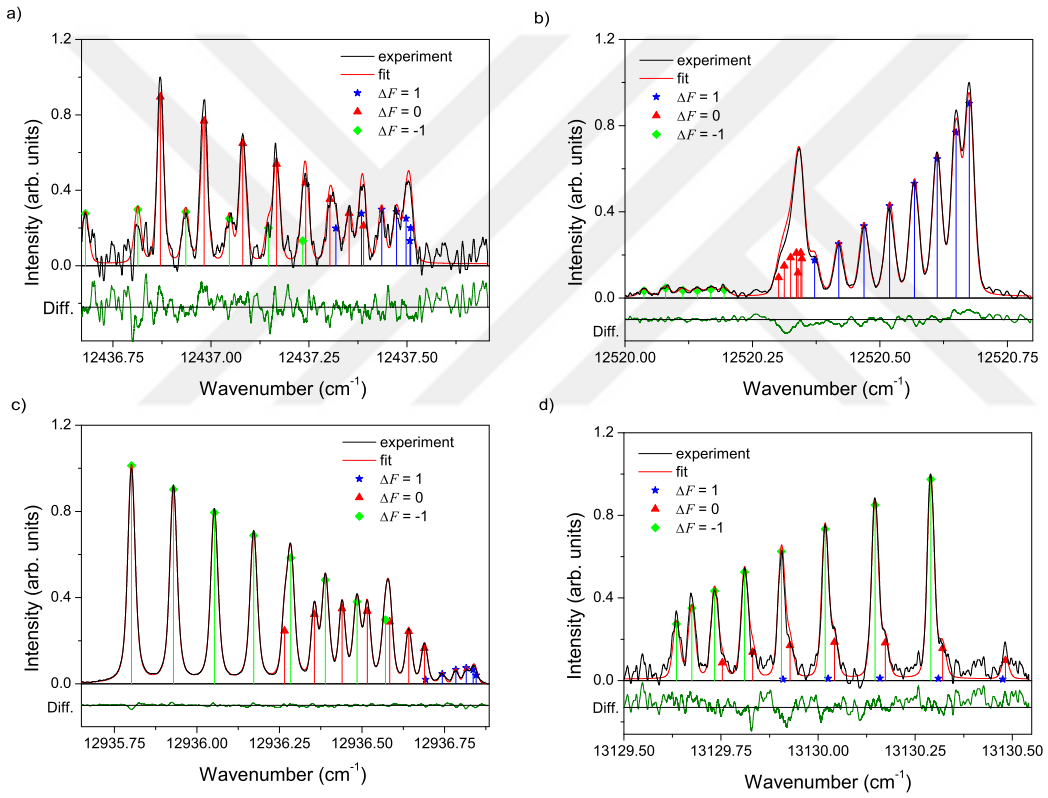


Figure 3.13 : Measured spectral lines in the discovery of the energy level E_{upper} = 40077.35 (0.08) cm^{-1}, J= 11/2 (o), with the monochromator fixed at λ_F=683.629 nm.
a) line at σ= 12437.11 cm^{-1} (λ= 803.824 nm), E_{lower}= 27640.05 cm^{-1}, J=11/2, (e) $\longrightarrow E_{upper}$
b) line at σ= 12520.54 cm^{-1} (λ= 798.468 nm), E_{lower}= 27556.90 cm^{-1}, J=9/2, (e) $\longrightarrow E_{upper}$
c) line at σ= 12936.16 cm^{-1} (λ= 772.815 nm), E_{lower}= 27141.28 cm^{-1}, J=13/2, (e) $\longrightarrow E_{upper}$
d) line at σ= 13130.00 cm^{-1} (λ= 761.405 nm), E_{lower}= 26947.33 cm^{-1}, J=13/2, (e) $\longrightarrow E_{upper}$

Brief note: Another starting point stated in Method 2 was the extra peaks observed in the measured OG spectrum. Since I was confronted with an example of this case during the measurements in search of the new energy level E_{upper}= 40077.43 cm^{-1},

it seemed appropriate to mention it. As already mentioned, the LIF and OG spectroscopic methods were used simultaneously. While measuring the laser line at σ= 12520.54 cm^{-1}(or λ= 798.468 nm), an extra peak was observed in the OG spectrum but not in the LIF spectrum, which means that it belongs to another possible undefined line. The extra peak in Fig.3.14 is highlighted with a green ellipse to clarify this point. This extra peak can be used as a starting point, which may also lead to an undefined line and, consequently, to an undiscovered fine structure energy level. For this example, the starting point with the extra peak did not lead to an undefined spectral line.

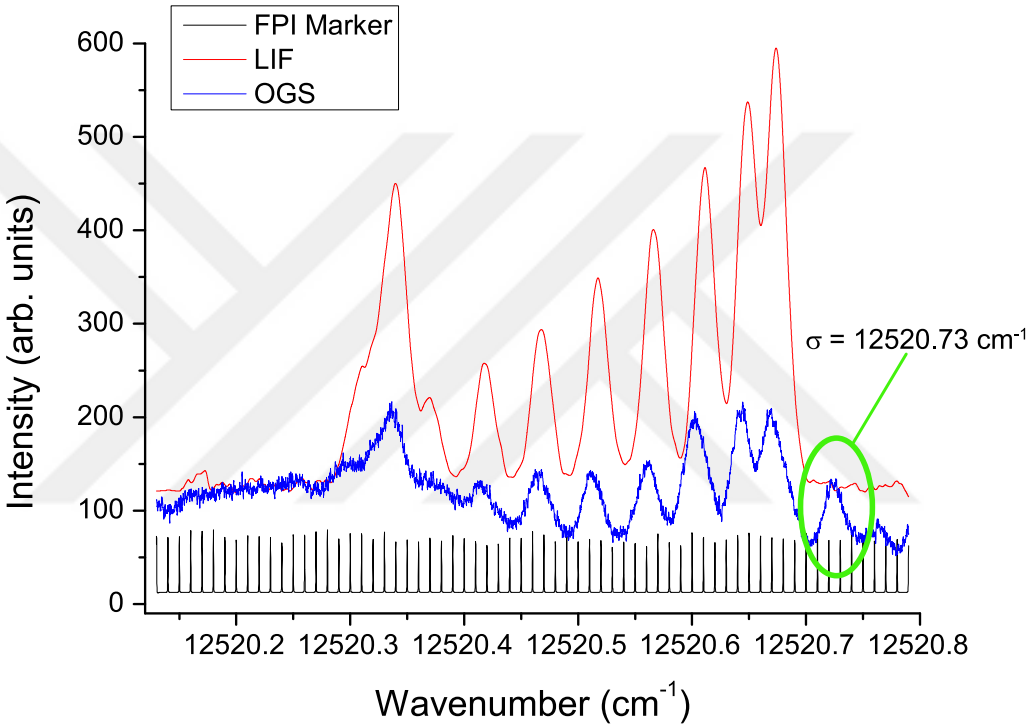


Figure 3.14 : Simultaneously measured LIF and OGS spectra of λ_{air}= 798.468 nm line with the monochromator set to the fluorescence line at λ_F= 683.629 nm. The highlighted extra peak observed in the OG spectrum at σ= 12520.73 cm^{-1} indicates a possible new starting point in the search for a new fine structure energy level.

So far, we have explained how to find new energy levels if the negative fluorescence line of the laser excitation line is defined. The discovery of energy levels in the presence of only positive fluorescence lines with undefined energy levels of the laser excitation line should be outlined. First, the spectral line was measured with the LIFS method with the monochromator fixed to the positive fluorescence line. Then, the fit process on the measured spectral line is performed by manually entering and altering

the estimated values of the J, A, and B of the upper and lower energy levels in the Hfs analysis program [64] until a good overlap is achieved with the experimental and theoretical spectra. The values obtained from the fit procedure are compared with the energy levels available in the literature. If a level corresponding to the lower or upper energy level (and their associated J, A, and B values) is found to overlap with the laser line, the unknown energy level can be determined from the laser line. However, the analysis process does not always yield good results in poorly resolved spectra, and determining the energy level is unsuccessful in such cases.

3.1.3 Discovered energy levels

The methods used to discover other energy levels will not be described hereafter; only the spectral lines measured with the LIFS method, along with the associated fluorescence lines, will be given under each discovered energy level heading. The list of spectral lines measured with the LIFS method for the discovery of new energy levels is given in Table 3.3. The energy levels discovered using Methods 1 and Method 2 are listed in order of discovery, i.e., the energy levels found in the first laser region are listed before the second laser region.

Level E= 36859.56(0.03) cm^{-1}

The FT-observed spectral line λ= 774.177 nm was undefined with unknown upper and lower energy levels. Fluorescence lines were measured with a monochromator scan with a fixed laser wavelength, as described in both methods. From the scan, only positive fluorescence lines were recorded, which led to the hfs analysis method for the discovery.

An Hfs analysis was performed on the measured LIF spectra of the spectral line λ= 774.177 nm. Fig.3.15 a) shows the theoretical and experimental overlapped spectra of the spectral line at σ= 12913.39 cm^{-1} (λ= 774.177 nm). From the hfs analysis performed, the J values and the hfs constants A and B, of the lower and upper energy levels were determined and searched within the energy level list of the literature for a match. From the search, a match was found with the lower energy level. By adding the energy value of the excitation line, the upper energy level was roughly found.

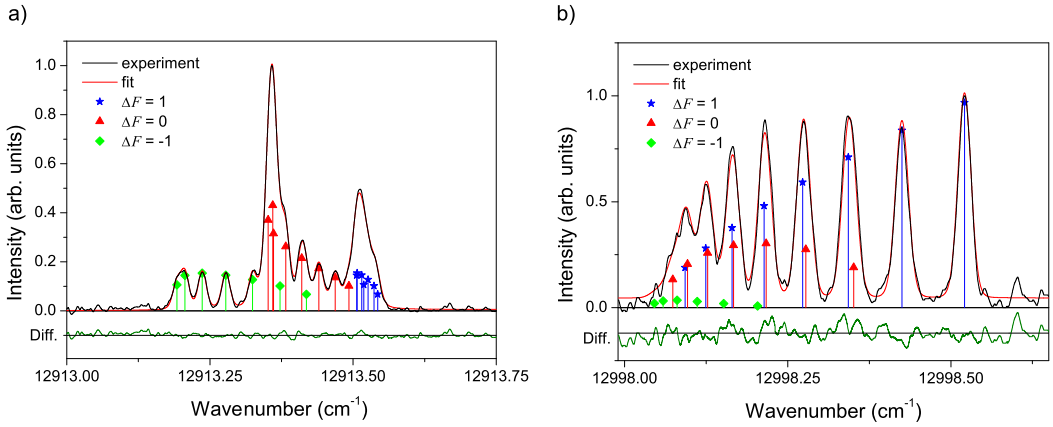


Figure 3.15 : Measured spectral lines (25 GHz) in the discovery of the energy level E_{upper} = 36859.56(0.03) cm^{-1}, J= 11/2 (o), with the monochromator fixed at λ_F=546.455 nm.
a) line at σ= 12913.39 cm^{-1} (λ= 774.177 nm), E_{lower}= 23946.16 cm^{-1}, J=11/2, (e) $\longrightarrow E_{upper}$
b) line at σ= 12998.32 cm^{-1} (λ= 769.119 nm), E_{lower}= 23861.17 cm^{-1}, J=9/2, (e) $\longrightarrow E_{upper}$

Using the Elements program, all possible theoretical spectral lines occurring from the discovered upper energy level of the laser transition are calculated. The LIFS method was applied with the laser set to one of the spectral lines, which was within our laser wavelength range. The measured and hfs analyzed spectral line at σ= 12998.32 cm^{-1} (λ= 769.119 nm) is shown in Fig.3.15 b). The value of the newly found energy level E= 36859.56(0.03) cm^{-1} was found with two spectral lines for precision, where each line was measured at least five times under the same conditions. The determined hfs constants of the discovered energy level are given in Table 3.1.

Level E= 40165.71(0.07) cm^{-1}

In the discovery of the energy level E= 40165.71(0.07) cm^{-1}, two spectral lines were measured with a 20 GHz scan using the LIFS method. The measured spectral lines involved in the discovery are shown in Fig.3.16. Spectral lines were measured with the monochromator fixed at different fluorescence wavelengths with different phases, as indicated in the caption of the figure. Hfs constants determined from both spectral lines are given in Table 3.1.

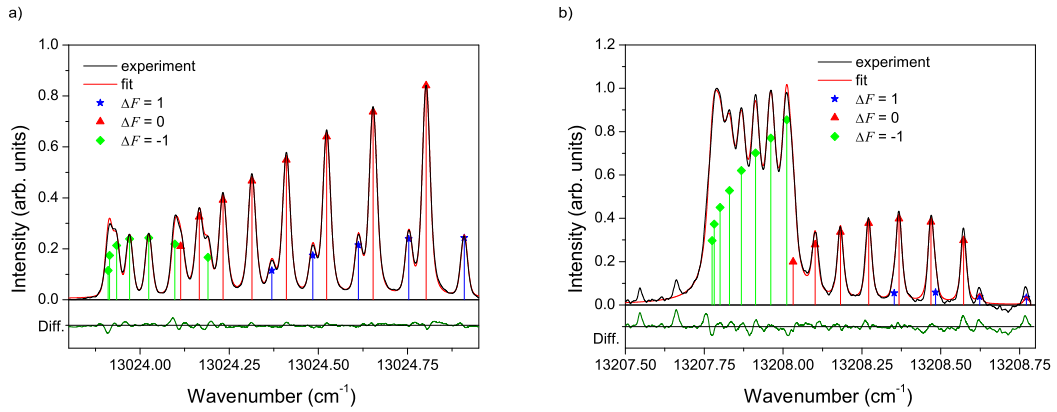


Figure 3.16 : Measured spectral lines in the discovery of the energy level E_{upper} = 40165.71(0.07) cm^{-1}, J= 13/2 (o), with the monochromator fixed at λ_F=684.995 nm and λ_F^-=464.165 nm, shown respectively in a) and b).
a) line at σ= 13024.48 cm^{-1} (λ= 767.574 nm), E_{lower}= 27141.28 cm^{-1}, J=13/2, (e) $\longrightarrow$ E_{upper}
b) line at σ= 13207.93 cm^{-1} (λ= 756.912 nm), E_{lower}= 26957.70 cm^{-1}, J=15/2, (e) $\longrightarrow$ E_{upper}

Level E= 39653.44(0.04) cm^{-1}

Spectral lines originating from undefined energy levels were measured using the LIFS method with a 30 GHz laser scan. The measured spectral lines involved in the discovery are shown and detailed in the caption. In the figure, the hfs spectra analyzed, labeled 'fit', and the LIFS method measured spectra, labeled 'experimental', are overlapped. The residual difference between the two spectra is shown graphically below the fitted and experimental spectra of each line. A and B of the newly discovered energy level are determined by performing hfs analysis on each spectrum of the repeated measurement of each spectral line for precision and are given in Table 3.1.

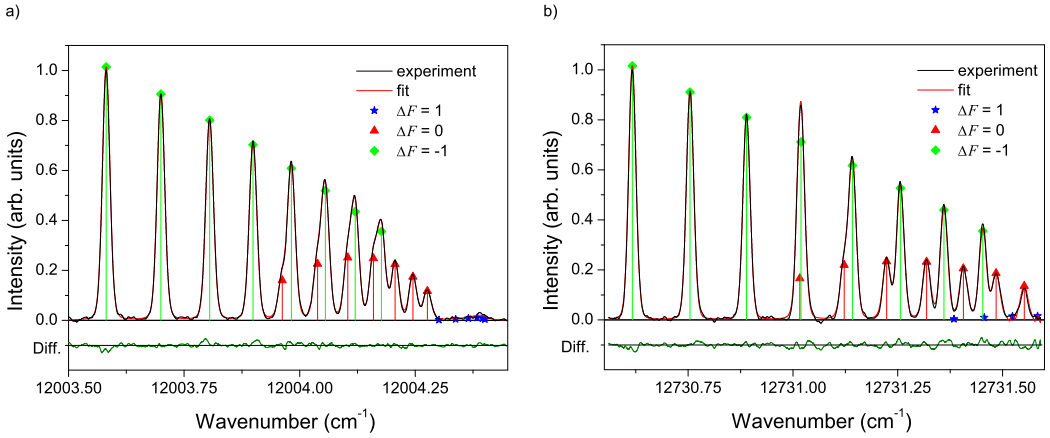


Figure 3.17 : Measured spectral lines in the discovery of the energy level E_{upper} = 39653.44(0.04) cm^{-1}, J= 13/2 (e), with the monochromator fixed at λ_F=480.962 nm.
a) line at σ= 12003.87 cm^{-1} (λ= 832.836 nm), E_{lower}= 27649.51 cm^{-1}, J=15/2, (o) $\longrightarrow$ E_{upper}
b) line at σ= 12730.98 cm^{-1} (λ= 756.912 nm), E_{lower}= 26922.40 cm^{-1}, J=15/2, (o) $\longrightarrow$ E_{upper}

Level E= 42407.40(0.10) cm^{-1} The spectral lines shown in Fig.3.18 contributed to the discovery of the energy level E= 42407.40(0.1) cm^{-1}. Both spectral lines were measured with the LIFS method with a 35 GHz scan. During measurements, the monochromator was fixed at different fluorescence wavelengths for each spectral line, with positive and negative phases, as indicated in the figure caption. A and B constants determined from the hfs analysis of the discovered energy level are given in Table 3.1.

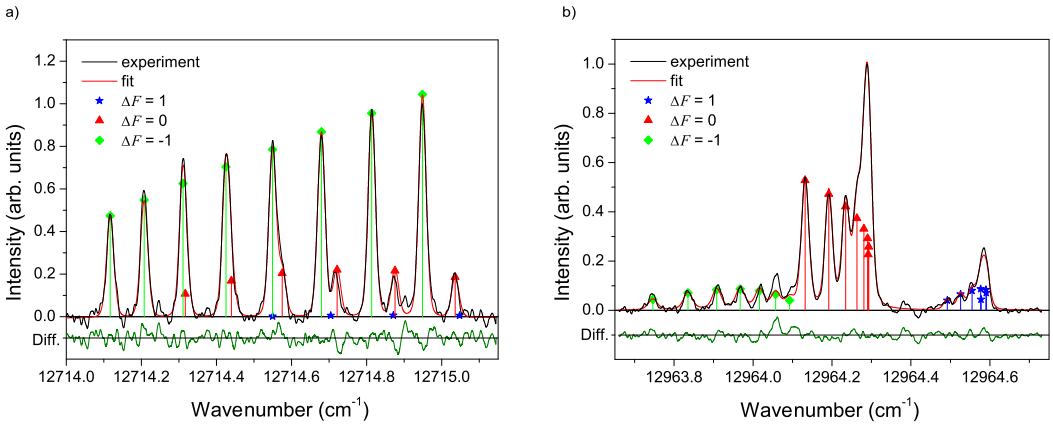


Figure 3.18 : Measured spectral lines in the discovery of the energy level E_{upper} = 42407.40(0.1) cm^{-1}, J= 17/2 (e), with the monochromator fixed at λ_F^-=555.311 nm for line a) and λ_F=475.406 nm for line b).
a) line at σ= 12714.58 cm^{-1} (λ= 786.282 nm), E_{lower}= 29692.67 cm^{-1}, J=19/2, (o) $\longrightarrow$ E_{upper}
b) line at σ= 12964.23 cm^{-1} (λ= 771.141 nm), E_{lower}= 29443.09 cm^{-1}, J=17/2, (o) $\longrightarrow$ E_{upper}

Level E= 36954.20(0.04) cm^{-1}

The energy level E= 36954.20(0.04) cm^{-1} was discovered with the spectral line, which was approximately 40 GHz broad, thus was measured with the LIFS method in two parts as shown in Fig.3.19 a) and b) with the monochromator fixed at a positive fluorescence line as indicated in the caption. Fig.3.19 c) shows the visually combined spectra for illustration. Hfs analysis was performed on each of the measured spectra shown in a) and b). The determined hfs constants are given in Table 3.1.

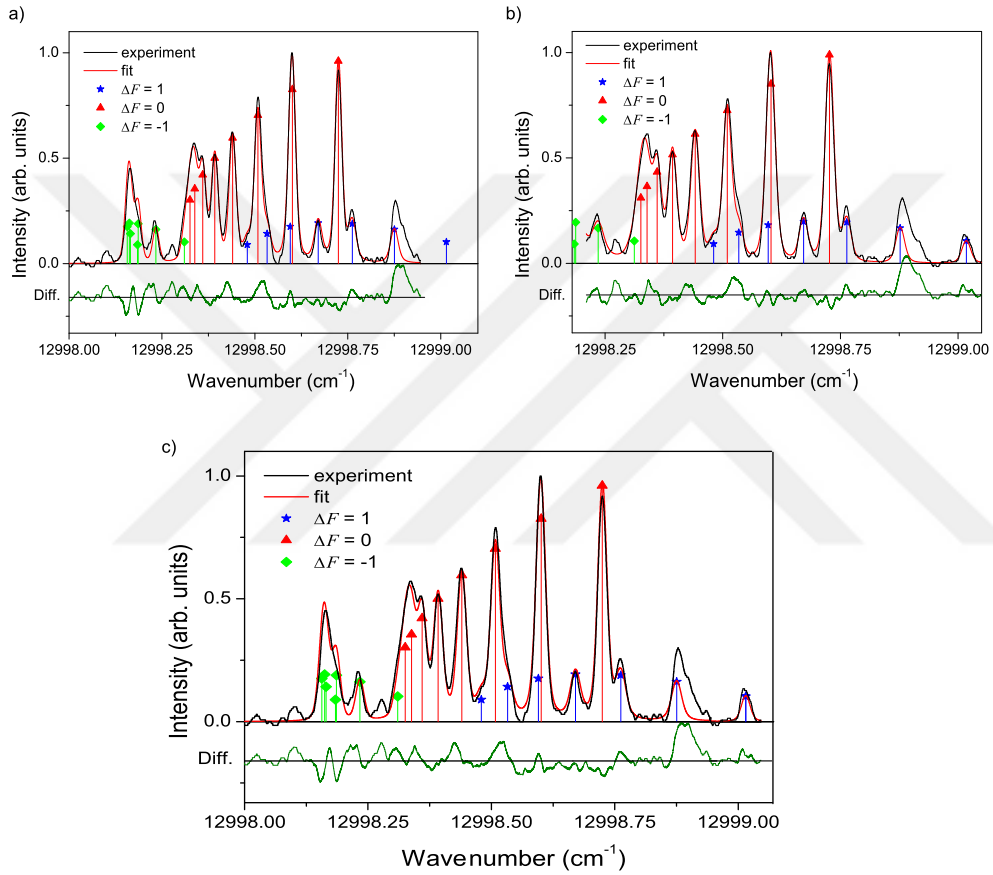


Figure 3.19 : Measured spectral line in the discovery of the energy level E_{upper} = 36954.20(0.04) cm^{-1}, J= 13/2 (o), with the monochromator fixed at λ_F=406.139 nm. c) shows the visually combined line spectrum of measured spectra a) and b) at σ= 12998.50 cm^{-1} (λ= 769.108 nm), E_{lower}= 23955.68 cm^{-1}, J=13/2, (e) $\longrightarrow$ E_{upper}

Level E= 42337.80(0.07) cm^{-1}

Three spectral lines contributed to the discovery of the energy level E= 42337.80(0.07) cm^{-1} as shown in Fig.3.20.

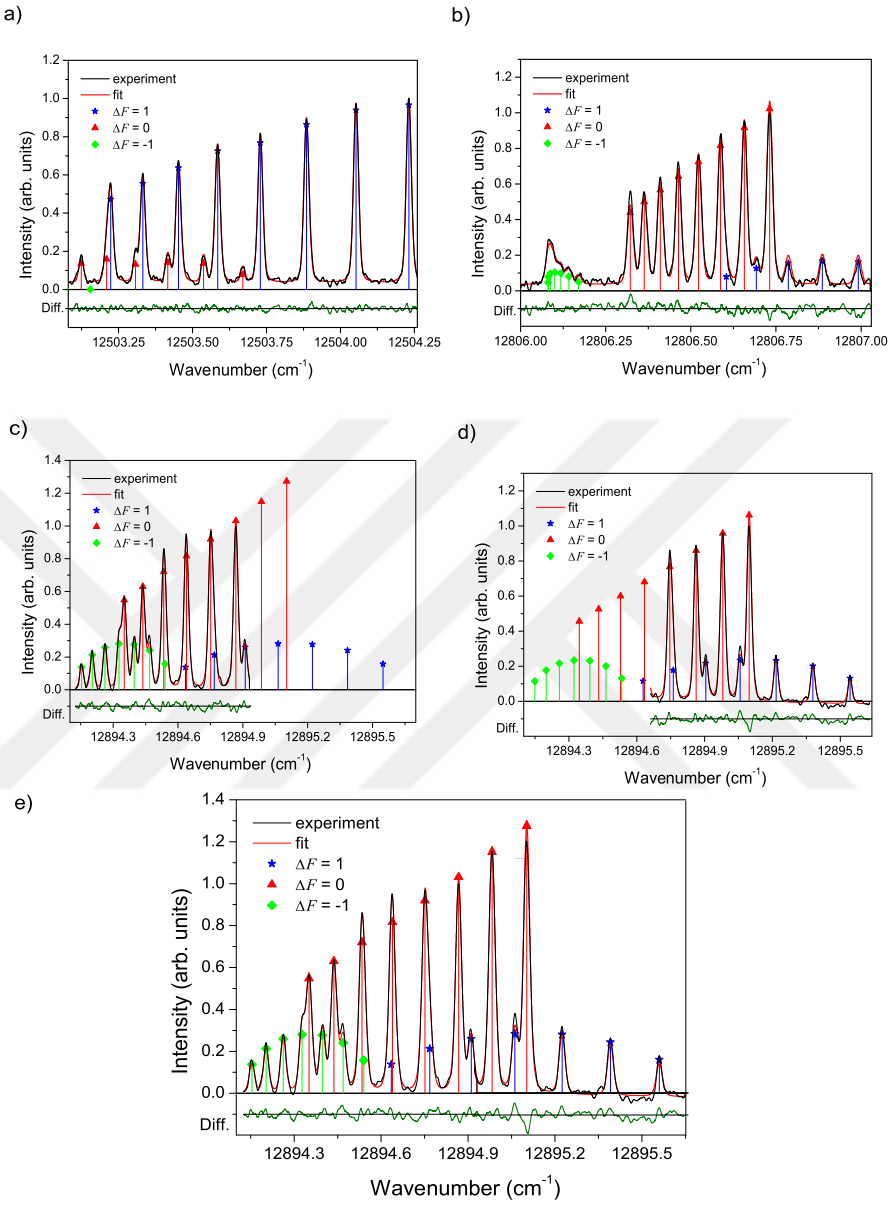


Figure 3.20 : Measured spectral lines in the discovery of the energy level E_{upper} = 42337.80(0.07) cm^{-1}, J= 17/2 (e), with the monochromator fixed at λ_F=548.617 nm for lines a) and b) and λ_F^-=475.695 nm for line e). e) shows the visually combined measured spectra of c) and d).
a) line at σ= 12503.75 cm^{-1} (λ= 799.540 nm), E_{lower}= 29834.05 cm^{-1}, J=15/2, (o) $\longrightarrow E_{upper}$
b) line at σ= 12806.54 cm^{-1} (λ= 780.636 nm), E_{lower}= 29531.25 cm^{-1}, J=17/2, (o) $\longrightarrow E_{upper}$
e) line at σ= 12894.77 cm^{-1} (λ= 775.295 nm), E_{lower}= 29443.09 cm^{-1}, J=17/2, (o) $\longrightarrow E_{upper}$

Lines were measured with the LIFS method with a 30 GHz Laser scan. The spectral line at σ= 12894.77 cm^{-1} (λ= 775.295 nm) exceeded our scan range and was therefore measured in two parts. The combined spectrum of the line is shown in Fig.3.20 e). The monochromator was fixed at positive and negative fluorescence lines for the measured spectral lines, which are indicated in the caption of the figure. The hfs analysis was performed for the repeated measurements of the three spectral lines, increasing the accuracy of the hfs constants of the discovered energy level. The hfs constants, A and B, resulting from the analysis of all three spectral lines are given in Table 3.1.

Level E= 27113.28(0.02) cm^{-1}

The spectral line shown in Fig.3.21 occurs from the newly discovered upper energy level E_{upper}= 40077.35 cm^{-1} of the laser transition, with an unknown lower level. The upper level was discovered in the first wavelength range of the laser, while the lower energy level E= 27113.28(0.02) cm^{-1} of the laser transition could be discovered after the mirror setup was changed to cover the second wavelength region. The undefined spectral line was measured with the LIFS method with a 25 GHz scan. Hfs constants were determined from the hfs analysis performed on each repeated measurement, as given in Table 3.1.

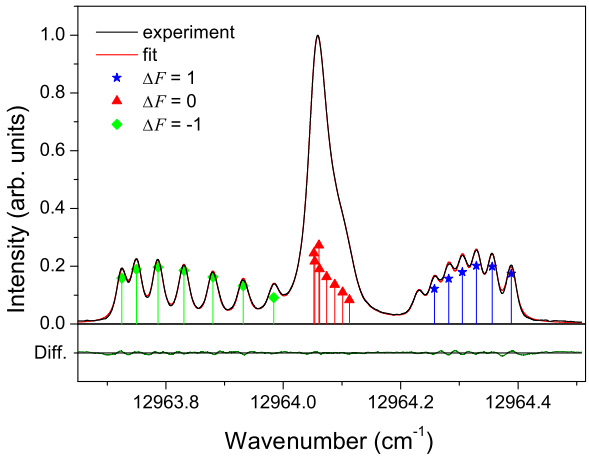


Figure 3.21 : Measured spectral line in the discovery of the energy level E_{lower}= 27113.28(0.02) cm^{-1}, J= 11/2 (e), with the monochromator fixed at λ_F=683.629 nm.
line at σ= 12964.07 cm^{-1} (λ= 771.151 nm), E_{upper}= 40077.35 cm^{-1}, J=11/2, (o) $\longrightarrow$ E_{lower}

Level E= 31062.22(0.02) cm^{-1}

The energy level E= 31062.22(0.02) cm^{-1} was determined with the LIFS method, measured spectral line as shown in Fig.3.22 with the monochromator fixed to the negative fluorescence line indicated in the caption. The spectrum of the spectral line was measured with a 25 GHz laser scan. Hfs constants of the discovered energy level resulting from the weighted mean of the hfs analysis performed for each repeated measured spectra are given in Table 3.1.

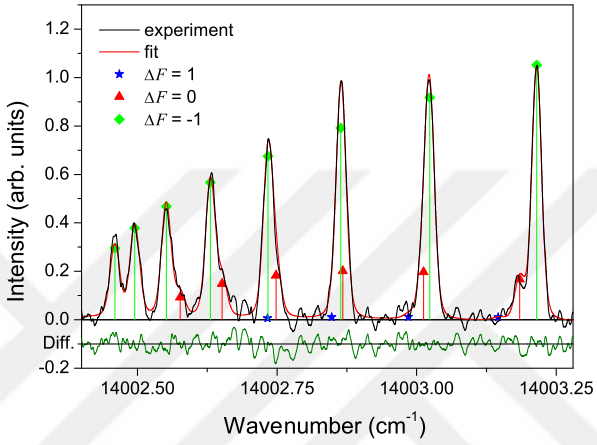


Figure 3.22 : Measured spectral line in the discovery of the energy level E_{upper}= 31062.22(0.02) cm^{-1}, J= 11/2 (o), with the monochromator fixed at λ_F^-=586.026 nm.
line at σ= 14002.85 cm^{-1} (λ= 713.943 nm), E_{lower}= 17059.35 cm^{-1}, J=13/2, (e) $\longrightarrow$ E_{upper}

Level E= 32663.47(0.04) cm^{-1}

The spectral line shown in Fig.3.23 c) contributed to the discovery of the energy level E= 32663.47(0.04) cm^{-1}. The spectral line at σ= 13842.15 cm^{-1} (λ= 722.232 nm) was wider than our scan range; therefore, it was measured in two parts as shown in Fig.3.23 a) and b). c) illustrates the combined spectrum of the spectral line occurring from the discovered energy level. The determined hfs constants are given in Table 3.1.

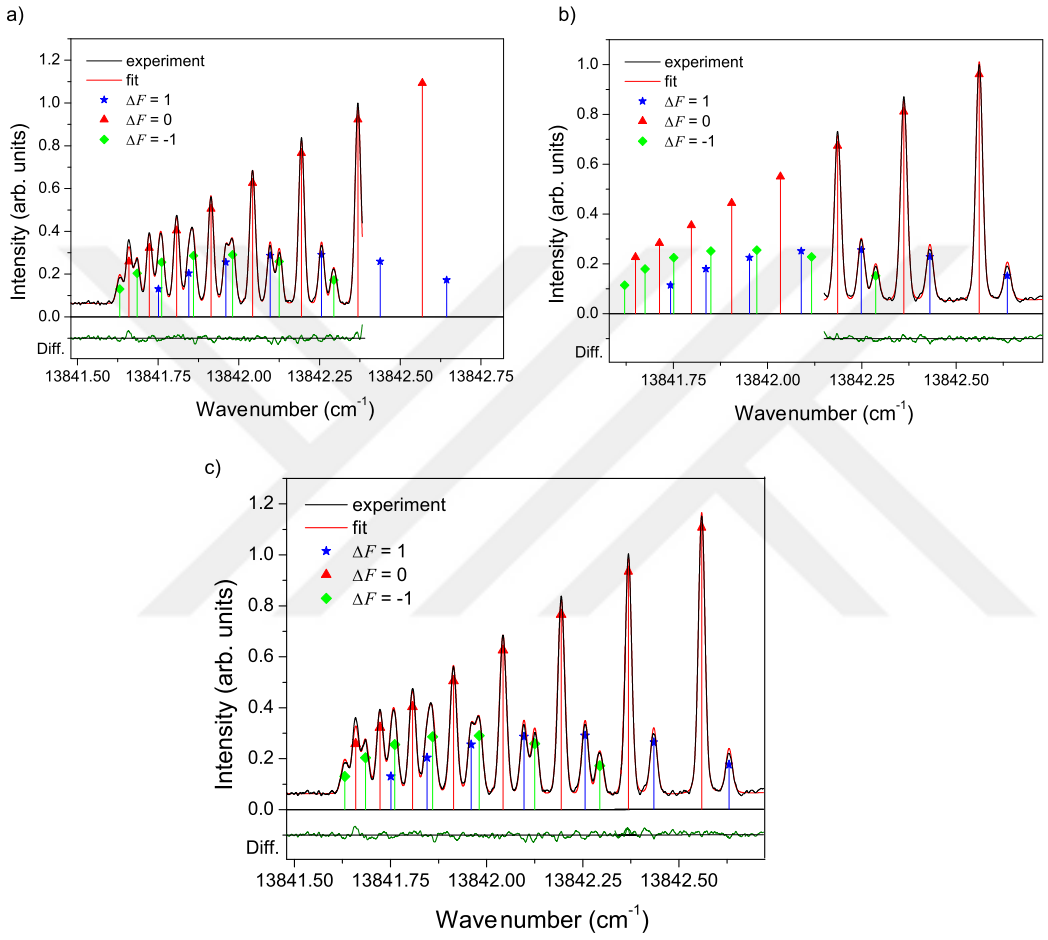


Figure 3.23 : Measured spectral line in the discovery of the energy level E_{upper} = 32663.47(0.04) cm^{-1}, J= 11/2 (o), with the monochromator fixed at λ_F=492.015 nm.
c) shows the visually combined line spectrum of the measured spectra a) and b).
c) line at σ= 13842.15 cm^{-1} (λ= 722.232 nm), E_{lower}= 18821.25 cm^{-1}, J=11/2, (e) $\longrightarrow$ E_{upper}

Level E= 37774.72(0.05) cm^{-1}

The discovery of the energy level E= 37774.72(0.05) cm^{-1} was found from the undefined spectral line shown in Fig.3.24. The line was measured with a 30 GHz laser scan and the spectrometer fixed at the negative fluorescence line as indicated in the caption of the figure. Hfs constants resulting from the hfs analysis performed are given in Table 3.1.

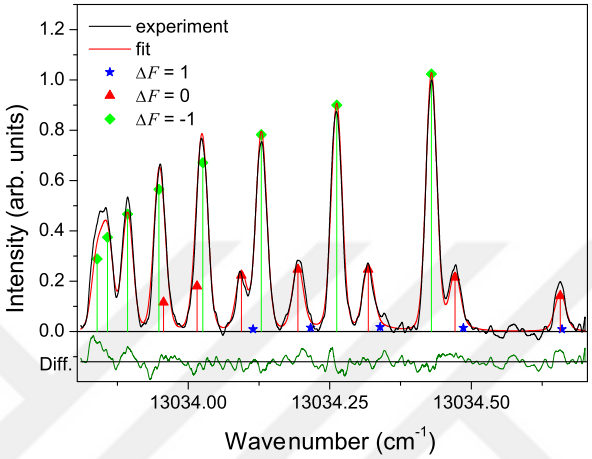


Figure 3.24 : Measured spectral line in the discovery of the energy level E_{upper} = 37774.72(0.05) cm^{-1}, J= 11/2 (o), with the monochromator fixed at λ_F^-=404.081 nm): Line at σ= 13034.14 cm^{-1} (λ = 786.282 nm), E_{lower}= 24740.52 cm^{-1}, J=13/2, (e) $-\!\!\rightarrow E_{upper}$

Level E= 37776.32(0.04) cm^{-1}

Spectral lines contributing to the discovery of the energy level E= 37776.32(0.04) cm^{-1} are shown in Fig.3.25. Both spectral lines are measured with a 25 GHz spectrometer fixed at a negative fluorescence line, as indicated in the caption. Hfs analysis on both spectral lines allowed for the precise determination of the hfs constants of the discovered energy level. The determined A and B constants are given in Table 3.1.

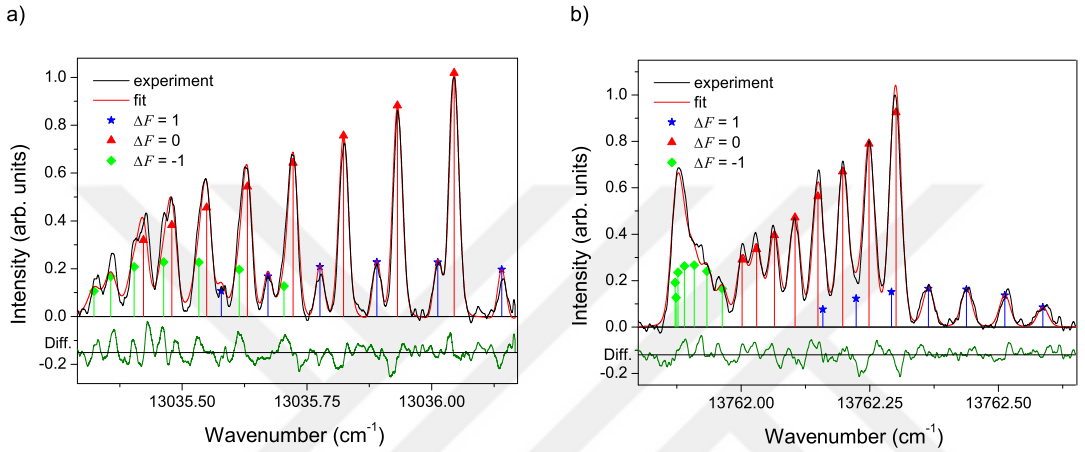


Figure 3.25 : Measured spectral lines in the discovery of the energy level E_{upper} = 37776.32(0.04) cm^{-1}, J= 13/2 (o), with the monochromator fixed at λ_F^-=404.081 nm for line a) and λ_F^-=416.300 nm for line b).
a) line at σ= 13035.77 cm^{-1} (λ= 766.099 nm), E_{lower}= 24740.52 cm^{-1}, J=13/2, (e) $\longrightarrow$ E_{upper}
b) line at σ= 13762.17 cm^{-1} (λ= 726.429 nm), E_{lower}= 24014.22 cm^{-1}, J=13/2, (e) $\longrightarrow$ E_{upper}

Level E= 38048.24(0.03) cm^{-1} The discovery of the energy level E= 38048.24(0.03) cm^{-1} was achieved with the measured spectral line shown in Fig.3.26. The line was measured with the LIFS method with a 20 GHz scan with the monochromator set to the negative and positive fluorescence lines that occur from the lower and upper energy levels of the excitation line, respectively, as indicated in the caption of the figure. From the hfs analysis performed, the constants A and B were determined and given in Table 3.1.

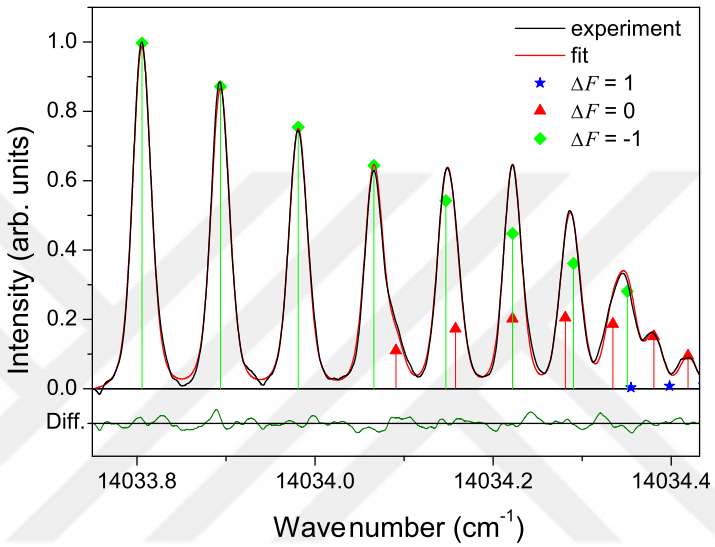


Figure 3.26 : Measured spectral line in the discovery of the energy level E_{upper} = 38048.24(0.03) cm^{-1}, J= 11/2 (o), with the monochromator fixed separately at λ_F^-=416.303 nm and λ_F=476.309 nm, where both gave the same hfs.
line at σ= 14034.05 cm^{-1} (λ= 712.356 nm), E_{lower}= 24014.22 cm^{-1}, J=13/2, (e) $\longrightarrow$ E_{upper}

Level E= 38087.78(0.06) cm^{-1}

The energy level E= 38087.78(0.06) cm^{-1} was found by measuring the spectral line shown in Fig.3.27. The spectral line was measured with a 30 GHz laser scan with the monochromator set to negative fluorescence line, which occurs from the lower energy level of the laser excitation as indicated in the caption. Hfs constants are determined from the hfs analysis and are given in Table 3.1.

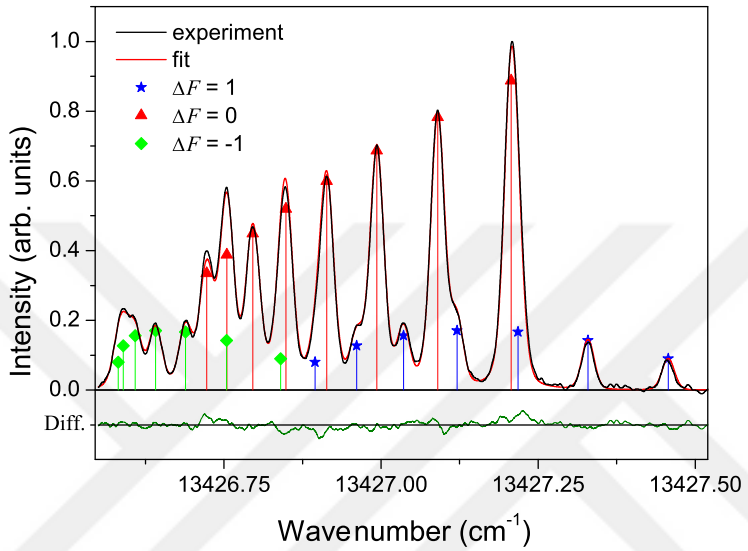


Figure 3.27 : Measured spectral line in the discovery of the energy level E_{upper} = 38087.78(0.06) cm^{-1}, J= 15/2 (o), with the monochromator fixed at λ_F^-=405.392 nm.
line at σ= 13426.96 cm^{-1} (λ= 744.565 nm), E_{lower}= 24660.80 cm^{-1}, J=15/2, (e) $\longrightarrow$ E_{upper}

Level E= 42770.41(0.04) cm^{-1}

Spectral lines contributing to the discovery of the energy level E= 42770.41(0.04) cm^{-1} are shown in Fig.3.28. The spectral line indicated with a) was measured with a 15 GHz and the line b) with a 25 GHz laser scan with the monochromator set to positive and negative fluorescence wavelengths, respectively, as indicated in the caption of the figure. From the hfs analysis performed on both spectral lines, the hfs constants were determined and given in Table 3.1.

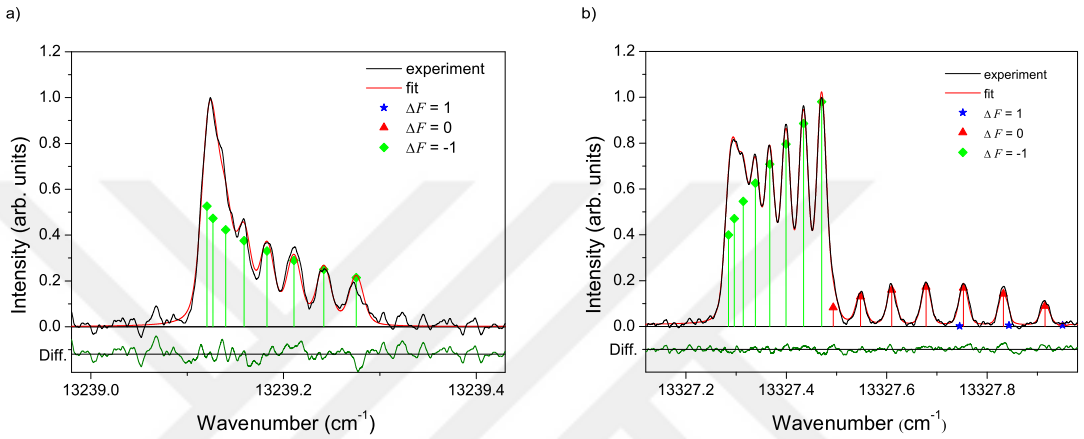


Figure 3.28 : Measured spectral lines in the discovery of the energy level E_{upper} = 42770.41(0.04) cm^{-1}, J= 15/2 (e), with the monochromator fixed at λ_F= 550.034 nm for line a) and λ_F^-=475.700 nm for line b).
a) line at σ= 13239.15 cm^{-1} (λ= 755.128 nm), E_{lower}= 29531.25 cm^{-1}, J=17/2, (o) $\longrightarrow$ E_{upper}
b) line at σ= 13327.37 cm^{-1} (λ= 750.129 nm), E_{lower}= 29443.09 cm^{-1}, J=17/2, (o) $\longrightarrow$ E_{upper}

Table 3.1 : New levels together with their hyperfine structure constants A and B (in MHz). Energy values and error bars resulting from the analysis of FT lines (see Table 3.5)

E (cm^{-1})	J	p	λ_{air} (nm)	A_{exp}	B_{exp}	A_{mean}	B_{mean}
27 113.28 (0.02)	11/2	e	771.151 f	1174.0 (1.3)	-2127 (16)		
31 062.22 (0.02)	11/2	o	713.943 f	1195.5 (0.9)	653 (48)		
31 964.93 (0.03)	13/2	o	760.614	594.8 (0.6)	-834 (36)	594.4 (0.5)	-849 (28)
			750.912 f	594.1 (0.6)	-883 (33)		
			741.982	593.6 (2.3)	-729 (80)		
			762.757	595.0 (2.1)	-847 (59)		
32 663.47 (0.04)	11/2	o	722.232	915.0 (2.0)	-77 (35)		
36 859.56 (0.03)	11/2	o	769.119 f	540 (5)	718 (310)	538 (4)	600 (120)
			774.177 f	535 (5)	580 (130)		
36 954.20 (0.04)	13/2	o	769.108 f	1205.8 (1.0)	1107 (21)		
37 774.72 (0.05)	11/2	o	767.005 f	1255.9 (1.2)	1541 (54)		
37 776.32 (0.04)	13/2	o	726.429 f	1082.8 (0.8)	-2098 (46)	1083.6 (1.1)	-2070 (56)
			766.909 f	1086.0 (1.5)	-1848 (130)		
38 048.24 (0.03)	11/2	o	712.356 f	666.1 (0.3)	-387 (110)		
38 087.78 (0.06)	15/2	o	744.565 f	1015.3 (0.7)	-540 (33)		
39 653.44 (0.04)	13/2	e	785.269	766.5 (0.4)	590 (26)	767.0 (0.6)	575 (16)
			832.836	768.4 (0.7)	567 (18)		
40 077.35 (0.08)	11/2	o	798.468 f	1143.9 (0.6)	-645 (21)	1143.8 (0.5)	-635 (10)
			761.405	1144.6 (2.0)	-640 (12)		
			772.815	1146 (3)	-642 (19)		
			771.151	1142.8 (0.8)	-602 (24)		
			803.824 f	1145.3 (1.6)	-621 (31)		
40 165.71 (0.07)	13/2	o	756.912	1870.8 (1.3)	-1129 (81)	1869.9 (0.7)	-1043 (13)
			767.574	1869.6 (0.8)	-1041 (13)		
42 337.80 (0.07)	17/2	e	780.636	1405.1 (2.5)	-298 (100)		
			775.295	1409.6 (0.7)	-155 (56)	1409.6 (0.8)	-178 (52)
			799.540 f	1413.3 (1.9)	-136 (110)		
42 407.4 (0.1)	17/2	e	771.141 f	980 (3)	-681 (150)	980.0 (2.1)	-655 (110)
			786.282 f	980 (3)	-627 (150)		
42 770.41 (0.04)	15/2	e	755.128 f	1289 (3)	943 (190)	1284.8 (0.6)	945 (39)
			750.129	1284.7 (0.5)	945 (40)		

Notes: f: hfs constants A and B of the other level were fixed during the fitting process and are provided in Table3.2

Table 3.2 : List of experimental hyperfine structure constants A and B which were fixed during the hfs analysis.

E (cm^{-1})	J	P	A (MHz)	B (MHz)	Ref.
17 059.35	13/2	e	556.1 (0.7)	-1217 (40)	[30]
18 651.53	15/2	e	863.40 (0.16)	-2740 (16)	[38]
23 861.17	9/2	e	279 (4.5)	-39 (300)	[17]
23 946.16	11/2	e	618.5 (0.5)	-2265 (18)	[38]
23 955.68	13/2	e	951.93 (0.21)	-2451 (15)	[38]
24 014.22	13/2	e	901.28 (0.21)	-1404 (13)	[38]
24 357.92	15/2	o	840 (3)	-1874 (150)	[17]
24 660.80	15/2	e	752.5 (0.3)	-2469 (29)	[38]
24 740.52	13/2	e	707.8 (1.1)	-771 (46)	[31]
26 957.70	15/2	e	1514.8 (0.5)	510 (40)	[37]
27 556.90	9/2	e	1121.1 (0.5)	847 (7)	[19]
27 640.21	11/2	o	1515.2 (0.5)	-645 (7)	[19]
29 443.09	17/2	o	1061 (3)	2084 (150)	[17]
29 531.25	17/2	o	1218.2 (3.0)	122 (182)	[65]
29 692.67	19/2	o	529 (3)	2143 (150)	[17]
29 834.05	15/2	o	1050.4 (1.9)	36 (103)	[30]
40 077.35	11/2	o	1143.8 (0.5)	-635 (10)	tw

Notes: The values of the hfs constants from [17] are converted from 10^{-3} cm^{-1} to MHz.
tw: this work

The four energy levels discovered during this thesis study, which were published by another research group [41,43] more quickly, will be presented hereafter. The hfs constants are presented in Table 3.4 with the values from the literature for comparison, if available. The energy values already published but also discovered in this study are emphasized with an asterisk. In this table, for the levels in the literature, the experimental hfs constants A_{exp} and B_{exp} were also determined as a by-product of this study. For three levels from the literature, unknown hfs constants could be determined with this work and are emphasized with the "tw" abbreviation in the reference column. Our obtained values for most levels with already known hfs constants agree within the error bars with the reference values.

Discovered level E= 37734.93(0.02) cm^{-1}

In the discovery of the energy level E= 37734.93(0.02) cm^{-1}, the spectral line shown in Fig.3.29 was measured with a 20 GHz laser scan with the monochromator fixed at a positive fluorescence wavelength, as indicated in the caption of the figure. Hfs analysis was performed to determine the hfs constants A and B, and are given in Table 3.4.

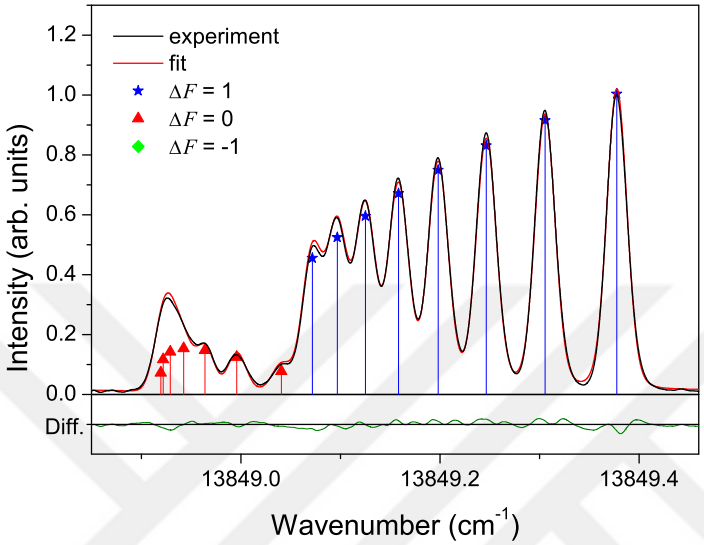


Figure 3.29 : Measured spectral line in the discovery of the energy level E_{upper} = 37734.93(0.02) cm^{-1}, J= 19/2 (e), with the monochromator fixed at λ_F =573.926 nm. Line at σ= 13849.21 cm^{-1} (λ = 721.864 nm), E_{lower}= 23885.74 cm^{-1}, J=17/2, (o) $\longrightarrow E_{upper}$

Discovered level E= 38665.37(0.08) cm^{-1}

For the discovery of the energy level E= 38665.37(0.08) cm^{-1} the spectral line shown in Fig.3.30 was investigated. The spectral line was measured with a 15 GHz scan and the monochromator was set to a negative fluorescence line, as indicated in the figure caption. Hfs constants resulting from the hfs analysis performed are given in Table 3.4.

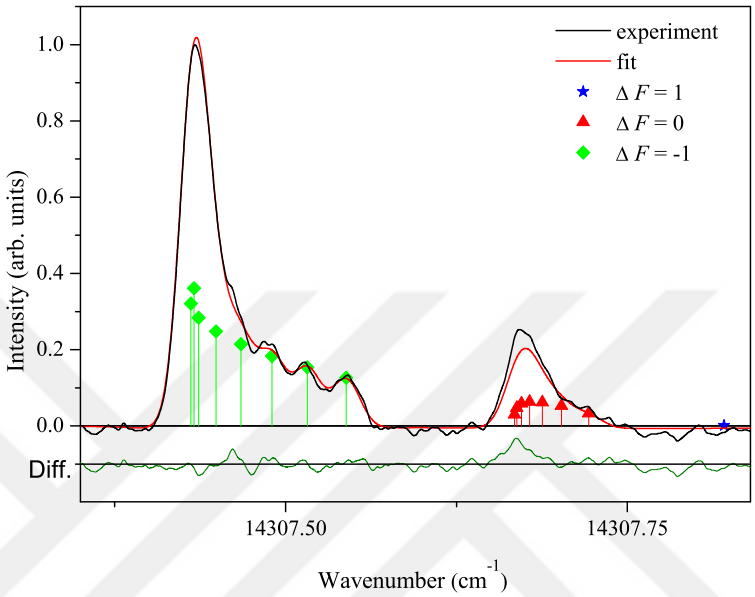


Figure 3.30 : Measured spectral line in the discovery of the energy level E_{upper} = 38665.37(0.08) cm^{-1}, J= 13/2 (e), with the monochromator fixed at λ_F = 410.380 nm. Line at σ= 14307.48 cm^{-1} (λ = 698.742 nm), E_{lower}= 24357.92 cm^{-1}, J=15/2, (o) $\longrightarrow$ E_{upper}.

Discovered level E= 38077.21(0.04) cm^{-1}

In the discovery of the energy level E= 38077.21(0.04) cm^{-1} the spectral line is illustrated in Fig.3.31 c). The whole spectrum was approximately 40 GHz wide, which exceeded our scan range and was therefore measured in two parts with the monochromator set to a negative fluorescence line as indicated in the caption of the figure. The identification of hfs constants was achieved by performing an hfs analysis on the measured spectra shown in a) and b), and are given in Table 3.4.

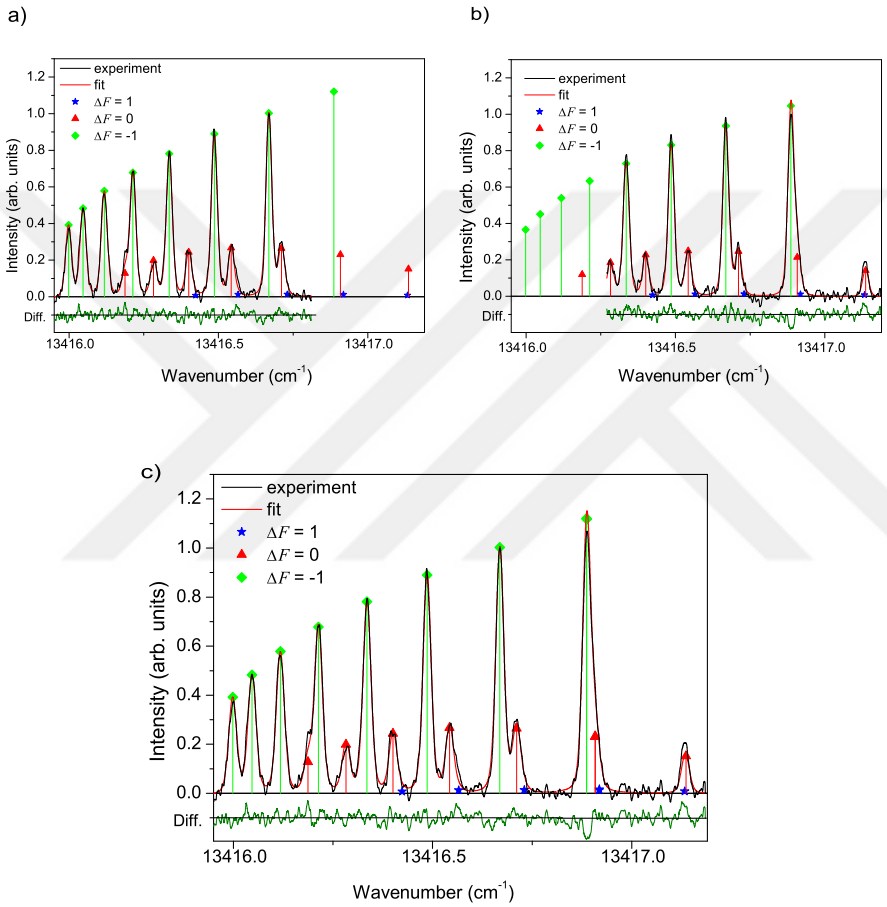


Figure 3.31 : Measured spectral lines in the discovery of the energy level E_{upper} = 38077.21(0.04) cm^{-1}, J= 13/2 (o), with the monochromator fixed at λ_F^-=405.393 nm. c) shows the visually combined line spectrum of a) and b) at
σ= 13416.45 cm^{-1} (λ= 745.148 nm), E_{lower}= 24660.80 cm^{-1}, J=15/2, (e) $\longrightarrow$ E_{upper}

Discovered level E= 38257.19(0.05) cm^{-1}

Two spectral lines contributed to the discovery of the energy level E= 38257.19(0.05) cm^{-1} as shown in Fig.3.32. The width of the measured spectral lines (approx. 40 GHz) exceeded our scan range, and thus were recorded in two parts with the monochromator set to negative fluorescence lines as indicated in the caption of the figure. Hfs analysis was performed on both spectra, which led to the identification of the hfs contacts given in Table 3.4.

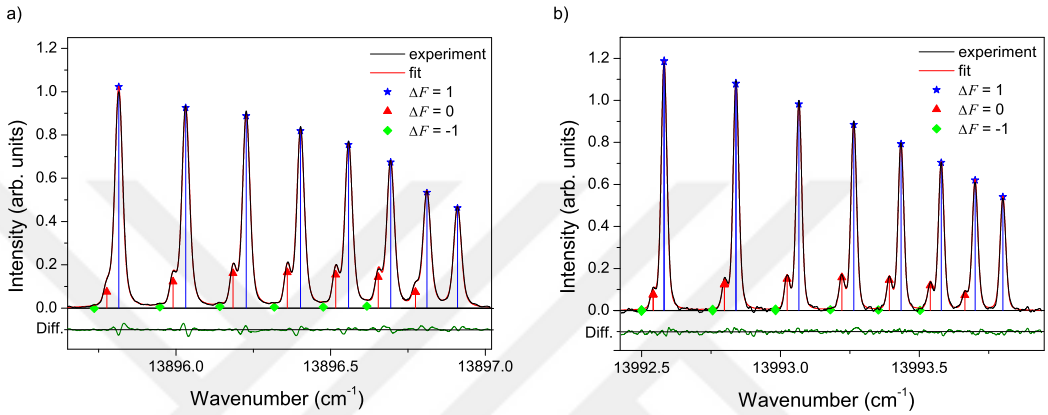


Figure 3.32 : Measured spectral lines in the discovery of the energy level E_{upper} = 38257.19(0.05) cm^{-1}, J= 19/2 (o), with the monochromator fixed at λ_F^-= 410.383 nm and λ_F^-= 501.883 nm for line a) and b), respectively. Both lines were measured in two parts; a) and b) show the visually combined spectra.
a) line at σ= 13896.34 cm^{-1} (λ= 719.416 nm), E_{lower}= 24360.81 cm^{-1}, J=17/2, (e) $\longrightarrow E_{upper}$
b) line at σ= 13993.18 cm^{-1} (λ= 714.437 nm), E_{lower}= 24263.96 cm^{-1}, J=17/2, (e) $\longrightarrow E_{upper}$

The energy values of the newly discovered energy levels, together with their determined parity, J value, hfs constants A and B, are saved in the classification program Elements [60,61] to calculate theoretically possible transitions that occur from or to the level. Table 3.5 lists all possible transitions to the newly discovered energy levels, sorted in wavelengths (nm).

The list also provides the cog of the observed line in units of wavenumber(cm^{-1}), which was identified from the FT spectra using a hfs simulation in the Elements program, allowing us to shift the theoretical fit with the relevant section of the FT spectra. This program allows us to accurately determine the cog by shifting the fit until a perfect overlap is achieved. The reading accuracy of the lines in the FT spectra for SNR>10 is estimated to be better than 0.0001 nm, for SNR$\leq$10 it is better than

0.0005 nm. Units were converted to wavenumber to add the calibration accuracy of the FT spectra, which was 0.005 cm^{-1}. The uncertainty of the determined wavenumber of the cog of the spectral line is given under the column $u_\sigma(cm^{-1})$. In column $\Delta\sigma$ the difference between the energy levels of the laser excitation line and the difference of the observed cog of the spectral line is given. The value observed in this column provides the measure of the accuracy of the determined energy value. The listed new energy level values result from weighted means of the repeated measurement of the spectral line and are found accordingly to the Ritz principle, namely, from the sum or subtraction of the defined energy level and the measured center of gravity wavenumber of the spectral line.

The same list for the four levels, which were published faster [41,43], but also discovered in this study, is provided in Table 3.6.

Table 3.3 : List of measured Ho I lines with the LIFS method to determine new energy levels with their classification. New levels are emphasized in bold.

line				lower level			upper level		
λ_{air} (nm)	σ (cm^{-1})	SNR	$\Delta\sigma$ (cm^{-1})	E (cm^{-1})	J	P	E (cm^{-1})	J	P
698.742	14 307.48 *	13	-0.03	24 357.92 f	15/2	o	38 665.37	13/2	e
712.356	14 034.05	9	-0.03	24 014.22 f	13/2	e	**38 048.24**	11/2	o
713.943	14 002.85	4	0.02	17 059.35 f	13/2	e	**31 062.22**	11/2	o
714.437	13 993.18 *	3	0.07	24 263.96	17/2	e	38 257.19	19/2	o
719.416	13 896.34 *	22	0.06	24 360.81	17/2	e	38 257.19	19/2	o
721.864	13 849.21 *	4	-0.02	23 885.74	17/2	o	37 734.93	19/2	e
722.232	13 842.15	4	0.09	18 821.25	11/2	e	**32 663.47**	11/2	o
726.429	13 762.17	3	-0.07	24 014.22 f	13/2	e	**37 776.32**	13/2	o
741.982	13 473.71	18	0.01	18 491.21	11/2	e	**31 964.93**	13/2	o
744.565	13 426.96	8	0.02	24 660.80 f	15/2	e	**38 087.78**	15/2	o
745.148	13 416.45 *	5	-0.04	24 660.80 f	15/2	e	38 077.21	13/2	o
750.129	13 327.37	–	-0.05	29 443.09	17/2	o	**42 770.41**	15/2	e
750.912	13 313.47	20	-0.07	18 651.53 f	15/2	e	**31 964.93**	13/2	o
755.128	13 239.15	–	0.01	29 531.25 f	17/2	o	**42 770.41**	15/2	e
756.912	13 207.93	14	0.08	26 957.70 f	15/2	e	**40 165.71**	13/2	o
760.614	13 143.66	48	0.02	18 821.25	11/2	e	**31 964.93**	13/2	o
761.405	13 130.00	–	0.02	26 947.33	13/2	e	**40 077.35** f	11/2	o
762.757	13 106.73	44	0.01	18 858.19	13/2	e	**31 964.93**	13/2	o
766.909	13 035.77	–	0.03	24 740.52 f	13/2	e	**37 776.32**	13/2	o
767.005	13 034.14	–	0.06	24 740.52 f	13/2	e	**37 774.72**	11/2	o
767.574	13 024.48	7	-0.05	27 141.28	13/2	e	**40 165.71**	13/2	o
769.108	12 998.50	–	0.02	23 955.68 f	13/2	e	**36 954.20**	13/2	o
769.119	12 998.32	–	0.07	23 861.17 f	9/2	e	**36 859.56**	11/2	o
771.141	12 964.23	–	0.08	29 443.09 f	17/2	o	**42 407.40**	17/2	e
771.151	12 964.07	19	0.00	**27 113.28**	11/2	e	**40 077.35**	11/2	o
772.815	12 936.16	4	-0.09	27 141.28	13/2	e	**40 077.35**	11/2	o
774.177	12 913.39	5	0.01	23 946.16 f	11/2	e	**36 859.56**	11/2	o
775.295	12 894.77	–	-0.06	29 443.09	17/2	o	**42 337.80**	17/2	e
780.636	12 806.54	–	0.01	29 531.25	17/2	o	**42 337.80**	17/2	e
785.269	12 730.98	–	0.06	26 922.40	15/2	o	**39 653.44**	13/2	e
786.282	12 714.58	–	0.15	29 692.67 f	19/2	o	**42 407.40**	17/2	e
798.468	12 520.54	–	-0.09	27 556.90 f	9/2	e	**40 077.35**	11/2	o
799.540	12 503.75	–	0.00	29 834.05 f	15/2	o	**42 337.80**	17/2	e
803.824	12 437.11	–	0.03	27 640.21 f	11/2	e	**40 077.35**	11/2	o
832.836	12 003.87	–	0.06	27 649.51	15/2	o	**39 653.44**	13/2	e

Notes: *: lines with levels already published in [41,43] and also discovered in tw;
SNR: in case the line is also observed in the FT spectra, the signal-to-noise ratio (SNR) from the Ho-Ar FT spectrum [34,66] is provided; lines without an SNR value are not observed in the FT spectra; $\Delta\sigma = E_{upper} - E_{lower} - \sigma$: difference between the difference in energy levels and the experimental wavenumber; f: fixed hfs constants, A and B, during the fit process of the investigated level.

Table 3.4 : Experimental hfs constants A and B (in MHz) for already known levels, together with values from literature if available.

E (cm^{-1})	J	p	λ_{air} (nm)	A_{exp}	B_{exp}	A_{mean}	B_{mean}	A_{ref}	B_{ref}	ref.
18 491.21	11/2	e	741.982	836.7 (2.5)	-244 (97)			842 (2)	-380 (29)	[32]
18 821.25	11/2	e	722.232	265.2 (1.0)	-417 (58)	265.0 (0.7)	-413 (31)	264.7 (0.6)	-446 (33)	[33]
18 821.25	11/2	e	760.614	264.9 (1.0)	-411 (37)					
18 858.19	13/2	e	762.757	466 (3)	-3117 (59)			465.45 (23)	-3158 (14)	[38]
23 885.74	17/2	o	721.864	705.8 (0.8)	-1697 (34)			708.9 (1.5)	-1473 (95)	[31]
24 263.96	17/2	e	714.437	716.7 (1.4)	1058 (100)					tw
24 360.81	17/2	e	719.416	658 (3)	-584 (330)					tw
26 922.40	15/2	o	785.269	1115.1 (0.6)	-891 (26)			1118 (3)	-908 (15)	[17]
26 947.33	13/2	e	761.405	582.1 (0.6)	-162 (47)					tw
27 141.28	13/2	e	767.574	1446.3 (0.4)	-1742 (11)	1446.3 (0.4)	-1752 (16)	1444.4 (1.9)	-1820 (100)	[35]
27 141.28	13/2	e	772.815	1450 (4)	-1817 (27)					
27 649.51	15/2	o	832.836	993.1 (0.5)	1600 (28)			991.6 (1.4)	1578 (88)	[67]
29 443.09	17/2	o	750.129	1055.5 (0.5)	2242 (39)	1055.7 (0.4)	2251 (36)	1061 (3)	2084 (150)	[17]
29 443.09	17/2	o	775.295	1055.9 (0.6)	2281 (72)					
29 531.25	17/2	o	780.636	1210.4 (2.5)	-19 (110)			1218.2 (3.0)	122 (18)	[65]
37 734.93 *	19/2	e	721.864	769.2 (0.7)	402 (29)			769.3 (0.1)	555 (88)	[43]
38 077.21 *	13/2	o	745.148 f	1408.3 (0.6)	-211 (57)			1408.9 (1.7)	-239 (35)	[41]
38 257.19 *	19/2	o	714.437	118.6 (1.3)	-1354 (140)	120.0 (1.0)	-1340 (87)	118.0 (1.6)	-1400 (121)	[41]
		o	719.416	120.9 (1.1)	-1332 (110)					
38 665.37 *	13/2	e	698.742 f	895.2 (1.1)	-691 (140)			901.6 (1.8)	-781 (218)	[41]

Values from [17] are converted from 10^{-3} cm^{-1} to MHz; f: hfs constants A and B of the other level were fixed during fitting process; tw: this work.

Table 3.5 : List of Holmium lines from the FT spectrum [29,34,66], classified by the new levels.

λ_{air} (nm)	σ (cm^{-1})	u_σ (cm^{-1})	SNR	com.	$\Delta\sigma$ (cm^{-1})	other level E (cm^{-1})	J
27113.28 (0.02) cm^{-1}, $J = 11/2$, e							
460.8371	21 693.567	0.029	8		0.013	5 419.70	13/2
540.1529	18 508.130	0.022	9		-0.010	8 605.16	11/2
771.1504	12 964.071	0.007	19	LIF	-0.001	40 077.35	11/2
31062.22 (0.02) cm^{-1}, $J = 11/2$, o							
456.1776	21 915.145	0.010	40		-0.005	9 147.08	13/2
534.1058	18 717.677	0.023	8	b	-0.007	12 344.55	13/2
713.9434	14 002.852	0.015	4	LIF	0.018	17 059.35	13/2
31964.93 (0.03) cm^{-1}, $J = 13/2$, o							
438.1304	22 817.845	0.031	8		0.005	9 147.08	13/2
509.3887	19 625.904	0.024	6	b	-0.014	12 339.04	15/2
662.8311	15 082.634	0.007	215		0.016	16 882.28	15/2
670.7054	14 905.562	0.007	19		0.018	17 059.35	13/2
741.9820	13 473.706	0.007	18	LIF	0.014	18 491.21	11/2
750.9126	13 313.464	0.007	20	LIF	-0.064	18 651.53	15/2
760.6131	13 143.670	0.007	48	LIF	0.010	18 821.25	11/2
762.7555	13 106.753	0.007	44	b, LIF	-0.013	18 858.19	13/2
32663.47 (0.04) cm^{-1}, $J = 11/2$, o							
492.0147	20 318.924	0.009	33		-0.004	12 344.55	13/2
722.2317	13 842.157	0.034	4	r LIF	0.063	18 821.25	11/2
1 076.8080	9 284.163	0.009	5		-0.004	23 379.31	11/2
36859.56 (0.03) cm^{-1}, $J = 11/2$, o							
546.4550	18 294.686	0.022	8	b	-0.026	18 564.90	13/2
610.8485	16 366.141	0.018	5	d	0.019	20 493.40	11/2
774.1774	12 913.383	0.013	5	LIF	0.017	23 946.16	11/2
36954.20 (0.04) cm^{-1}, $J = 13/2$, o							
406.1388	24 615.171	0.011	14	b	-0.011	12 339.04	15/2
406.2302	24 609.637	0.035	7		0.013	12 344.55	13/2
472.4111	21 162.083	0.029	17	r	-0.013	15 792.13	11/2
499.4432	20 016.714	0.025	7		0.056	16 937.43	11/2
549.3576	18 198.022	0.022	6	b	-0.042	18 756.22	15/2

Table 3.5 (continued) : List of Holmium lines from the FT spectrum [29,34,66], classified by the new levels.

						other level	
λ_{air} (nm)	σ (cm^{-1})	u_σ (cm^{-1})	SNR	com.	$\Delta\sigma$ (cm^{-1})	E (cm^{-1})	J
37774.72 (0.05) cm^{-1}, $J = 11/2$, o							
349.2130	28 627.627	0.013	20		0.013	9 147.08	13/2
404.8790	24 691.760	0.011	27		0.030	13 082.93	11/2
570.1799	17 533.460	0.020	7		-0.050	20 241.31	13/2
37776.32 (0.04) cm^{-1}, $J = 13/2$, o							
404.8518	24 693.420	0.011	12		-0.030	13 082.93	11/2
726.4331	13 762.100	0.014	3	LIF	0.000	24 014.22	13/2
38048.24 (0.03) cm^{-1}, $J = 11/2$, o							
388.9386	25 703.715	0.038	6		-0.025	12 344.55	13/2
476.3102	20 988.852	0.009	158		0.038	17 059.35	13/2
520.9587	19 190.037	0.023	8		0.013	18 858.19	13/2
712.3574	14 034.029	0.015	9	LIF	-0.009	24 014.22	13/2
38087.78 (0.06) cm^{-1}, $J = 15/2$, o							
345.4361	28 940.619	0.047	8		0.081	9 147.08	13/2
449.6654	22 232.519	0.010	41		-0.019	15 855.28	15/2
455.7947	21 933.556	0.010	13		0.014	16 154.21	15/2
467.6386	21 378.049	0.010	20		-0.089	16 709.82	17/2
506.1877	19 750.012	0.025	10		-0.032	18 337.80	17/2
744.5654	13 426.955	0.014	8	LIF	0.025	24 660.80	15/2
39653.44 (0.04) cm^{-1}, $J = 13/2$, e							
480.9616	20 785.870	0.009	23		0.030	18 867.54	13/2
490.6233	20 376.546	0.009	13	b	-0.026	19 276.92	15/2
40077.35 (0.08) cm^{-1}, $J = 11/2$, o							
370.3421	26 994.378	0.041	6		0.042	13 082.93	11/2
655.6906	15 246.884	0.017	4		0.036	24 830.43	11/2
683.6290	14 623.783	0.007	12	b, a	0.077	25 453.49	9/2
689.1664	14 506.281	0.016	10		-0.081	25 571.15	13/2
772.8142	12 936.161	0.013	4	LIF	-0.091	27 141.28	13/2
40165.71 (0.07) cm^{-1}, $J = 13/2$, o							
681.8315	14 662.333	0.016	8	b	0.047	25 503.33	11/2
684.9956	14 594.607	0.016	10	b	-0.047	25 571.15	13/2
756.9120	13 207.938	0.007	14	LIF	0.072	26 957.70	15/2
767.5731	13 024.491	0.013	7	LIF	-0.061	27 141.28	13/2

Table 3.5 (continued) : List of Holmium lines from the FT spectrum [29,34,66], classified by the new levels.

						other level	
λ_{air} (nm)	σ (cm^{-1})	u_σ (cm^{-1})	SNR	com.	$\Delta\sigma$ (cm^{-1})	E (cm^{-1})	J
42337.80 (0.07) cm^{-1}, $J = 17/2$, e							
548.5214	18 225.767	0.022	10	b	-0.007	24 112.04	15/2
548.6177	18 222.568	0.022	10		0.062	24 115.17	17/2
566.1096	17 659.522	0.008	11		0.028	24 678.25	19/2
672.4173	14 867.613	0.016	7		-0.083	27 470.27	19/2
42407.4 (0.1) cm^{-1}, $J = 17/2$, e							
448.6439	22 283.139	0.030	4		-0.009	20 124.27	19/2
42770.41 (0.04) cm^{-1}, $J = 15/2$, e							
535.8020	18 658.422	0.022	10		-0.052	24 112.04	15/2
535.8940	18 655.217	0.022	8		0.023	24 115.17	17/2
550.0339	18 175.650	0.008	18		0.010	24 594.75	13/2
664.4437	15 046.028	0.016	5		0.022	27 724.36	13/2

Notes: λ_{air}: observed center-of-gravity wavelength in air from FT spectrum; σ: observed center-of-gravity vacuum wavenumber of the transition; SNR: observed signal-to-noise ratio of the transition in the Ho-Ar-spectrum; u_σ: uncertainty in observed wavenumber from FT spectra; $\Delta\sigma = E_{upper}$-E_{lower} - σ: difference between the difference of the level energies and the observed wavenumber; comment (com.): a: hfs constants, A and B, of lower level are unknown; b: blend but not preventing the determination of cog; r: blend line, reduces the accuracy in the determination of cog; LIF: also measured with LIF.

3.2 Determination of hfs constants

As mentioned in Sec.3, an additional study was carried out on the investigation of energy levels already defined in the literature to identify their corresponding hfs constants. During this study, the spectral lines observed in the FT spectrum in the first wavelength region (680–750 nm) were examined. The list of spectral lines investigated for the purpose using the LIFS method is given in Table 3.7 with their wavenumber, upper and lower energy levels, with their values of parity (P) and J, respectively. The energy levels and their determined corresponding hfs constants are given in Table 3.8. The fixed hfs constants of the energy levels from the literature during the hfs analysis are provided in Table 3.9.

Table 3.6 : List of Holmium lines from the FT spectrum [29,34,66], classified by the levels already published in [41,43], but also discovered by us.

						other level	
λ_{air} (nm)	σ (cm^{-1})	u_σ (cm^{-1})	SNR	com.	$\Delta\sigma$ (cm^{-1})	E (cm^{-1})	J
37734.93 (0.02) cm^{-1}, $J = 19/2$, e							
573.9246	17 419.059	0.008	118		-0.019	20 315.89	17/2
583.9116	17 121.133	0.008	84		-0.003	20 613.80	17/2
688.3386	14 523.727	0.007	14		-0.007	23 211.21	19/2
721.8656	13 849.178	0.015	4	LIF	0.012	23 885.74	17/2
38077.21 (0.04) cm^{-1}, $J = 13/2$, o							
471.6797	21 194.900	0.027	8	b	0.030	16 882.28	15/2
475.6536	21 017.826	0.009	25	b	0.034	17 059.35	13/2
514.6378	19 425.731	0.009	14	b	-0.051	18 651.53	15/2
710.8895	14 063.007	0.015	4	b	-0.017	24 014.22	13/2
745.1499	13 416.423	0.014	5	b LIF	-0.013	24 660.80	15/2
38257.19 (0.05) cm^{-1}, $J = 19/2$, o							
458.1845	21 819.153	0.040	14	r	0.027	16 438.03	17/2
463.9624	21 547.439	0.010	62	b	-0.049	16 709.82	17/2
501.8829	19 919.412	0.009	93		-0.002	18 337.80	17/2
714.4373	13 993.172	0.035	3	r LIF	-0.029	24 263.96	17/2
719.4157	13 896.340	0.007	22	LIF	0.060	24 360.81	17/2
38665.37 (0.08) cm^{-1}, $J = 13/2$, e							
515.6245	19 388.557	0.009	14	b	-0.107	19 276.92	15/2
537.3540	18 604.534	0.008	30	b	0.076	20 060.76	11/2
550.1577	18 171.558	0.008	22		0.052	20 493.76	13/2
698.7426	14 307.475	0.007	13	LIF	-0.025	24 357.92	15/2

Determination of hfs constants of the levels E= 38124.76 cm^{-1}, J=17/2 (e) and E= 23885.74 cm^{-1}, J=17/2 (o)

The already defined line at λ_{air}= 702.106 nm (σ=14238.94 cm^{-1}), which corresponds to the excitation from E_{lower}= 23885.74 cm^{-1}, J= 17/2, (o) to E_{upper}= 38124.76 cm $^{-1}$ J= 17/2, (e) was determined in the FT spectrum. The laser wavelength was adjusted to λ_{air}= 702.106 nm, and the LIFS method was performed by adjusting the monochromator to the fluorescence wavelength at λ_F= 561.360 nm. The measured and analyzed LIF spectrum is shown in Fig.3.33. The residual of the difference between the experiment and the fit is shown in the lower part of the plots.

Table 3.7 : List of spectral lines defined in the FT spectrum and investigated with the LIFS method. Both wavelength and wave number are given as fit result of the measured lines.

$\lambda_{air}\ (nm)$	$\sigma\ (cm^{-1})$	$E_{upper}\ (MHz)$	J_{upper}	P_{upper}	$E_{lower}\ (MHz)$	J_{lower}	P_{lower}
702.106	14238.94	38124.76	17/2	e	23885.74	17/2	o
702.191	14237.22	30029.36	13/2	o	15792.13	11/2	e
705.144	14177.59	37388.72	17/2	e	23211.21	19/2	o
707.196	14136.46	37971.48	17/2	o	23834.94	15/2	e
719.821	13888.51	34055.69	15/2	o	20167.18	15/2	e
724.179	13804.93	30242.96	15/2	o	16438.01	17/2	e
725.056	13788.22	26127.22	13/2	o	12339.04	15/2	e
736.079	13581.75	26664.67	11/2	o	13082.93	11/2	e

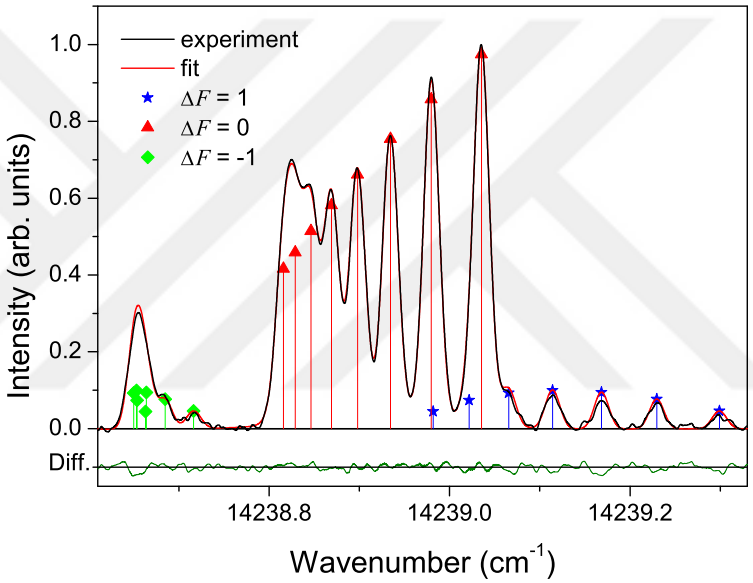


Figure 3.33 : Experimental LIF spectrum of the line at λ_{air}= 702.106 nm (σ=14238.94 cm^{-1}) measured with λ_F = 561.360 nm and best-fit curve superposed.

From the analysis of the measured LIF spectra, the already known hfs constants of the lower and upper energy levels were determined and found to be slightly improved for the A values of both energy levels with a smaller margin of error compared to the reference values in Table3.8. The B values of both energy levels were determined differently from the reference value. From the least-squares simulation fit of the measured line, it was found that the obtained hfs constants were better matched with the fit than the reference values [30,37].

Determination of hfs constants of the level E= 30029.36 cm^{-1}, J=13/2 (o)

The line at λ_{air}= 702.191 nm (σ= 14237.22 cm^{-1}), which corresponds to the excitation from E_{lower}= 15792.13 cm^{-1}, J= 11/2, (e) to E_{upper}= 30029.36 cm $^{-1}$ J= 13/2, (o) was determined. The laser wavelength was adjusted to λ_{air}= 702.191 nm, and the LIFS method was performed by adjusting the monochromator to the fluorescence wavelength at λ_F= 462.800 nm. The measured and analyzed LIF spectrum is shown in Fig.3.33. The residual difference between experiment and fit is shown in the lower part of the plots.

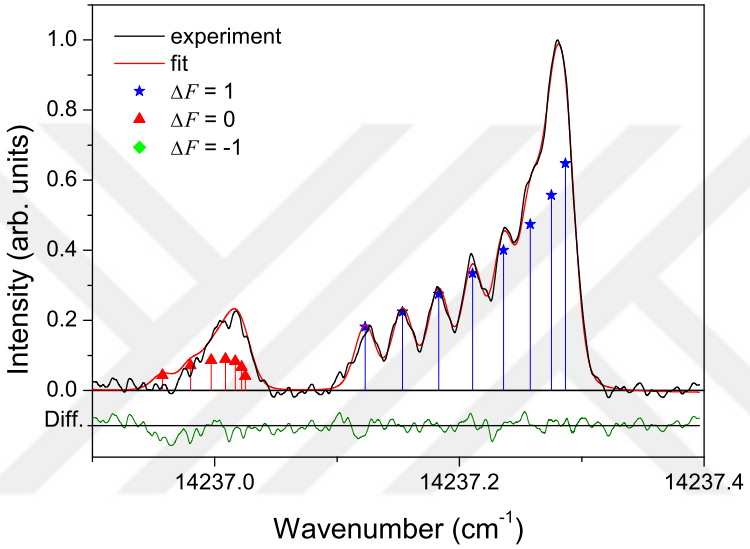


Figure 3.34 : Experimental LIF spectrum of the line at λ_{air}= 702.191 nm (σ=14237.22 cm^{-1}) measured with λ_F = 462.800 nm and best-fit curve superposed.

Since the spectrum was noisy and the hfs constants of the lower energy level had been determined by our research group using laser spectroscopic methods [38], the measured LIF spectrum was analyzed keeping the lower energy value and its hfs constants fixed during the least-squares fit procedure. From the analysis of the measured LIF spectra, the hfs constants of the upper energy level were determined for the first time with this study and are given in Table 3.8.

Determination of the hfs constants of the level E= 37388.72 cm^{-1}, J=17/2 (e)

The line at λ_{air}= 705.143 nm (σ= 14177.59 cm^{-1}), which corresponds to the excitation from E_{lower}= 23211.21 cm^{-1}, J= 19/2, (o) to E_{upper}= 37388.72 cm $^{-1}$ J= 17/2, (e) was determined. The laser wavelength was adjusted to λ_{air}= 705.143 nm, and the LIFS method was performed by adjusting the monochromator to the fluorescence wavelength at λ_F^-= 410.700 nm. The measured and analyzed LIF spectrum is shown in Fig.3.35.

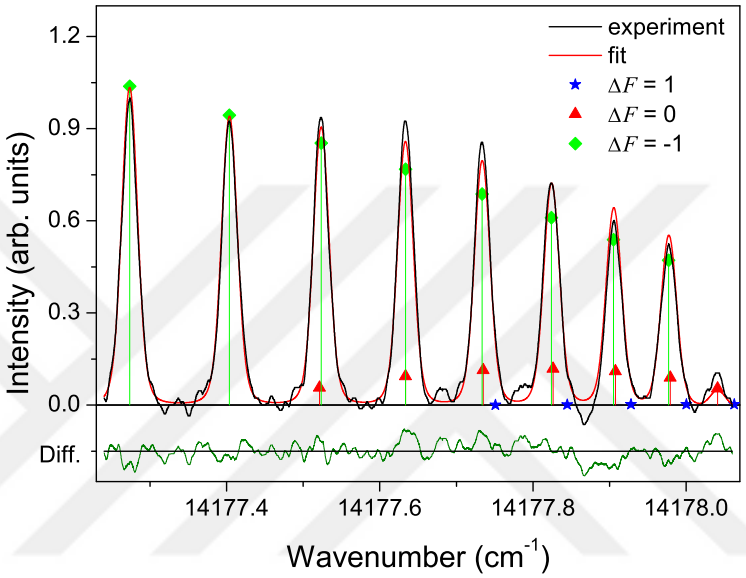
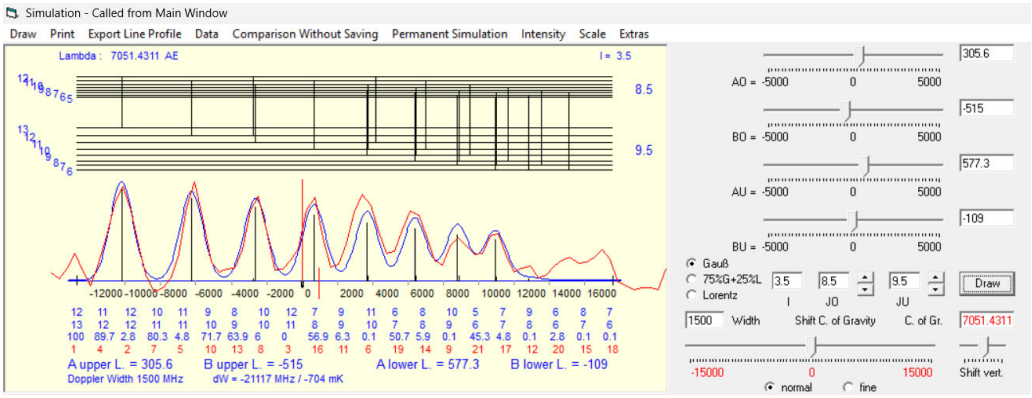


Figure 3.35 : Experimental LIF spectrum of the line at λ_{air}= 705.143 nm (σ= 14177.59 cm^{-1}) measured with the monochromator adjusted to λ_F^-= 410.700 nm and best-fit curve superposed.

Although the spectral lines appear to be resolved, small components are hidden beneath large maxima. As shown in Fig.3.35. Therefore, the measured LIF spectrum was analyzed by keeping the lower energy value and its hfs constants fixed during the least squares fit procedure. From the analysis of the measured LIF spectra, the hfs constants of the upper energy level were determined and showed a large difference from the reference values published by Reddy et al. [20] given in Table 3.8.

Figs.3.36 a) and b) show screenshots from the hfs simulation program within the Elements program [1,2], where the red line is the measured spectrum, and the blue line is the theoretical fit. As evidence, the A and B values of the lower energy level have been fixed for both simulations to show that the constant hfs values of the upper energy level determined from our measurements give a better theoretical fit compared

a)



b)

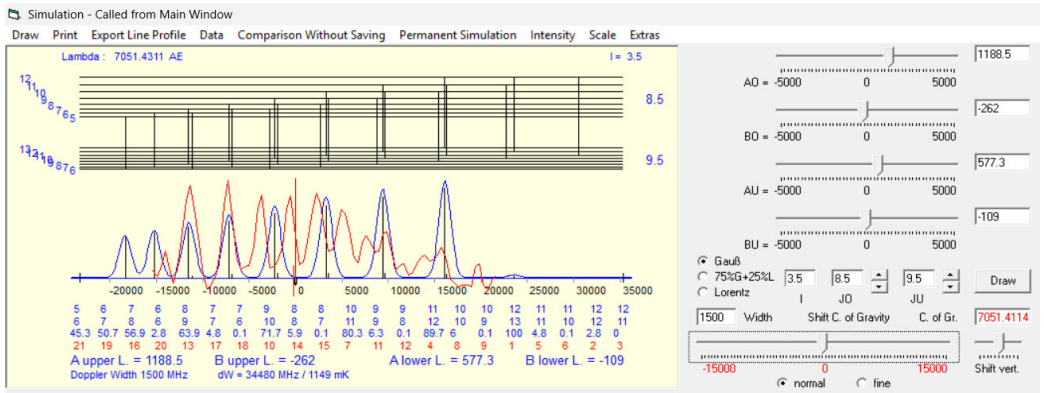


Figure 3.36 : Theoretical fit (blue line) of the line at λ_{air}= 705.143 nm of the FT observed spectrum (red line) using the hfs simulation program.
a) Fit with the hfs constants of the upper energy determined from this study.
b) Theoretical fit (blue line) of the line at λ_{air}= 705.143 nm with the upper energy level *A* and *B* constants from [20].

to the reference fit hfs values from the literature, which do not overlap with the line at all. Screenshots of the simulation program using the hfs values from this work and the reference values given in [20] are shown for comparison in Figs.3.36 a) and b), respectively. The fit with the reference hfs constants does not overlap with the measured spectra and gives a completely different hfs structure result, as can be seen in Fig.3.36 b), supporting the accuracy of the hfs constants determined in this study.

Determination of hfs constants of the level E= 37971.48 cm^{-1}, J=17/2 (o)

The line at λ_{air}= 707.196 nm (σ= 14136.46 cm^{-1}), which corresponds to the excitation from E_{lower}= 23834.94 cm^{-1}, J= 15/2, (e) to E_{upper}= 37971.48 cm $^{-1}$ J= 17/2, (o) was determined. The laser wavelength was adjusted to λ_{air}= 707.196 nm, and the LIFS method was performed by adjusting the monochromator to the fluorescence wavelength at λ_F= 707.196 nm. The measured and analyzed LIF spectrum is shown in Fig.3.37.

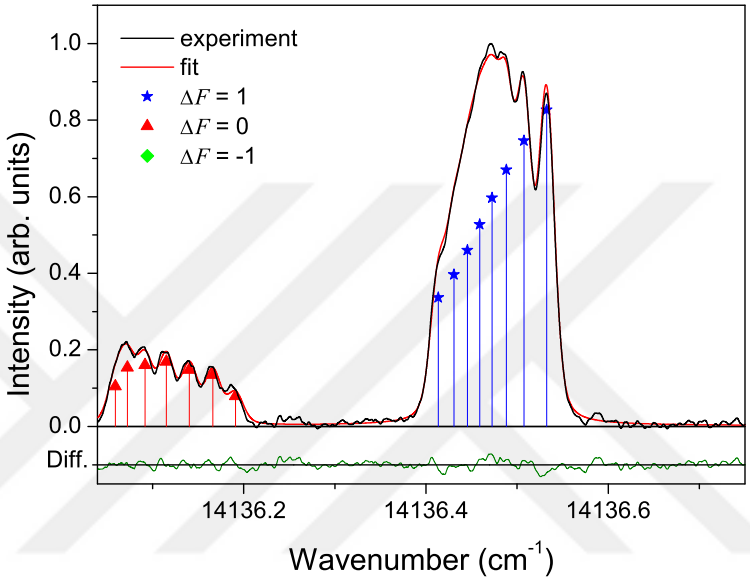


Figure 3.37 : Experimental LIF spectrum of the line at λ_{air}= 707.196 nm (σ=14136.45 cm^{-1}) measured with the monochromator adjusted to λ_F = 509.188 nm and best-fit curve superposed.

For a better fit, the measured LIF spectrum was analyzed by keeping the lower energy value and its hfs constants fixed during the least squares fit procedure. From the analysis of the measured LIF spectra, the hfs constants of the upper energy level were determined and the A value was in good agreement with the reference value given in Table3.8. The B value was determined slightly differently from [41].

Determination of hfs constants of the level E= 20167.18 cm^{-1}, J=15/2 (e)

The line at λ_{air}= 719.821 nm (σ= 13888.51 cm^{-1}), which corresponds to the excitation from E_{lower}= 20167.18 cm^{-1}, J= 15/2, (e) to E_{upper}= 34055.69 cm $^{-1}$ J= 15/2, (o) was determined. The laser wavelength was adjusted to λ_{air}= 719.821 nm, and the LIFS method was performed by adjusting the monochromator to the fluorescence wavelength at λ_F= 390.080 nm. The measured and analyzed LIF spectrum is shown in Fig.3.38.

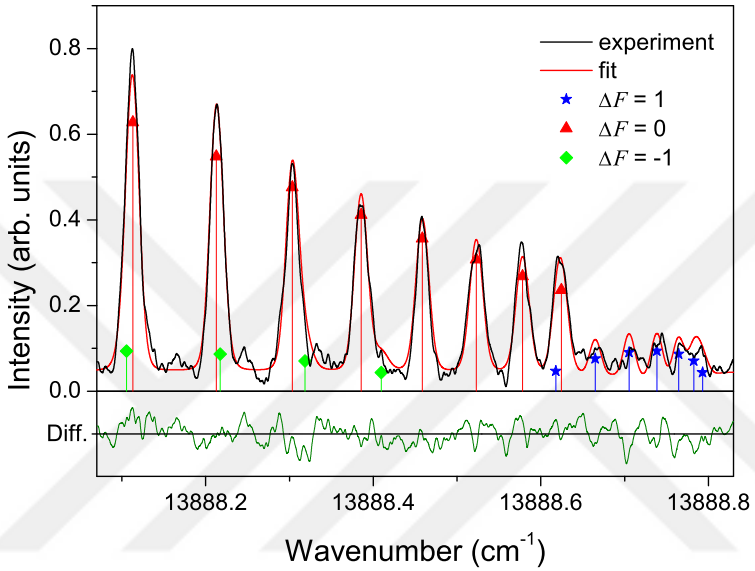


Figure 3.38 : Experimental LIF spectrum of the line at λ_{air}= 719.821 nm (σ=13888.51 cm^{-1}) measured with the monochromator adjusted to λ_F = 390.080 nm and best-fit curve superposed.

For a better fit, the measured LIF spectrum was analyzed by keeping the upper energy value and its hfs constants fixed during the least squares fit procedure. From the analysis of the measured LIF spectra, it was determined that the hfs constants of the lower energy level improved with a smaller error margin compared to the values in Table 3.8.

Determination of hfs constants of the level E= 30242.96 cm^{-1}, J=15/2 (o)

The line at λ_{air}= 724.178 nm (σ= 13804.93 cm^{-1}), which corresponds to the excitation from E_{lower}= 16438.0 cm^{-1}, J= 17/2, (e) to E_{upper}= 30242.96 cm $^{-1}$ J= 15/2, (o) was determined. The laser wavelength was adjusted to λ_{air}= 724.178 nm, and the LIFS method was performed by adjusting the monochromator to the fluorescence

wavelength at λ_F^-= 608.176 nm. The measured and analyzed LIF spectrum is shown in Fig.3.39.

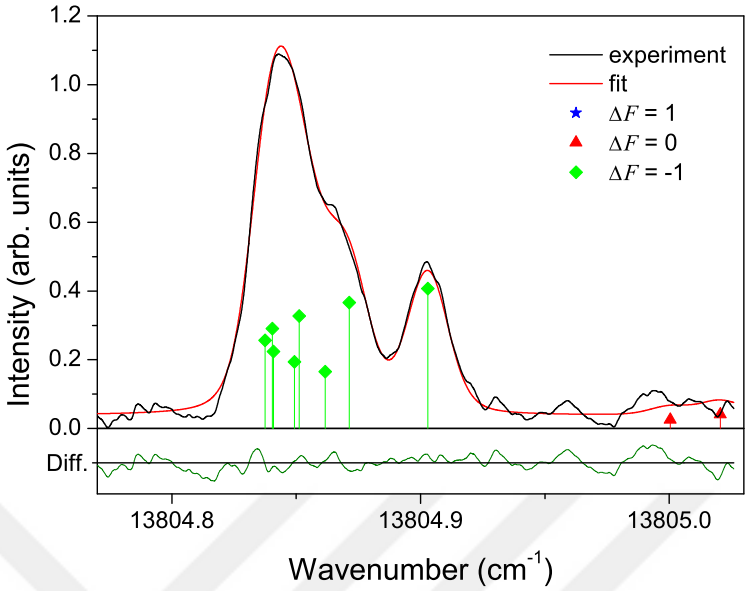


Figure 3.39 : Experimental LIF spectrum of the line at λ_{air}= 724.179 nm (σ= 13804.93 cm^{-1}) measured with the monochromator adjusted to λ_F = 462.800 nm and best-fit curve superposed.

For a better fit, the measured LIF spectrum was analyzed by keeping the lower energy value and its hfs constants fixed during the least squares fit procedure. From the analysis of the measured LIF spectra, the hfs constants of the upper energy level were determined for the first time with this study and are given in Table 3.8.

Determination of hfs constants of the level E= 12339.04 cm^{-1}, J=15/2 (e)

The line at λ_{air}= 725.056 nm (σ= 13788.22 cm^{-1}), which corresponds to the excitation from E_{lower}= 12339.04 cm^{-1}, J= 15/2, (e) to E_{upper}= 26127.22 cm $^{-1}$ J= 13/2, (o) was determined. The laser wavelength was adjusted to λ_{air}= 725.056 nm, and the LIFS method was performed by adjusting the monochromator to the fluorescence wavelength at λ_F= 564.811 nm. The measured and analyzed LIF spectrum is shown in Fig.3.40. T The laser could only scan a part of the spectral line. Although attempts were made to measure the entire spectrum at different time intervals, the laser scan could not be completed.

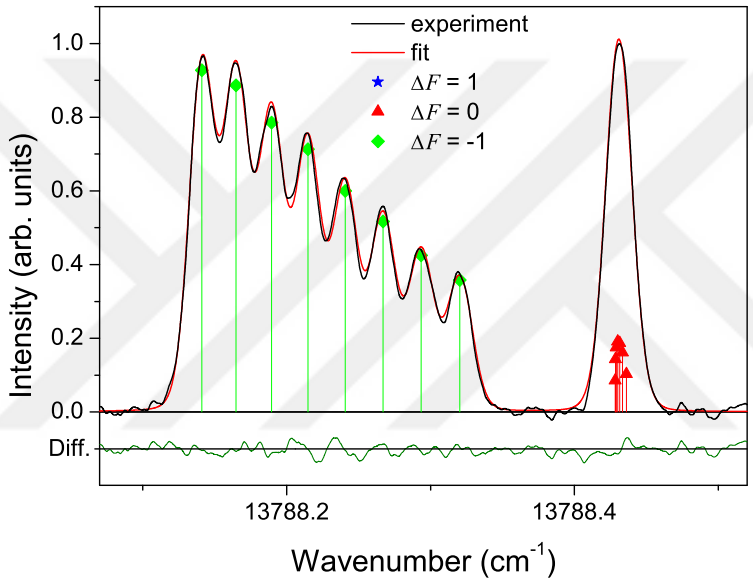


Figure 3.40 : Experimental LIF spectrum of the line at λ_{air}= 725.056 nm (σ=13788.22 cm^{-1}) measured with the monochromator adjusted to λ_F = 564.811 nm and best-fit curve superposed.

The measured LIF spectrum was analyzed by keeping the upper energy value and its hfs constants fixed during the least squares fit procedure for a better fit. From the analysis of the measured LIF spectra, the hfs constants of the lower energy level were determined and it was found to improve for the constant A with a smaller error margin, while for B, the constant value obtained of the hfs was found to be off the reference value given in Table 3.8.

A least squares simulation fit was applied for comparison with the hfs constants obtained from the measured line spectra and the reference values in [17]. As a result,

the fit with the hfs constants determined from this study overlapped better with the measured line spectra.

Determination of hfs constants of the level E= 13082.93 cm^{-1}, J=11/2 (e) and E= 26664.67 cm^{-1}, J=11/2 (o)

The line at λ_{air}= 736.079 nm (σ= 13581.75 cm^{-1}), which corresponds to the excitation from E_{lower}= 13082.9 cm^{-1}, J= 11/2, (e) to E_{upper}= 26664.67 cm $^{-1}$ J= 11/2, (o) was determined. The laser wavelength was adjusted to λ_{air}= 736.079 nm, and the LIFS method was performed by adjusting the monochromator to the fluorescence wavelength at λ_F= 570.695 nm. The measured and analyzed LIF spectrum is shown in Fig.3.41.

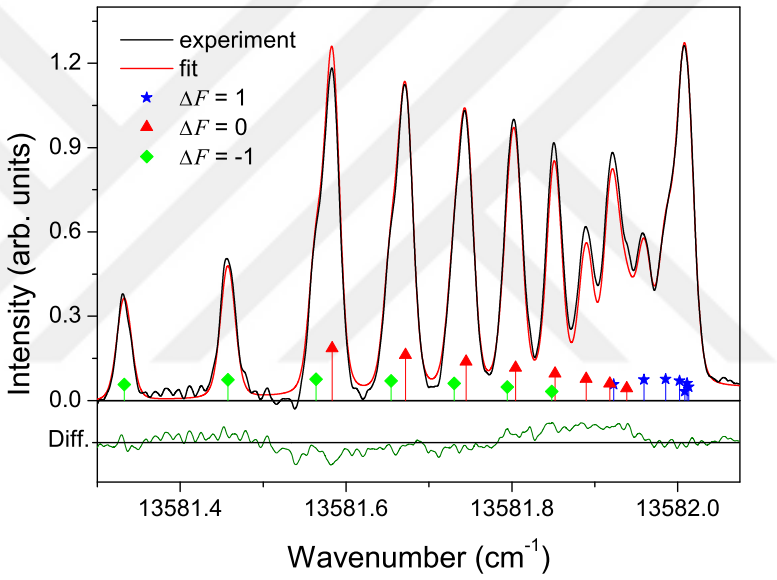


Figure 3.41 : Experimental LIF spectrum of the line at λ_{air}= 736.079 nm (σ=13581.75 cm^{-1}) measured with the monochromator adjusted to λ_F = 570.695 nm and best-fit curve superposed.

From the fit procedure, the hfs constants of the lower and upper energy levels were obtained as given in Table 3.8. The hfs constants obtained for the upper level improved with a smaller error margin compared to the reference values, whereas the values of the hfs constant for the lower energy level were found to agree well with the reference value of [38].

Table 3.8 : Energy levels with their hyperfine structure constants A and B (in MHz.). Energy values and error bars were found from the analysis of multiple LIF measurements of each laser line.

E (MHz)	J	Parity	λ_{air} (nm)fit	A(MHz)	B(MHz)	$A\,(\mathrm{MHz})_{\mathrm{ref}}$	$B\,(\mathrm{MHz})_{\mathrm{ref}}$	Ref.
12339.04*	15/2	e	725.056	806.7(1.3)	-31(23)	807(3)	243(10)	[17]
13082.93	11/2	e	736.079	1036.7(7)	2428(11)	1037.1(0.7)	2388(12)	[38]
20167.18*	15/2	e	719.821	1337.5(3)	1331(28)	1335.9(1.5)	1250(60)	[17]
23885.74	17/2	o	702.106	704.8(6)	-1853(56)	708.9(1.5)	-1473(95)	[30]
26664.67	11/2	o	736.079	779.5(6)	1472(20)	778.0(2.0)	1443(83)	[19]
30029.36**	13/2	o	702.191	976.7(7)	332(70)	tw	tw	
30242.96**	15/2	o	724.179	946.3(8)	3156(50)	tw	tw	
37388.72**	17/2	e	705.144	305.6(3)†	-515(46)†	1188.5(70)	-262(22)	[20]
37971.48**	17/2	o	707.196	1189.2(5)	-286(26)	1190.6(3)	-346(13)	[41]
38124.76	17/2	e	702.106	811.5(6)	-560(57)	812.3(1.2)	-300(80)	[37]

tw: this work
*: upper level fixed during fit procedure
**: lower level fixed during fit procedure
†: reference value of hfs constants shows big difference, discussed in text.

Table 3.9 : Experimental hyperfine structure constants A and B (in MHz.) of Ho I which kept fixed during the fit procedure.

E (MHz)	J	Parity	A(MHz)	B(MHz)	Ref.
15792.13	11/2	e	1025.5(4)	858(11)	[38]
16438.01	17/2	e	819.7(5)	2035(20)	[19]
23211.21	19/2	o	576.5(9)	-219(52)	[17]
23834.94	15/2	e	1270.90(22)	-1715(17)	[38]
26127.37	13/2	o	811.8(5)	50.9(7.0)	[19]
34055.69	15/2	o	1063.8(0.8)	1432(11)	[40]

4. Conclusion and Recommendation

Data on the spectral lines of rare earth elements are of great interest for applications in the field of astrophysics in means of determination of abundance ratios of elements in stars, galaxies, or interstellar media; determination of physical conditions such as the temperature, density, and chemical composition of stellar atmospheres and nebulae [68]; in understanding stellar evolution or determining the evolutionary stage of a star form the width of a spectral line [69]; studies on the expansion of the universe from line shifts [70].

Recent astrophysics studies highlight that hyperfine structure data in the line database are still incomplete and contain significant inaccuracies [13]–[16]. The findings of this study made further contributions to the experimental data of complex atoms, which will be available as a resource in the National Institute of Standards and Technology (NIST) Atomic and Molecular Database.

In total, 20 fine structure energy levels of Ho I have been discovered. However, four of them were also found by another research group and the findings were published faster, leaving us with 16 new energy levels discovered, comprising five levels with even parity and 11 with odd parity. From this study, the hfs contacts of the discovered energy levels were determined. Additionally, as a byproduct of the hfs analysis of the spectral lines, the hfs constants of three levels already experimentally known were also determined for the first time. The results of this study have been published in [63].

An additional study of defined spectral lines from the literature within our laser wavelength range was conducted to determine the hfs constants. Spectral lines were measured using the LIFS method, and the hfs analysis was performed to determine the corresponding hfs constants of the energy levels involved in the transition. A total of eight spectral lines were measured and the hfs constants of 10 energy levels were determined by hfs analysis. Among these 10 energy levels, the hfs constants of two energy levels were determined for the first time and corrected for one energy level. The

results of the findings, together with the ongoing study and search for spectral lines of already defined levels in the literature that fall within the wavelength range of our laser setup, are planned to be published as soon as they are completed.

During this study, significant inaccuracies in the energy level values of Ho I in the literature were revealed, affecting the precision of our findings. Inaccuracies in the energy levels were already observed in previous work by our research group [28,35,66]. The accuracy of the experimental data plays a significant role in improving theoretical calculations and semi-empirical atomic structure analysis.

In future studies, a revision study, of all published Ho I energy levels should be carried out, which was already achieved by our research group for lanthanum [71].

REFERENCES

[1] **RSC** (2025). *Holmium*, https://periodic-table.rsc.org/element/67/holmium.

[2] **Stone, N. J.** (2005). Table of nuclear magnetic dipole and electric quadrupole moments, *Atomic Data and Nuclear Data Tables,* 90, 75-176, *https://doi.org/10.1016/j.add.2005.04.001.*

[3] **Lawler, J.**, **Sneden, C. and Cowan, J.** (2004). Improved atomic data for Ho II and new holmium abundances for the sun and three metal-poor stars, *The Astrophysical Journal*, 604(2), 850. 90, 75-176

[4] **Bord, D.J. and Cowley, C.R.** (2002). On the Abundance of Holmium in the Sun, *Solar Physics*, 211, 3–15.

[5] **Przybylski, A.** (1963). Lines of Holmium in the Spectrum of HD 101065, *Acta Astronomica*, 13, 33–42.

[6] **Roederer, I.U.**, **Cowan, J.J.**, **Preston, G.W.**, **Shectman, S.A.**, **Sneden, C.**, **Thompson, I.B. and Burles, S.M.** (2014). The Ubiquity of the r-process, *The Astrophysical Journal*, 791(1), 32.

[7] **McWilliam, A.** (1997). Abundance Ratios and Galactic Chemical Evolution, *Annual Review of Astronomy and Astrophysics*, 35, 503–556.

[8] **Thomas, D.** (2001). Abundance ratios in hierarchical galaxy formation, *Astrophysics and Space Science*, 277, 209.

[9] **Prochaska, J.X.**, **Howk, J.C. and Wolfe, A.M.** (2003). The Elemental Abundance Pattern in a Galaxy at z = 2.626, *Nature*, 423, 57-59.

[10] **Johnson, J.A. and Cowan, J.J.** (2006). Nucleosynthesis: Stellar and Solar Abundances and Atomic Data, *Astrophysical Journal*, 639, L123–L126.

[11] **Sneden, C. and Others** (2022). Application of Laboratory Atomic Physics to Some Significant Stellar Chemical Composition Questions, *Elements*, 18, 123–145.

[12] **Chen, M.H.**, **Li, L.X.**, **Liang, E.W. and Wang, N.** (2025). Impact of Nuclear Mass Models on r-Process Nucleosynthesis and Heavy Element Abundances in r-Process-Enhanced Metal-Poor Stars, *Astronomy & Astrophysics*, 693, A1.

[13] **Denis, P.A.**, **Quinet, P.**, **Palmeri, P. and Biémont, É.** (2020). The DREAM Database of Lanthanide Atomic Data: Status and Perspectives, *Monthly Notices of the Royal Astronomical Society*, 495(1), 1234–1244.

[14] **Kitamura, H.**, **Takeda, Y.**, **Honda, S. and Aoki, W.** (2017). Spectral Line Identification and Calibration in the Ca II Infrared Triplet Region of the Solar Spectrum, *Astronomy & Astrophysics*, 601, A50.

[15] **Smith, V.V.**, **Cunha, K.**, **Shetrone, M.**, **Hasselquist, S.**, **Andrews, B.H.**, **García-Hernández, D.A.**, **Zasowski, G. and et al.** (2021). The APOGEE Data Release 16 Spectral Line List, *The Astrophysical Journal Supplement Series*, 253(2), 42.

[16] **Shetrone, M.**, **Majewski, S.R.**, **Smith, V.V.**, **Bizyaev, D.**, **García Pérez, A.E.**, **Lawler, J.E. and et al.** (2015). The SDSS-III Apache Point Observatory Galactic Evolution Experiment (APOGEE), *The Astrophysical Journal Supplement Series*, 221(1), 24.

[17] **Wyart, J.F.**, **Camus, P. and Vergès, J.** (1977). Etude du spectre de l'holmium atomique: I. Spectre d'emission infrarouge niveaux d'émission infrarouge niveaux d'énergie de Ho I et structures hyperfines, *Physica B+ C*, 92(3), 377–396.

[18] **Burghardt, B.**, **Buttgenbach, S.**, **Glaeser, N.**, **Harzer, R.**, **Meisel, G.**, **Roski, B. and Traber, F.** (1982). Hyperfine structure measurements in metastable states of ^{165}Ho, *Zeitschrift für Physik A Atoms and Nuclei,* 307, 193-200. *https://doi.org/10.1007/bf01438640*.

[19] **Childs, W.**, **Cok, D.R. and Goodman, L.** (1983). New line classifications in Ho I based on high-precision hyperfine-structure measurement of low levels, *Journal of the Optical Society of America*, 73(2), 151–155.

[20] **Reddy, M. N.**, **Ahmad, S. A. and Rao, G. N.** (1992). Laser optogalvanic spectroscopy of holmium, *J.Opt.Soc. Am.B,* 9(1), 22-26. *https://doi.org/10.1364/JOSAB.9.000022*.

[21] **Smirnov, Yu. M.** (2013). Excitation of low-lying even levels of the holmium atom in the electron-atom collisions, *Opt. Spectrosc.* 114,485. *https://doi.org/10.1134/S0030400X13040188*.

[22] **Kröger S.**, **Wyart J. F. and Luc P.** (1997). Theoretical interpretation of hyperfine structures in doubly-excited configurations $4f^{10}5d6s6p$ and $4f^{10}5d^26s$ and new energy levels in neutral holmium (Ho I), *Phys. Scr. ,* 55, 579 *https://doi.org/10.1088/0031-8949/55/5/010*.

[23] **Den Hartog E. A.**, **Wiese L. M. and Lawler J. E.** (1999). Radiative lifetimes of Ho I and Ho II, *J. Opt. Soc. Am. B,* 16, 2278 *https://doi.org/10.1364/JOSAB.16.002278*.

[24] **Nave, G.** (2003). Atomic transition rates for neutral holmium (Ho I), *Opt.Soc.Am.B, 20, 2193-2202*
https://doi.org/10.1364/JOSAB.20.002193.

[25] **Lawler, J., E.**, **Sneden, C. and Cowan, J. J.** (2004). Improved Atomic Data for Ho II and New Holmium Abundances for the Sun and Three Metal-poor Stars, *Astrophys. J.* 604, 850-860
https://doi.org/10.1086/38206.

[26] **Sansonetti, J.E. and Martin, W.C.** (2005). *Handbook Of Basic Atomic Spectroscopic Data*, volume 34, American Institute of Physics for the National Institute of Standards and Technology.

[27] **Gurell, J.**, **Wahlgren, G.M.**, **Nave, G. and Wyart, J.F.** (2009). Wavelengths, energy levels and hyperfine structure constants in Ho ii, *Physica Scripta*, 79(3), 035306.

[28] **Al-Labady, N.**, **Özdalgiç, B.**, **Er, A.**, **Güzelçimen, F.**, **Öztürk, I.**, **Kröger, S.**, **Kruzins, A.**, **Tamanis, M.**, **Ferber, R. and Başar, G.** (2017). Line identification of atomic and ionic spectra of holmium in the near-UV. Part I. Spectrum of Ho I, *The Astrophysical Journal Supplement Series*, 228(2), 16.

[29] **Başar, G.**, **Al-Labady, N.**, **Özdalgiç, B.**, **Güzelçimen, F.**, **Er, A.**, **Öztürk, I.**, **Ak, T.**, **BİLİr, S.**, **Tamanis, M.**, **Ferber, R.** *et al.* (2017). Line identification of atomic and ionic spectra of holmium in the near-UV. II. Spectra of Ho II and Ho III, *The Astrophysical Journal Supplement Series*, 228(2), 17.

[30] **Stefanska, D. and Furmann, B.** (2018). Hyperfine structure investigations for the odd-parity configuration system in atomic holmium, *Journal of Quantitative Spectroscopy and Radiative Transfer*, 206, 286–295.

[31] **Stefanska D.**, **Ruczkowski J.**, **Elantkowska M. and Furmann, B.** (2018). Fine- and hyperfine structure investigations of the even-parity configuration system of the atomic holmium, *JQSRT,* 213, 180-195.

[32] **Stefanska D.**, **Furmann B. and Gl-owacki P.** (2018). Possibilities of investigations of the temporal variation of the α constant in the holmium atom, *JQSRT,* 213, 159-1687 .

[33] **Furmann B.**, **Stefanska D.**, **Suski M. and Wilman S.** (2018). Identification of new electronic levels in the holmium atom and investigation of their hyperfine structure, *JQSRT,* 219, 117.

[34] **Özdalgıç, B.**, **Başar, G.**, **Güzelçimen, F.**, **Öztürk,** , **Ak, T.**, **Bilir, S.**, **Tamanis, M.**, **Ferber, R. and Kröger, S.** (2019). Line Identification of Atomic and Ionic Spectra of Holmium in the Visible Spectral Range. II. Spectrum of Ho II and Ho III, *Astrophys J Suppl Ser,* 240 (2), 27 .

[35] **Özdalgiç, B.**, **Güzelçimen, F.**, **Öztürk, I.**, **Kröger, S.**, **Kruzins, A.**, **Tamanis, M.**, **Ferber, R. and Başar, G.** (2019). Line identification of atomic and ionic spectra of holmium in the visible spectral range. I. Spectrum of Ho I, *The Astrophysical Journal Supplement Series*, 240(2), 27.

[36] **Elantkowska M.**, **Ruczkowski J.and Sikorski A. and Wilman S.** (2019). Fine- and hyperfine structure investigations of the odd-parity configuration system in atomic holmium, *JQRST,* 237, 106642 .

[37] **Özdalgıç B.**, **Başar G. and Kröger S.** (2019). Hyperfine Structure Analysis of Atomic Holmium in an FT Spectrum in the Visible Spectral Range, *The Astrophysical Journal Supplement Series,* 244, 41 .

[38] **Başar, G.**, **Başar, G.**, **Özdalgiç, B.**, **Öztürk, I.**, **Güzelçimen, F.**, **Bingöl, D. and Kröger, S.** (2020). Laser spectroscopic investigation of atomic holmium in the wavelength range from 780 nm to 830 nm: Hyperfine structure measurements and a new energy level, *JQRST,* 243, 106809.

[39] **Chomski M.**, **Furmann B.**, **Ruczkowski J.**, **Suski M. and Stefanska D.** (2021). Landé g_J factors of the electronic levels of the holmium atom, *JQSRT,* 274, 107865.

[40] **Chomski M.**, **Furmann B.**, **Suski M.**, **Głowacki, P.**, **Stefanska D. and Mieloch S.** (2022). Landé g_J factors of odd-parity electronic levels of the holmium atom, *JQSRT,* 279, 108045 .

[41] **Chomski M.**, **Furmann B.**, **Suski M.**, **Głowacki, P.**, **Stefanska D. and Mieloch S.** (2023). Determination of the energies of new electronic levels of the holmium atom and investigation of their hyperfine structure, *JQSRT,* 297, 108480.

[42] **Bingöl D.**, **Başar Gö .**, **Başar Gü .**, **Öztürk İ. K.**, **Güzelçimen F.**, **Kın Barka S. and Kröger S.** (2023). Verification of the Existence of Recently Published New Energy Levels of Atomic Holmium, *Physics and Astronomy Reports,* 1, 85.

[43] **Furmann D.**, **Klemska S.**, **Mieloch S. and Stefańska D.** (2024). Hyperfine structure and even-parity new levels evaluation in the holmium atom, *JQSRT,* 316, 108903.

[44] **Foot, C.** (2005). *Atomic Physics*, OUP Oxford, ISBN:9780198506959.

[45] **Laska, A.** (2012). *Program for the combinatoric assignment of LS-and jj-coupling term symbols*, Friedrich-Alexander-Universität Erlangen-Nürnberg.

[46] **Martin W. C.**, **Zalubas R. and Hagan L.** (1978). *Atomic Energy Levels–The Rare Earth Elements*, Institute for Basic Standards, National Bureau of Standards, Washington, D.C.20231
https://cir.nii.ac.jp/crid/1363388845421931008.

[47] **Haken, H. and Wolf, H.C.** (2013). *Molecular Physics And Elements Of Quantum Chemistry: Introduction To Experiments And Theory*, Springer Science & Business Media.

[48] **Haigh, C.** (1995). The theory of atomic spectroscopy: jj coupling, intermediate coupling, and configuration interaction, *Journal of Chemical Education*, 72(3), 206.

[49] **Eisberg R. and Resnick R.** (1985). *Quantum Physics Of Atoms, Molecules, Solids, Nuclei, And Particles*, Wiley.

[50] **Demtröder, W.** (2006). *Atoms, Molecules And Photons: An Introduction To Atomic-, Molecular- And Quantum-Physics*, Springer Science & Business Media, ISBN:9783540206316.

[51] **Cowan, R.D.** (1981). *The Theory Of Atomic Structure And Spectra.*, UNIVERSITY OF CALIFORNIA PRESS, ISBN:0520038215.

[52] **Bransden, B.H. and Joachain, C.J.** (2003). *Physics Of Atoms And Molecules*, Pearson Education India.

[53] **Thorne, A.P.** (1988). *Spectrophysics*, Springer, ISBN:9780412274701.

[54] **Demtröder, W.** (2014). *Laser Spectroscopy 1: Basic Principles*, Springer, ISBN:978364253852.

[55] **Goeckner, M.**, **Goree, J. and Sheridan, T.** (1993). Saturation broadening of laser-induced fluorescence from plasma ions, *Review of scientific instruments*, 64(4), 996–1000.

[56] **Demtröder, W.** (2008). *Laser Spectroscopy Vol.2: Experimental Techniques*, Springer e-Books, ISBN:978364253852.

[57] **Barbieri, B.**, **Beverini, N. and Sasso, A.** (1990). Optogalvanic spectroscopy, *Reviews of modern physics*, 62(3), 603.

[58] **Kröger, S.** (1996). *Hyperfeinstruktur Des Thuliums Und Weiterer Lanthanide (Gd, Ho, Er, Yb)* [Doctoral Dissertation, Berlin, Techn. Universitaet].

[59] **Helmrich, G.** (1997). *Spektroskopie: Eine Einführung In Dei Praxis Der Fluoreszenz-Und Laserspektroskopie*, Univ. der Bundeswehr.

[60] **Windholz, L. and Guthöhrlein, G.** (2003). Classification of spectral lines by means of their hyperfine structure. Application to Ta I and Ta II levels, *Physica Scripta*, 2003(T105), 55.

[61] **Windholz, L.** (2016). Finding of previously unknown energy levels using Fourier-transform and laser spectroscopy, *Physica Scripta*, 91(11), 114003.

[62] **Özdalgıç, B.** (2019).Holmiyum elementinin görünür bölgedeki spektral çizgilerinin sınıflandırılması ve aşırı ince yapısının incelenmesi [Doktora Tezi, İ.Ü.].

[63] **Barka, S.**, **Basar Gü.**, **Kröger S. and Basar G.** (2024). New energy levels of atomic holmium discovered by laser spectroscopy in the near infrared spectral range, Spectrochimica Acta Part B Atomic Spectroscopy, 216, 106946.

[64] **Zeiser, A.**, **Kröger, S.**, **Pooyan-Weis, L.**, **Windholz, L. and Guthöhrlein, G.** (2022). A new version of the program fitter for fitting atomic hyperfine structure in optical spectra including the calculation of confidence intervals, *Journal of Quantitative Spectroscopy and Radiative Transfer*, 290, 108294.

[65] **Furmann B.**, **Stefanska D.**, **Wilman S.**, **Chomski M. and Suski M.** (2019). Hyperfine structure studies of the odd-parity electronic levels in the holmium atom. II: New levels, *JQSRT,* 235, 70.

[66] **Zengin, M.**, **Barka, S.K.**, **Öztürk, İ.K.**, **Klincare, I.**, **Kröger, S. and Başar, G.** (2024). Line identification of atomic and ionic spectra of Holmium in the near infrared spectral range from 700 nm to 1750 nm, *Spectrochimica Acta Part B: Atomic Spectroscopy*, 217, 106950.

[67] **Furmann, B.**, **Stefańska, D.**, **Suski, M.**, **Wilman, S. and Chomski, M.** (2019). Hyperfine structure studies of the odd-parity electronic levels of the holmium atom. I: Levels with known energies, *Journal of Quantitative Spectroscopy and Radiative Transfer*, 234, 115–123.

[68] **Gray, D.F.** (2005). *The Observation and Analysis of Stellar Photospheres*, Cambridge University Press, 3rd edition.

[69] **Herwig, F.** (2005). Evolution of asymptotic giant branch stars, *Annu. Rev. Astron. Astrophys.*, 43(1), 435–479.

[70] **Hubble, E.** (1929). A Relation between Distance and Radial Velocity among Extra-galactic Nebulae, *Proceedings of the National Academy of Sciences*, 15, 168–173.

[71] **Güzelçimen, F.**, **Windholz, L.**, **Başar, G. and Kröger, S.** (2022). Revised Energy Levels of Atomic Lanthanum Considering Hyperfine Structure, *The Astrophysical Journal Supplement Series*, 258(2), 28.

[72] **Dankwort, W.**, **Ferch, G. and Gebauer, H.** (1974). Hexadecapole interaction in the atomic ground state of ^{165}Ho, *The European Physical Journal A,* 267(3), 229–237.

[73] **Wyart, J.F. and Camus, P.** (1978). Etude du spectre de l'holmium atomique: II. Interprétation paramétrique des niveaux d'énergie et des structures hyperfines, *Physica B+ C*, 93(2), 227–236.

APPENDICES

APPENDIX A:

APPENDIX A: Energy Levels of Atomic Holmium

Table A.1 : Energy levels of Ho from the literature with their corresponding hfs constants, if available. (Ref 1 and Ref 2 indicate the references of the energy levels and hfs constants, respectively).

J	Parity	$E(\mathrm{cm}^{-1})$	A (MHz)	B (MHz)	Ref 1	Ref 2
15/2	o	0.00	800.4(3.0)	-1167.0(150)	[46]	[17]
			800.583173(36)	-1668.07870(330)		[72]
			800.58309(6)	-1668.089(8)		[18]
			809.2	-1576.9		[73]
13/2	o	5419.70	941.3(3.0)	-1229.1229(150)	[46]	[17]
			937.2088(3)	-1438.065(25)		[18]
			940.5(40)	-1222(19)		[20]
			937.2	-1376.1		[73]
17/2	e	8378.91	778.5(0.6)	217(34)	[46]	[67]
			783.3(1.9)	90(110)		[37]
			775.8(4.5)	569.7(300)		[17]
			784.9	587.6		[17]
			784.7(60)	601(23)		[20]
15/2	e	8427.11	844.6(1.5)	597(108)	[46]	[67]
			842.4(4.5)	800.5(300)		[17]
			843.9	731.5		[73]
			842.5(1.8)	340(110)		[37]
			839.3(0.2)	385(43)		[41]
11/2	o	8605.16	1034.6(0.5)	-1051(7)	[46]	[19]
			1035.1396(9)	-1052.556(30)		[18]
			1039.9(50)	-1052(16)		[20]
			1035.8	-1035.8		[73]
13/2	e	9147.08	918.6(4.5)	2884(300)	[46]	[17]
			910.2	2752.2		[73]
			916.6(0.5)	2668(7)		[19]
			912.0(60)	2659(20)		[20]
			916.5(0.5)	2730(30)		[38]
19/2	e	9741.50	745.3(2.0)	1660(100)	[46]	[37]
			749.5	1952		[73]
			742.9(4.5)	1679(300)		[17]
			740.1(70)	1672(28)		[20]
			745.1(1.4)	1747(78)		[31]

Table A.1 (continued) : Energy levels of Ho from the literature with their corresponding hfs constants, if available. (Ref 1 and Ref 2 indicate the references of the energy levels and hfs constants, respectively).

J	Parity	E(cm^{-1})	A (MHz)	B (MHz)	Ref 1	Ref 2
9/2	o	10695.75	1138.1(0.5)	-491(4)	[46]	[19]
			1137.87(13)	-493.7(1.3)		[18]
			1080.2	-176.9		[73]
21/2	e	11322.31	691.7(0.3)	3487(17)	[46]	[38]
			693.4(4.5)	3316(300)		[17]
			681.1	3642.6		[73]
			711.3(90)	3360(31)		[20]
			694.6(0.8)	3540(11)		[31]
17/2	e	11530.56	770.2(3.0)	1295(150)	[46]	[17]
			775.3	587.6		[73]
			772.8(1.2)	1011(20)		[31]
19/2	e	11689.77	730.9(0.5)	2990(40)	[46]	[38]
			732.1(3.0)	3322(150)		[17]
			735.4	3144.9		[73]
			756.1(70)	2606(24)		[20]
			735.5(0.8)	3022(36)		[31]
15/2	e	12339.04	807(3.0)	243(150)	[46]	[17]
			814.6	-78.8		[73]
			806.7(1.4)	-139(19)		[31]
13/2	e	12344.55	906.9(3.0)	752(150)	[46]	[17]
			915	731.5		[73]
			908.6(0.6)	424(23)		[31]
11/2	e	13082.93	1037.1(0.7)	2388(12)	[46]	[38]
			1037.3(4.5)	2548.5(300)		[17]
			1041.5	2515.3		[73]
			1042.2(1.8)	2358.9(7.7)		[31]
9/2	o	13094.42	884.5(2.0)	1752(22)	[22]	[30]
13/2	e	15081.12	891.0(1.5)	264(60)	[46]	[17]
			912	-365.8		[73]
			891.0(0.4)	119(12)		[31]
17/2	e	15130.31	807.6(3.0)	2257(150)	[46]	[37]
			808.5(1.8)	2120(27)		[31]
			808.2(1.5)	2257.6(60)		[17]
			816.4	2188.5		[73]
15/2	e	15136.06	860.8(0.9)	217(80)	[46]	[38]
			862.4(0.6)	234(14)	[46]	[31]

Table A.1 (continued) : Energy levels of Ho from the literature with their corresponding hfs constants, if available. (Ref 1 and Ref 2 indicate the references of the energy levels and hfs constants, respectively).

J	Parity	E(cm^{-1})	A (MHz)	B (MHz)	Ref 1	Ref 2
			863.1(1.5)	477(60)		[17]
			881.7	566.6		[73]
11/2	e	15792.13	1025.5(0.4)	858(11)	[46]	[38]
			1026.8(1.5)	1043(60)		[17]
			1030.4	1094.27		[73]
			1029.9(2.0)	835(41)		[31]
			1026.5(3.6)	887(57)		[33]
15/2	e	15855.28	1142.4(1.1)	-410(35)	[46]	[33]
			1140.1(1.5)	-243(60)		[17]
			990.8	24.0		[73]
			1143.5(2.4)	-367(60)		[31]
			1142.9(1.9)	-410(56)		[32]
15/2	e	16154.21	903.4(0.9)	439(31)	[46]	[33]
			903.9(1.5)	567(60)		[17]
			1054.4	173.9		[73]
			903.1(1.3)	489(37)		[31]
			903.3(1.0)	446(36)		[32]
17/2	e	16438.01	820.8(1.5)	2263(60)	[46]	[17]
			777.4	-2443.4(4)		[73]
			816.9(50)	2040(18)		[20]
			822.0(0.4)	2000(19)		[31]
			819.7(0.5)	2035(20)		[19]
19/2	e	16683.52	739.9(1.5)	3424(60)	[46]	[17]
			724.6	3513.7		[73]
			739.7(0.5)	3389(12)		[31]
17/2	e	16709.82	1135.6 (0.5)	-1984(30)	[46]	[38]
			1138.0(1.5)	-1805(60)		[17]
			1168.6	-2092.6)		[73]
			1137.9(60)	-1806(20)		[20]
			1140.1(0.8)	-2098(42)		[31]
			1139.7(0.8)	-2045(41)		[33]
9/2	e	16719.62	1208.5(3.0)	2138(150)	[46]	[17]
			1197.4	2233.5		[73]
13/2	e	16735.95	882.7(1.7)	-26(30)	[46]	[33]
			883.6(1.7)	-4(64)	[46]	[31]

Table A.1 (continued) : Energy levels of Ho from the literature with their corresponding hfs constants, if available. (Ref 1 and Ref 2 indicate the references of the energy levels and hfs constants, respectively).

J	Parity	E(cm^{-1})	A (MHz)	B (MHz)	Ref 1	Ref 2
			883.8(1.5)	-192(60)		[17]
			781.3	-119.9)		[73]
			881.6(1.1)	-23(41)		[32]
15/2	e	16882.28	481.3(2.7)	-671(21)	[46]	[31]
			478.8(1.5)	-405(60)		[17]
			483.9	-455.7		[73]
			480.6(50)	-716(19)		[20]
			479.3(1.3)	-641(26)		[32]
			477.7(0.5)	-675(20)		[19]
11/2	e	16937.43	1022.3(3.0)	2069(150)	[46]	[17]
			1029.8	2182.5		[73]
			1024.4(0.7)	1899(26)		[31]
			1024.0(0.6)	1883(19)		[32]
13/2	e	17059.35	557.0(50)	-981(21)	[46]	[20]
			556.7(3.0)	-977(150)		[17]
			644.3	-665.6		[73]
			556.4(0.8)	-1332(18)		[31]
			556.1(0.7)	-1217(40)		[32]
19/2	e	17883.57	1220.50(0.19)	-73(12)	[46]	[38]
			1222.0(4.5)	288(300)		[17]
			1228.9	461.7		[73]
			1224.1(1.6)	-152(36)		[31]
17/2	e	18337.80	1102.2 (0.4)	-1831(13)	[46]	[38]
			1104.0(3.0)	-1517(150)		[17]
			1094.3	-1475.0		[73]
			1105.7(1.5)	-1792(107)		[31]
			1104.7(1.2)	-1782(20)		[33]
11/2	e	18491.21	839.1(3.0)	-228.228(150)	[46]	[17]
			833.7	-263.8(8)		[73]
			842.0(2.0)	-380(29)		[32]
13/2	e	18564.90	869.6 (0.3)	390(40)	[46]	[38]
			868.0(4.5)	594(300)		[17]
			869.7	716.5		[73]
			869.3(0.3)	389(19)		[32]
15/2	o	18572.28	808(4)	1990(180)	[46]	[37]
			805.8(0.8)	1663(318)		[41]

Table A.1 (continued) : Energy levels of Ho from the literature with their corresponding hfs constants, if available. (Ref 1 and Ref 2 indicate the references of the energy levels and hfs constants, respectively).

J	Parity	E(cm^{-1})	A (MHz)	B (MHz)	Ref 1	Ref 2
			798.1	1930.7		[73]
15/2	e	18651.53	863.40 (0.16)	-2740(16)	[46]	[38]
			863.4(1.5)	-257260)		[17]
			838.8	-2491.3		[73]
			866.9(0.4)	-2643(23)		[32]
			865.4(1.4)	-2670(19)		[33]
17/2	o	18737.79	900.5(3.0)	980.4(150)	[46]	[17]
			889.8	950.4		[73]
15/2	e	18756.22	852.7(0.8)	2679(33)	[46]	[33]
			848.7(4.5)	3151(300)		[17]
			867.9	2674.2		[73]
9/2	e	18757.87	1141.8(2.4)	376(78)	[46]	[33]
			1154.2(4.5)	525(300)		[17]
			1144.9	557.6		[73]
11/2	e	18821.25	264.7(0.6)	-446(33)	[46]	[33]
			265.3(1.5)	-228(60)		[17]
			280.9	-71.95		[73]
			264.4(0.7)	-435(40)		[32]
13/2	e	18858.19	465.45(0.23)	-3158(14)	[46]	[38]
			466.0(3.0)	-2956(150)		[17]
			489.3	-2956.0		[73]
			465.0(0.1)	-3154(1)		[32]
			467.8(0.9)	-3185(41)		[33]
13/2	o	18867.54	1478.3(70)	-478(25)	[46]	[20]
			1480.6(1.5)	-474(60)		[17]
			1492.4	-524.7		[73]
			1486.7(2.0)	-848(81)		[30]
15/2	o	19276.94	1301.1(1.5)	-1883(60)	[46]	[17]
			1298.7(70)	-1881(27)		[20]
			1319.7	-1831.8		[73]
11/2	o	20060.76	553.4(40)	-544(16)	[46] [20]	
			549.2(1.5)	-549(60)		[17]
			555.5	-485.7		[73]
15/2	e	20074.89	824.1(0.5)	1658(80)	[46]	[38]
			827.6(3.2)	1561(40)		[33]
			823.2 (1.5)	1430(30)		[37]

Table A.1 (continued) : Energy levels of Ho from the literature with their corresponding hfs constants, if available. (Ref 1 and Ref 2 indicate the references of the energy levels and hfs constants, respectively).

J	Parity	E(cm^{-1})	A (MHz)	B (MHz)	Ref 1	Ref 2
			817	1714(9)		[73]
19/2	o	20124.25	922.8(1.5)	-788(60)	[46]	[17]
			920.2(40)	-783(19)		[20]
			946.8	-869.4		[73]
15/2	e	20167.17	1335.9(1.5)	1250(60)	[46]	[17]
			1335.9(0.2)	1249(5)		[32]
21/2	o	20210.60	1027.7	-194.9	[46]	[73]
			1021.8(1.3)	-600(90)		[37]
			1022.2(1.3)	-663(95)		[41]
13/2	e	20241.31	995.50 (0.22)	252(19)	[46]	[38]
			995.6(3.0)	345(150)		[17]
			919.2	347.8		[73]
			1092.6(50)	429(17)		[20]
			996.2(1.5)	286(61)		[31]
			998.0(1.8)	270(17)		[32]
13/2	e	20258.27	1426.8(1.6)	1755(70)	[46]	[31]
			1426.7(3.0)	1889(150)		[17]
			1424.6(50)	1902(22)		[20]
17/2	o	20315.89	612.4(60)	-1310(27)	[46]	[20]
			615.8(1.5)	-1304(60)		[17]
			747.1	-1433.0		[73]
11/2	e	20493.40	1012.5(0.7)	641(28)	[46]	[32]
			1014.3 (1.1)	790(90)		[37]
			1012.1	812.5		[73]
9/2	e	20493.40	1019.3(1.4)	277(70)		[41]
13/2	o	20493.77	516.9	-1759.8	[46]	[73]
			494.1(3.0)	-1871(150)		[17]
17/2	e	20498.73	1224.0(1.5)	381(60)	[46]	[17]
17/2	e	20568.63	795.1(1.5)	3286(73)	[17]	[67]
			792.9(4.5)	3178(300)		[17]
			773.2	3468.7		[73]
			796.5(2.4)	3358(104)		[31]
17/2	o	20613.81	695.5	-833.4	[46]	[73]
			786.0(1.5)	-1019(60)		[17]
			792.2(1.3)	-1323(78)		[30]
19/2	o	20831.18	963.7(1.1)	-1005(77)	[46]	[30]

Table A.1 (continued) : Energy levels of Ho from the literature with their corresponding hfs constants, if available. (Ref 1 and Ref 2 indicate the references of the energy levels and hfs constants, respectively).

J	Parity	E(cm^{-1})	A (MHz)	B (MHz)	Ref 1	Ref 2
			962.3(3.0)	-1124.3(150)		[17]
			941.7	-590.6		[73]
11/2	e	20849.13	984.1(0.9)	85(14)	[46]	[38]
			977.3	245.8		[73]
13/2	e	21044.81	971.3(2.1)	2240(170)	[46]	[37]
			973.5	2863.1		[73]
15/2	o	21069.22	425.8(1.6)	-2078(84)	[46]	[30]
			425.7(1.5)	-1858.9(60)		[17]
			409.8	-1765.8		[73]
			424.1(60)	-1851(20)		[20]
19/2	e	21217.11	1080.7(1.5)	863(60)	[46]	[17]
9/2	e	21373.17	1197.1(4.5)	2239(300)	[46]	[17]
			1196.8	2305.5		[73]
			1205.2(2.9)	1983(75)		[31]
			1205(2.8)	1983(75)		[30]
17/2	o	21378.54	800.8(1.3)	452(65)	[46]	[30]
			798.1(3.0)	719.6(150)		[17]
			751.3	872.4		[73]
19/2	o	21485.02	803.7(3.0)	3696.8(150)	[46]	[17]
			807.4	3762.5		[73]
21/2	e	21494.89	1031.9(1.2)	1258(88)	[46]	[33]
			1032.5(1.5)	1091(60)		[17]
17/2	o	21552.02	834.8(1.9)	-804(97)	[46]	[30]
			832.8(3.0)	-588(150)		[17]
			862.2	-743.5		[73]
13/2	e	21584.89	1219.6(1.5)	-681(60)	[46]	[17]
			1228.6	-770.5		[73]
15/2	o	21682.90	793.8(0.3)	-586(30)	[46]	[38]
			788.4(3.0)	-359.9(150)		[17]
			813.4	-296.8		[73]
13/2	e	21980.67	1012.1(3.0)	1580(150)	[46]	[17]
15/2	o	22014.13	630.8	-1445.0	[46]	[73]
			649.9(1.5)	-1331.2(60)		[17]
13/2	o	22024.20	747.3(1.1)	1690(30)	[46]	[38]
			748.3(3.0)	1885.9(150)		[17]
			868.2	2458.4		[73]

Table A.1 (continued) : Energy levels of Ho from the literature with their corresponding hfs constants, if available. (Ref 1 and Ref 2 indicate the references of the energy levels and hfs constants, respectively).

J	Parity	E(cm^{-1})	A (MHz)	B (MHz)	Ref 1	Ref 2
13/2	e	22157.86	732.6(40)	222(14)	[46]	[20]
			742.9(3.0)	228(150)		[17]
			743.2	77.9		[73]
			739.3(1.1)	156(49)		[31]
9/2	o	22157.88	360.4(0.9)	-495(80)	[46]	[38]
			385.8	-356.8		[73]
11/2	e	22197.69	876.9(3.0)	1784(150)	[17]	[17]
15/2	e	22227.34	1308.6(1.5)	-2117(60)	[46]	[17]
			1305.3	-1768.8		[73]
			1318.8(60)	-2068(27)		[20]
			1310.3(1.4)	-2081.2081(71)		[31]
15/2	e	22227.36	1308.6(0.5)	-2122(20)	[46]	[19]
13/2	o	22392.88	392.1	-1397.1	[46]	[73]
			512.9(3.0)	-749(150)		[17]
11/2	e	22413.14	617.7(50)	-661(15)	[46]	[20]
			618.5(1.5)	-666(60)		[17]
			614.6	-914.4		[73]
13/2	e	22414.04	818.9(0.8)	587(35)	[46]	[31]
			823.5(3.0)	522(150)		[17]
17/2	e	22476.89	743(3.0)	609(150)	[46]	[17]
15/2	e	22500.62	747.4(0.8)	431(37)	[46]	[31]
			752.5(3.0)	263.8(150)		[17]
11/2	o	22518.59	526	-1277.1	[46]	[73]
			682.6(1.5)	-1187.3(60)		[17]
11/2	o	22593.53	771.9	245.9	[46]	[17]
			870	-6.0		[73]
19/2	e	22866.55	764.2(3.0)	953(150)	[46]	[17]
13/2	e	22978.19	933.0(0.1)	-1150.3(6)	[46]	[31]
			935(3.0)	1120(40)		[37]
			900.3	1286.1		[73]
19/2	o	23211.21	576.5(0.9)	-219(52)	[17]	[30]
			576.5(3.0)	-359.8(150)		[17]
			587.9	-209.9		[73]
21/2	e	23366.71	822(3.0)	1211(150)	[46]	[17]
25/2	e	23375.28	971(3.0)	2632(150)	[46]	[17]
11/2	e	23379.31	985.1(0.4)	-167(23)	[46]	[38]

Table A.1 (continued) : Energy levels of Ho from the literature with their corresponding hfs constants, if available. (Ref 1 and Ref 2 indicate the references of the energy levels and hfs constants, respectively).

J	Parity	E(cm^{-1})	A (MHz)	B (MHz)	Ref 1	Ref 2
			921.9	-77.9		[73]
17/2	e	23498.57	1351(3.0)	120(150)	[46]	[17]
			13711	617.6		[73]
			1348.1(1.1)	90(100)		[37]
13/2	o	23585.31	1078.3(1.5)	-770.5(60)	[46]	[17]
			1036.1	-182.878		[73]
11/2	o	23612.92	1254(3.0)	-383.8(150)	[46]	[17]
			1300.2	-506.7		[73]
15/2	o	23818.54	962.3(3.0)	704.6(150)	[46]	[17]
			962.4	1094.3		[73]
15/2	e	23834.94	1270.96(0.22)	-1715(17)	[46]	[38]
			1274.0(3.0)	-1643(150)		[17]
			1267.9	-1523.0		[73]
9/2	e	23861.17	279(4.5)	-39(300)	[46]	[17]
			260.5	51.0		[73]
17/2	o	23885.74	708.9(1.5)	-1473(95)	[46]	[30]
			705(3.0)	-1445(150)		[17]
			700.9	-1397.1		[73]
13/2	o	23942.71	953.0(3.0)	725.6(150)	[46]	[17]
			990.5	201		[73]
11/2	e	23946.16	618.5(0.5)	-2265(18)	[46]	[38]
			614.0(4.5)	-2338(300)		[17]
			629.9	-2506.3		[73]
13/2	e	23955.69	1005.5	-2344.4	[46]	[73]
			951.93(0.21)	-2451(15)		[38]
13/2	e	24006.23	825(3.0)	2129(150)	[46]	[17]
13/2	e	24014.22	901.28(0.21)	-1404(13)	[46]	[38]
			833.4	-626.6		[73]
15/2	o	24112.04	1212.9(3.0)	1349.2(150)	[46]	[17]
17/2	o	24115.17	1192.4(1.7)	-1682(121)	[46]	[67]
			1196.2			[22]
11/2	e	24141.21	723.0(1.1)	-550(50)	[46]	[37]
			752.2	-113.9		[73]
17/2	e	24263.96	719.5		[46]	[22]
9/2	e	24355.64			[46]	
			949.8	-299.8		[73]

Table A.1 (continued) : Energy levels of Ho from the literature with their corresponding hfs constants, if available. (Ref 1 and Ref 2 indicate the references of the energy levels and hfs constants, respectively).

J	Parity	E(cm^{-1})	A (MHz)	B (MHz)	Ref 1	Ref 2
15/2	o	24357.90	840.3(3.0)	-1873.9(150)	[46]	[17]
			855.9	-2017.7		[73]
17/2	e	24360.81			[46]	
			675.1	344.8		[73]
15/2	e	24376.91	578(4.5)	198(300)	[17]	
19/2	e	24404.19	502.7(3.0)	1583(150)	[46]	[17]
			496.9(1.2)	1491(76)		[31]
13/2	o	24594.75	1359.5(3.0)	3220.1(150)	[46]	[17]
15/2	e	24660.80	752.5(0.3)	-2469(29)	[46]	[38]
			787.6	-3549.6		[73]
19/2	o	24678.25	1209.3(0.4)	-1026(17)	[46]	[38]
			1211.4(3.0)	-1034.4(150)		[17]
			1215.6(70)	-1057(24)		[20]
21/2	e	24714.34	693.7(3.0)	1760(150)	[46]	[17]
13/2	e	24740.52	707.8(1.1)	-771.4(2.3)	[46]	[31]
			707.3(1.7)	-700(100)		[37]
			724.3	-1013.3		[73]
13/2	e	24760.13	626.2(0.5)	445(18)	[46]	[31]
			626.6			[22]
			596.6	456		[22]
17/2	e	24795.58	1135.0(1.5)	1316(88)	[46]	[33]
			1135.9(3.0)	1454(150)		[17]
11/2	e	24830.43	865(4.5)	-354(300)	[17]	[17]
			918.9	-638.6		[73]
11/2	e	24961.42	764.5(4.5)	570(300)	[17]	[17]
11/2	e	25261.55	1026.7(0.1)	970(11)	[46]	[31]
			1027.7(4.5)	989(300)		[17]
11/2	e	25261.55	1120.1	1205.2	[46]	[73]
11/2	e	25261.55	1025.9(0.5)	934(7)	[46]	[19]
15/2	e	25272.63	555.0(0.1)	-768.6(3.5)	[46]	[31]
			556.5(2.1)	-850(150)		[37]
			536	-1328.1		[73]
9/2	e	25453.49			[17]	
			631.1	-827.4		[73]
11/2	e	25503.33	1227.9(4.5)	645(300)	[17]	[17]
			11000	620.6		[73]

Table A.1 (continued) : Energy levels of Ho from the literature with their corresponding hfs constants, if available. (Ref 1 and Ref 2 indicate the references of the energy levels and hfs constants, respectively).

J	Parity	E(cm^{-1})	A (MHz)	B (MHz)	Ref 1	Ref 2
			1227.0(0.1)	639.4(5.0)		[31]
21/2	e	25545.07	1101(3.0)	1214(150)	[46]	[17]
			1107.7(1.7)	576(96)		[31]
19/2	e	25548.26	603(3.0)	1226(150)	[46]	[17]
13/2	e	25571.15	1409.0(4.5)	-1289(300)	[73]	[17]
			1396.8	-1205.2		[73]
			1407.15(3)	-1378.6(2.1)		[18]
			1412.1(60)	-1275(22)		[20]
			1407.9(0.9)	-1369.1(8.4)		[31]
15/2	o	25591.43	375.3(3.0)	-92.9(150)	[46]	[17]
			389.7	-398.7		[73]
11/2	o	25616.48	1737.2(1.5)	-440.7(60)	[46]	[17]
			1721.2	-464.69(69)		[73]
17/2	o	25660.40	969.8(3.0)	-620.6(150)	[46]	[17]
			989.3	-365.8		[73]
9/2	o	25805.04	936.2(3.0)	-425.7(150)	[46]	[17]
			948.3	-368.8		[73]
11/2	e	25914.31	697.2(0.2)	-844.5(6.7)	[22]	[31]
			695.4(1.1)	-1050(60)		[37]
13/2	e	25930.66	1010.3(0.1)	3205.5(7.4)	[46]	[31]
			1022.0(1.6)	3210(90)		[37]
			983.3	3559		[73]
15/2	e	25967.69	830.4		[22]	
21/2	o	25980.35	1171.3(3.0)	443.7(150)	[46]	[17]
15/2	o	26023.52	810.0(3.0)	45(150)	[46]	[17]
9/2	e	26039.99	10677	-245.8	[46]	[73]
			1244.27(13)	-167.2(1.5)		[18]
13/2	o	26127.22	812.1(3.0)	-305.8(150)	[46]	[17]
			812.0(0.7)	23(29)		[38]
			811.8(0.5)	50.9(7.0)		[19]
17/2	o	26143.57	776.7(3.0)	989.4(150)	[46]	[17]
15/2	o	26198.39	1075.9(3.0)	-1298.2(150)	[46]	[17]
			1116.8	-1184.2		[73]
13/2	o	26225.76	732.4(3.0)	-1055.4(150)	[46]	[17]
			741.4	-1618.92		[73]
13/2	o	26288.10	1215.0(3.0)	-1520.1(150)	[46]	[17]

Table A.1 (continued) : Energy levels of Ho from the literature with their corresponding hfs constants, if available. (Ref 1 and Ref 2 indicate the references of the energy levels and hfs constants, respectively).)

J	Parity	E(cm^{-1})	A (MHz)	B (MHz)	Ref 1	Ref 2
			1169.2	-1501.998		[73]
19/2	e	26293.14	986.3		[17]	[22]
17/2	e	26394.99	542.6		[17]	[22]
11/2	o	26443.11	969.2(3.0)	-569.7(150)	[46]	[17]
			1045.4	-1439.04		[73]
15/2	o	26456.72	907.1(3.0)	950.4(150)	[46]	[17]
			861.9	710.5		[73]
17/2	o	26480.47	1091.8(3.0)	66(150)	[46]	[17]
			1064.6	-449.7		[73]
11/2	o	26529.83	752.2(3.0)	1888.9(150)	[46]	[17]
			751.0(60)	1895(20)		[20]
17/2	o	26637.82	1023.2(1.5)	1451.1(60)	[46]	[17]
			948.6	2416.4		[73]
17/2	e	26655.52	1023.2(3.0)	2368(150)	[46]	[17]
11/2	o	26664.67	778.0(2.0)	1443(83)	[46]	[67]
			783.0(3.0)	1469.1(150)		[17]
			849.9	1529.0		[73]
17/2	o	26664.68	1073.8(3.0)	1322.2(150)	[17]	[17]
13/2	o	26673.72	945.5(3.0)	-209.9(150)	[46]	[17]
			965.4	-323.8		[73]
19/2	o	26770.17	729.4(1.4)	1291(73)	[46]	[30]
			727.9(3.0)	1229(150)		[17]
15/2	o	26811.32	1326.7(6.0)	588(19)	[46]	[20]
			1319.3(3.0)	584.6(150)		[17]
9/2	o	26818.67	669.1(3.0)	-989.4(150)	[17]	[73]
			630.8	-1205.2		[73]
15/2	o	26922.41	1134.1	-1253.2	[46]	[73]
			1117.6(3.0)	-908.5(150)		[17]
13/2	e	26947.33	581.6		[17]	[22]
15/2	e	26957.70	1514.8(0.5)	510(40)	[46]	[37]
			1509.2	899.4		[73]
13/2	o	26977.37	884.1	-1346.1	[46]	[73]
			856.2(3.0)	-1478.1(150)		[17]
11/2	o	27049.80	534.2(4.5)	-722.6(300)	[46]	[17]
			527.3	-812.458		[73]
11/2	e	27113.28	1174.0(1.3)	-2127(16)	[63]	[63]

Table A.1 (continued) : Energy levels of Ho from the literature with their corresponding hfs constants, if available. (Ref 1 and Ref 2 indicate the references of the energy levels and hfs constants, respectively).

J	Parity	E(cm^{-1})	A (MHz)	B (MHz)	Ref 1	Ref 2
13/2	e	27141.28	1444.4(1.9)	-1820(100)	[17]	[37]
			1434.8	-1448.0		[73]
21/2	o	27358.81	1161.1(80)	1896(29)	[46]	[20]
			1163.2(3.0)	1888.9(150)		[17]
13/2	o	27423.79	1039.1(3.0)	1565.1(150)	[46]	[17]
			1040.6	1313.1		[73]
19/2	o	27470.27	1121.2(3.0)	2038.8(150)	[46]	[17]
9/2	e	27556.90	1121.1(0.5)	847(7)	[19]	[19]
7/2	e	27575.09	582.1(0.5)	50.9(7)	[19]	[19]
11/2	e	27640.21	1515.2(0.5)	-645(7)	[19]	[19]
11/2	o	27643.13	955.4(3.0)	1733(150)	[46]	[17]
			947.4	1625		[73]
15/2	o	27649.51	991.6(1.4)	1578(88)	[46]	[67]
			995.3(3.0)	1499.1(150)		[17]
19/2	o	27670.98	1038.6(1.5)	2233.8(10.1)	[46]	[67]
			1040.5(3.0)	2128.7(150)		[17]
23/2	o	27697.56	1117.9(3.0)	2686.4(150)	[46]	[17]
13/2	o	27724.36	936.5(3.0)	1310.2(150)	[46]	[17]
17/2	o	27923.18	1142.6 (0.8)	1588(80)	[46]	[38]
			1155.7(3.0)	1430.1(150)		[17]
17/2	o	28244.29	661.6(1.1)	731(27)	[46]	[30]
			660.1(3.0)	578.7(150)		[17]
15/2	o	28315.79	875.7(1.2)	267(60)	[46]	[30]
			875.4			[22]
19/2	o	28393.24	876.6(0.4)	1245(6)	[46]	[67]
19/2	o	28393.24	877.2(3.0)	1028.4(150)	[46]	[17]
19/2	o	28393.24	876.2(1.5)	1239(106)	[46]	[30]
21/2	o	28481.24	1029.6(1.4)	2067(104)	[46]	[30]
			1031.9(3.0)	1828.9(150)		[17]
13/2	o	28561.18	606.5(0.4)	1521(13)	[46]	[38]
			608.6			[22]
13/2	o	28598.25	357.3(3.0)	269.8(150)	[17]	[17]
			334.6	110.9		[73]
11/2	o	28642.79	439.4(0.4)	504(14)	[22]	[38]
			438.0(1.0)	577(42)		[67]
11/2	e	28793.03	620.0(1.1)	-520(80)	[22]	[37]

Table A.1 (continued) : Energy levels of Ho from the literature with their corresponding hfs constants, if available. (Ref 1 and Ref 2 indicate the references of the energy levels and hfs constants, respectively).

J	Parity	E(cm^{-1})	A (MHz)	B (MHz)	Ref 1	Ref 2
17/2	o	28861.41	615.9(0.5)	-78(21)	[46]	[30]
			617.9(3.0)	-179.9(150)		[17]
			634.0(60)	201(19)		[20]
21/2	o	28887.78	954.3(0.1)	1809(13)	[46]	[30]
			956(3.0)	1589(150)		[17]
			905.7(70)	1388(31)		[20]
15/2	o	28952.03	1002.5(3.0)	0(150)	[17]	[17]
			989.9	-128.9		[73]
13/2	o	29013.43	636.3 (2.0)	-392(65)	[38]	[38]
			635.4(0.2)	-561(47)		[41]
11/2	e	29069.78	950.1	-827.4(4)	[46]	[73]
			958.2(2.1)	-1400(80)		[37]
15/2	o	29086.67	396.1(2.8)	-550(34)	[46]	[30]
			399.6(3.0)	-615(150)		[17]
11/2	e	29096.77	1050.7(2.7)	200(110)	[22]	[37]
11/2	o	29116.10	496.0(2.3)	-498(107)	[17]	[67]
			497.9(4.5)	-449.7(300)		[17]
11/2	o	29207.00	562.4(4.5)	75(300)	[17]	[17]
11/2	o	29208.43	488.7(4.5)	360(300)	[17]	[17]
			330.7	-887.4		[73]
9/2	o	29248.34	622.4	-1037.3	[17]	[73]
23/2	o	29266.91	1090.9(3.0)	2743(150)	[46]	[17]
13/2	o	29324.82	1001.6(4.5)	-1679(300)	[17]	[17]
13/2	o		973.5	-1505.0		[73]
9/2	o	29422.14	1273.3	290.8	[17]	[73]
17/2	o	29443.09	1061(3.0)	2084(150)	[46]	[17]
19/2	o	29465.60	978.5(0.6)	1842(50)	[46]	[38]
			984.8(3.0)	1628(150)		[17]
17/2	o	29531.25	1218.2(3.0)	122(182)	[65]	[65]
9/2	o	29544.70	712(3.0)	1889(150)	[17]	[17]
21/2	o	29558.07	975(3.0)	3028(150)	[46]	[17]
25/2	o	29576.42	1081.9(3.0)	5666(150)	[46]	[17]
9/2	e	29638.41	704(3)	-420(60)	[22]	[37]
15/2	e	29642.60	771.39	434.71	[46]	[73]
13/2	o	29660.86	961.4(3.0)	-1349(150)	[17]	[17]
19/2	o	29692.67	528.8(3.0)	2143(150)	[46]	[17]

Table A.1 (continued) : Energy levels of Ho from the literature with their corresponding hfs constants, if available. (Ref 1 and Ref 2 indicate the references of the energy levels and hfs constants, respectively).

J	Parity	E(cm^{-1})	A (MHz)	B (MHz)	Ref 1	Ref 2
11/2	o	29702.04	1362.2(4.5)	-1277(300)	[17]	[17]
13/2	e	29751.91	13811(5)	1470(280)	[46]	[37]
			908.4	-3363.8		[73]
9/2	o	29760.74	1189.0(4.5)	255.(300)	[17]	[17]
			1109.9	260.8		[73]
15/2	o	29834.05	1050.4(1.9)	36(103)	[17]	[30]
			1051.7(3.0)	-90(150)		[17]
13/2	o	29842.26	1149.1(0.5)	404(91)	[17]	[30]
			1145.5(3.0)	450(150)		[17]
11/2	o	29930.22	1177.6	992.3	[17]	[73]
15/2	o	29979.51	1229.4(3.0)	96(150)	[46]	[17]
23/2	o	30011.00	1017.2(3.0)	3058(150)	[46]	[17]
13/2	o	30029.36	956.7	377.7	[46]	[73]
15/2	o	30049.10	1285.7(0.6)	348(40)	[46]	[38]
			1293.3(4.5)	135(300)		[17]
			1242.7	3.0		[73]
19/2	o	30049.71	638.9(0.4)	1449(30)	[17]	[38]
			644.0(3.0)	1199(150)		[17]
21/2	o	30067.84	784(3.0)	2009(150)	[17]	[17]
9/2	o	30071.29	1784.1(4.5)	-570(300)	[17]	[17]
			1766.4	-482.7		[73]
17/2	o	30135.31	1049.7(3.1)	2400(195)	[46]	[67]
			1050.2(3.0)	2278(150)		[17]
11/2	o	30146.15	1104.9(1.8)	538(81)	[46]	[30]
			1023.2	-24.0		[73]
15/2	o	30242.96	992.3	2827.1	[17]	[73]
11/2	o	30280.49	1193.7(1.6)	1623(50)	[22]	[30]
			1178.2			[22]
			1187.6(1.9)	1810(150)		[37]
17/2	o	30327.49	788.1(3.0)	552(150)	[46]	[17]
13/2	o	30339.01	1444.7(1.8)	461(73)	[46]	[30]
			1442.0(4.5)	480(300)		[17]
11/2	e	30423.60	792.2(2.1)	-1441(23)	[22]	[31]
19/2	o	30425.58	947.4(0.6)	1840(19)	[46]	[38]
			951.7(0.5)	1835(18)		[67]
			950.4			[22]

Table A.1 (continued) : Energy levels of Ho from the literature with their corresponding hfs constants, if available. (Ref 1 and Ref 2 indicate the references of the energy levels and hfs constants, respectively).

J	Parity	E(cm^{-1})	A (MHz)	B (MHz)	Ref 1	Ref 2
21/2	o	30484.68	974.6(3.0)	1349(150)	[46]	[17]
17/2	o	30582.15	707.2(3.0)	1619(150)	[46]	[17]
13/2	o	30589.44	1444.3(3.6)	-1245(92)	[17]	[67]
15/2	o	30773.59	838.2(3.0)	1184(150)	[46]	[17]
17/2	o	30805.90	761.84(0.19)	-275(19)	[46]	[38]
			767.5			[22]
			764.5(2.4)	-293(51)		[30]
19/2	o	31018.63	951.0(3.0)	654(150)	[46]	[17]
			945.18(0.22)	665(30)		[38]
15/2	o	31042.44	734.5(3.0)	1199(150)	[46]	[17]
11/2	o	31062.22	1195.5(0.9)	653(48)	[63]	[63]
17/2	o	31116.22	1532.8(0.5)	-1653(9)	[46]	[38]
			1539(2.5)	-1539(124)		[67]
			1534.7(0.9)	-1380(40)		[37]
13/2	o	31272.03	673.2(1.7)	349(92)	[22]	[30]
			665.6		[22]	[30]
17/2	o	31286.69	849.3(3.0)	815(150)	[17]	[17]
15/2	o	31339.46	627.41(0.20)	193(11)	[17]	[38]
			627.2(1.3)	1218(41)	[17]	[30]
			632.6			[22]
13/2	o	31380.04	747.5(2.6)	840(22)	[17]	[67]
			744.9(1.7)	818(48)		[30]
			747.7(2.9)	1090(160)		[37]
			734.5			[22]
11/2	o	31394.02	784.6(1.6)	394(71)	[17]	[67]
			800.5			[22]
15/2	o	31443.26	1025.55(0.20)	-1100(14)	[46]	[38]
			1028.8(0.4)	-1099(30)		[67]
21/2	o	31515.70	1134.1(4.5)	2590(300)	[46]	[17]
15/2	o	31540.19	811.9(0.3)	200(13)	[46]	[38]
			814.1(0.9)	217(101)		[67]
			809.5			[22]
19/2	o	31605.80	1167.3(0.4)	702(27)	[65]	[65]
13/2	e	31662.00			[21]	
13/2	e	31698.45			[21]	
11/2	o	31707.40	906.4(1.6)	1782(73)	[17]	[30]

Table A.1 (continued) : Energy levels of Ho from the literature with their corresponding hfs constants, if available. (Ref 1 and Ref 2 indicate the references of the energy levels and hfs constants, respectively).

J	Parity	E(cm^{-1})	A (MHz)	B (MHz)	Ref 1	Ref 2
			893.4			[22]
17/2	o	31793.06	858.6(4.5)	2054(300)	[46]	[17]
13/2	o	31816.26	43.5(0.6)	-1672(12)	[46]	[38]
			41.8(1.7)	-1584(24)		[67]
11/2	e	31903.28	764.0(1.3)	0(50)	[22]	[37]
13/2	o	31964.93	594.4(0.5)	-849(28)	[63]	[63]
17/2	o	31984.62	809.4(4.5)	1919(300)	[17]	[17]
9/2	e	32039.76	812.1(1.8)	-360(60)	[46]	[37]
15/2	o	32134.09	545.1(3.5)	1512(131)	[65]	[65]
11/2	o	32280.32	586.4(0.9)	-411(80)	[65]	[65]
19/2	o	32331.28	980.6(4.5)	2518(300)	[17]	[17]
15/2	o	32334.47	650.1(0.2)	492(105)	[41]	[41]
11/2	o	32542.31	1026.5	77.9	[17]	[73]
9/2	e	32613.12	898.9(2.1)	1282(58)	[41]	[41]
13/2	o	32623.42	771.9(0.1)	1747(28)	[65]	[65]
7/2	e	32633.75	1089.5(1.9)	950(60)	[22]	[37]
11/2	o	32663.47	915.0(2.0)	-77(35)	[63]	[63]
15/2	o	32671.45	848.8(1.1)	1232(35)	[46]	[67]
15/2	o	32671.45	849.5(1.1)	1218(41)	[46]	[30]
15/2	o	32671.45	845(3)	1280(140)	[46]	[37]
7/2	e	32758.37	866.0(2.8)	1070.(70)	[22]	[37]
9/2	e	32785.21	845.8(1.5)	-525.(43)	[46]	[31]
			847.3(2.3)	-980.(90)		[37]
17/2	o	32809.73	863.6(0.4)	2756.(27)	[65]	[65]
11/2	e	32837.21	10677(6)	-2010.(430)	[22]	[37]
13/2	o	32898.14	12677(7)	120.(380)	[17]	[37]
			1005.2	3019.0		[73]
11/2	e	32917.77	1158.3(0.7)	280(40)	[22]	[37]
7/2	e	32931.51	887.7(0.6)	-1136(24)	[22]	[30]
			897.9(1.9)	-1360(60)		[37]
15/2	o	33005.31	663.24(0.22)	-361(16)	[46]	[38]
			662.1(1.6)	-132(76)		[30]
15/2	o	33091.50	674.4(0.4)	304.(60)	[46]	[38]
7/2	e	33188.42	846.4(2.1)	-670(60)	[22]	[37]
17/2	o	33268.75	788.6(1.3)	1981(82)	[22]	[30]
			784.0(1.9)	2130(130)		[37]

Table A.1 (continued) : Energy levels of Ho from the literature with their corresponding hfs constants, if available. (Ref 1 and Ref 2 indicate the references of the energy levels and hfs constants, respectively).

J	Parity	E(cm^{-1})	A (MHz)	B (MHz)	Ref 1	Ref 2
11/2	e	33312.51	962(30)	-1140(820)	[22]	[37]
17/2	o	33466.85	1164.8(0.6)	2165(20)	[33]	[33]
15/2	o	33523.57	937.6(0.8)	921(54)	[22]	[33]
9/2	e	33577.20			[22]	
15/2	o	33651.60	748.9(0.3)	2503(19)	[65]	[65]
13/2	o	33689.15	1255.5(0.7)	609(34)	[65]	[65]
13/2	o	33784.23	793.4(3.1)	785(13)	[65]	[65]
15/2	o	33808.02	1127.1(1.2)	1189(29)	[33]	[33]
13/2	e	33907.40			[22]	
17/2	o	33983.40	1014.7(1.9)	1591(34)	[22]	[30]
15/2	o	33983.68	979.7(0.6)	1163(54)	[22]	[67]
			979.8(0.8)	1123(50)		[30]
11/2	e	33986.71	1103.4(2.2)	680(100)	[22]	[37]
15/2	o	34055.69	1063.8(0.8)	1432(11)	[41]	[41]
19/2	o	34013.03	1077.9(0.2)	1228(21)	[22]	[67]
			1078.1(0.2)	1219(25)		[30]
			1078.3(1.7)	1260(160)		[37]
11/2	o	34108.80	885.1(0.4)	561(40)	[65]	[65]
13/2	o	34185.82	747.7(0.4)	641(18)	[22]	[30]
11/2	e	34270.67			[22]	
19/2	o	34277.91	1125.0(0.5)	1644(54)	[22]	[67]
			1125.0(0.5)	-1644.1644(54)		[30]
			1123.9(1.4)	1640(80)		[37]
17/2	o	34293.91	905.1(1.6)	261(34)	[22]	[67]
			903.5(0.9)	228(51)		[30]
			909.1(2.0)	250(110)		[37]
13/2	o	34309.15	1051.2(0.5)	1485(29)	[22]	[67]
			1051.5(0.4)	1481(40)		[30]
			1052(3)	2120(170)		[37]
15/2	o	34346.46	697.2(4.0)	799(48)	[22]	[67]
			693.2(2.9)	846(69)		[30]
11/2	e	34366.07			[46]	
19/2	o	34502.26	921.8(2.6)	3257(82)	[22]	[67]
			923(3)	2990(160)		[37]
13/2	o	34534.53	807.0(1.0)	658(27)	[22]	[67]
			806.4(0.9)	680(32)		[30]

Table A.1 (continued) : Energy levels of Ho from the literature with their corresponding hfs constants, if available. (Ref 1 and Ref 2 indicate the references of the energy levels and hfs constants, respectively).

J	Parity	E(cm^{-1})	A (MHz)	B (MHz)	Ref 1	Ref 2
17/2	o	34537.92	883.7(0.9)	1613(26)	[22]	[30]
			885.8(2.1)	1610(110)		[37]
9/2	o	34564.81	1222.7(6.6)	1443(115)	[65]	[65]
11/2	o	34584.43	1391.3(0.7)	543(27)	[22]	[30]
21/2	o	34648.05	1091.8(2.4)	3590(140)	[22]	[37]
13/2	o	34653.56	962.1(1.6)	589(70)	[46]	[30]
15/2	o	34706.50	751.7(2.3)	-495(122)	[65]	[65]
19/2	o	34737.11	915.4(0.1)	1910(30)	[22]	[67]
			915.4(1.1)	1884(55)		[30]
			914(3)	1830(160)		[37]
11/2	o	34714.29	744(5)	650(300)	[22]	[37]
15/2	o	34853.26	650.6(1.2)	504(71)	[22]	[30]
17/2	o	34868.26	431.2(0.6)	1276(27)	[22]	[67]
			430.5(1.9)	1300(160)		[37]
21/2	o	34879.66	791.2(1.3)	3862(93)	[22]	[30]
			792(4)	4080(230)		[37]
15/2	o	34888.46	557.0(0.7)	1442(36)	[22]	[67]
			556.8(1.0)	1474(29)		[30]
			556.3 (1.4)	1270(100)		[37]
15/2	o	35034.88	632.4(0.9)	445(168)	[41]	[41]
9/2	e	35040.75	960.7(0.7)	-831(90)	[46]	[38]
			962.3(1.6)	-750(60)		[37]
11/2	o	35051.06	972.1(0.9)	1243(16)	[65]	[65]
19/2	o	36071.92	980.6(1.5)	2043(103)	[41]	[41]
7/2	e	35078.45			[22]	
13/2	o	35085.06	736.0(1.0)	1219(22)	[65]	[65]
9/2	e	35270.88	977.0(1.4)	-470(50)	[22]	[37]
13/2	o	35270.88	709.0(1.9)	569(32)	[33]	[33]
13/2	o	35359.94	620.7(0.7)	599(20)	[65]	[65]
15/2	o	35397.77	688.0(1.3)	1695(21)	[65]	[65]
13/2	o	35434.63	897.6(0.3)	-1271(39)	[22]	[67]
			897.9(0.4)	-1253(58)		[30]
			896.9(2.9)	-970(190)		[37]
21/2	o	35473.43	1161.5(1.1)	1660(110)	[22]	[37]
19/2	o	35498.58	1090.2(0.3)	702(27)	[65]	[65]
11/2	o	35514.11	670.8(1.4)	1357(28)	[22]	[32]

Table A.1 (continued) : Energy levels of Ho from the literature with their corresponding hfs constants, if available. (Ref 1 and Ref 2 indicate the references of the energy levels and hfs constants, respectively).

J	Parity	E(cm^{-1})	A (MHz)	B (MHz)	Ref 1	Ref 2
			671.0(2.3)	1329(27)		[30]
			673(4)	1370(180)		[37]
17/2	o	35599.50	882.0(4.0)	887(44)	[22]	[67]
			885.7(2.2)	930(77)		[30]
15/2	o	35633.95	1239.5(0.9)	1980(14)	[65]	[65]
15/2	o	35671.30	889.7(0.6)	550(47)	[33]	[33]
17/2	o	35692.30	858.1(1.4)	1677(91)	[22]	[30]
13/2	o	35737.24	840.4(0.6)	945(40)	[32]	[32]
11/2	o	35819.64	705.2(2.8)	601(224)	[41]	[41]
15/2	o	35919.52	854.6(0.6)	866(20)	[33]	[33]
7/2	e	36001.87	11655(3)	260(130)	[22]	[37]
11/2	e	36011.48	864.4(0.3)	5.7(5.8)	[23]	[32]
13/2	o	36016.09	1089.2(1.1)	706(20)	[30]	[30]
17/2	o	36152.56	827.5(0.6)	855(57)	[33]	[33]
15/2	o	36203.63	1045.8(0.6)	813(31)	[65]	[65]
19/2	o	36229.59	880.7(0.4)	718(16)	[22]	[67]
			880.3(1.2)	733(70)		[32]
13/2	o	36328.99	821.1(0.6)	1576(45)	[30]	[30]
15/2	e	36344.52	1997.6(70)	-284(20)	[46]	[20]
17/2	e	36367.65	715(3.0)	2690(200)	[46]	[37]
13/2	o	36445.54	1063.2(0.8)	599(20)	[65]	[65]
7/2	e	36504.15			[22]	
11/2	o	36646.34	948.5(5.3)	-30(1)	[41]	[41]
13/2	e	36663.94	850.0(80)	1340(23)	[46]	[20]
15/2	o	36665.85	1009.9(0.7)	1212(59)	[65]	[65]
17/2	o	36677.81	1238.8(2.1)	251(116)	[22]	[67]
19/2	e	36726.65	1305.2(70)	-617(32)	[46]	[20]
17/2	e	36791.24	1620.0(80)	1615(28)	[46]	[20]
11/2	o	36859.56	538(4)	600(120)	[63]	[63]
15/2	e	36860.75	1416(4)	-1263(190)	[46]	[38]
13/2	o	36873.76	1145.5(0.4)	-1156(28)	[46]	[30]
			1142.29 (0.14)	-1146(10)		[38]
			1145.5 (0.4)	-1156(28)		[30]
19/2	o	36888.64	926.3(0.4)	1750(40)	[22]	[67]
			925.9(0.4)	1737(85)		[32]
17/2	o	36889.6	1148.5(1.3)	-117(18)	[41]	[41]

Table A.1 (continued) : Energy levels of Ho from the literature with their corresponding hfs constants, if available. (Ref 1 and Ref 2 indicate the references of the energy levels and hfs constants, respectively).

J	Parity	E(cm^{-1})	A (MHz)	B (MHz)	Ref 1	Ref 2
13/2	e	36895.69			[46]	
15/2	o	36905.61	1299.6(0.3)	-617(78)	[65]	[65]
13/2	o	36954.20	1205.8(1.0)	1107(21)	[63]	[63]
15/2	e	36958.59	187(3)	-1110(260)	[46]	[37]
19/2	o	36997.50	1137.5(1.2)	1704(51)	[33]	[33]
11/2	o	37029.70	55(3)	-1240(160)	[46]	[37]
13/2	o	37128.86	843.9(1.7)	153(76)	[65]	[65]
15/2	o	37150.34	1309.0(1.1)	576(24)	[33]	[33]
11/2	o	37226.97	963.3(1.3)	313(51)	[22]	[30]
			962.4(1.5)	313(62)		[32]
15/2	e	37233.47	714.2(2.7)	620(190)	[22]	[37]
17/2	o	37252.22	1073.1(1.3)	1237(41)	[41]	[41]
15/2	e	37324.64			[46]	
17/2	e	37388.72	1188.5(70)	-262(22)	[46]	[20]
13/2	e	37404.14			[46]	
15/2	e	37404.14			[46]	
17/2	o	37412.14	1125.9(0.4)	1399(24)	[65]	[65]
15/2	o	37426.02	1101.8(0.5)	321(30)	[22]	[67]
			1100.7(2.2)	390(130)		[37]
11/2	e	37438.53			[46]	
13/2	e	37481.94	778.0(60)	639(31)	[46]	[20]
13/2	o	37492.43	1067.5(0.9)	153(24)	[65]	[65]
13/2	o	37550.85			[22]	
15/2	o	37550.85			[22]	
19/2	o	37619.29	1287.8(1.3)	-1268(91)	[22]	[30]
			1280.8(1.1)	-1340(80)		[37]
15/2	o	37623.09	720.5(50)	919(20)	[46]	[20]
15/2	e	37623.18	645.1(0.6)	59(57)	[41]	[41]
15/2	e	37651.71			[46]	
17/2	o	37652.23	977.2(1.8)	380(130)	[22]	[38]
			977.5(1.4)	457(75)		[30]
17/2	o	37664.13			[22]	
21/2	o	37709.99	1170.9(1.7)	-1426(83)	[23]	[30]
			11733(5)	-1270(300)		[37]
15/2	o	37717.23	881.6(2.5)	1659(49)	[33]	[33]
17/2	o	37762.23	1297.5(2.4)	-658(164)	[41]	[41]

Table A.1 (continued) : Energy levels of Ho from the literature with their corresponding hfs constants, if available. (Ref 1 and Ref 2 indicate the references of the energy levels and hfs constants, respectively).

J	Parity	E(cm^{-1})	A (MHz)	B (MHz)	Ref 1	Ref 2
11/2	o	37774.72	1255.9(1.2)	1541(54)	[63]	[63]
17/2	o	37762.26	1304.0(2.5)	-669(104)	[22]	[30]
			1298.7(2.0)	-670(100)		[37]
19/2	o	37772.62	1219.4(0.7)	-1531(56)	[22]	[67]
			12177(3)	-1360(150)		[37]
13/2	o	37776.32	1083.6(1.1)	-2070(56)	[63]	[63]
15/2	o	37842.85	1454.3(1.2)	-1026(52)	[22]	[67]
			1450.3(0.5)	-974(21)		[38]
17/2	o	37864.95	1239.2(1.8)	423(101)	[22]	[67]
15/2	e	37865.77	1094.7(70)	-2744(34)	[46]	[20]
17/2	o	37971.48	1190.6(0.3)	-346(13)	[41]	[41]
17/2	o	37971.23	1192.5(1.2)	-44(45)	[33]	[33]
19/2	o	38035.35	870.6(0.3)	2071(15)	[33]	[33]
11/2	o	38048.24	666.1(0.3)	-387(110)	[63]	[63]
13/2	o	38051.38	966.0(0.8)	409(53)	[65]	[65]
13/2	o	38077.21	1408.9(1.7)	-239(35)	[41]	[41]
21/2	o	38078.98	639.0(0.1)	1782(36)	[33]	[33]
15/2	o	38087.78	1015.3(0.7)	-540(33)	[63]	[63]
17/2	e	38124.76	812.3(1.2)	-300(80)	[22]	[37]
17/2	o	38229.97	243.0(0.4)	-1212(64)	[65]	[65]
13/2	o	38241.67	613.9(2.4)	-698(118)	[22]	[67]
			610.7(2.0)	-800(70)		[37]
13/2	e	38244.65			[46]	
15/2	e	38244.65			[46]	
11/2	o	38250.32	648.7(3.1)	-180(58)	[22]	[30]
			651.8(1.9)	-122(30)		[32]
19/2	o	38257.25	118.0(1.6)	-1400(121)	[41]	[41]
15/2	o	38273.6	965.4(0.2)	1449(160)	[41]	[41]
17/2	o	38303.27	943.3(0.7)	1628(201)	[41]	[41]
17/2	o	38317.38	655.4(0.4)	0.8(18.0)	[33]	[33]
15/2	e	38320.93	616(4)	3920(250)	[22]	[37]
15/2	o	38343.62	960.0(0.5)	-648(62)	[65]	[65]
15/2	o	38345.8	523.4(2.1)	471(102)	[22]	[32]
			521(3)	530(270)		[37]
13/2	o	38397.18			[46]	
17/2	o	38405.86	330.0(0.3)	-823(39)	[33]	[33]

Table A.1 (continued) : Energy levels of Ho from the literature with their corresponding hfs constants, if available. (Ref 1 and Ref 2 indicate the references of the energy levels and hfs constants, respectively).

J	Parity	E(cm^{-1})	A (MHz)	B (MHz)	Ref 1	Ref 2
13/2	o	38445.46	1333.3(2.4)	-560(150)	[22]	[37]
13/2	o	38482.43	672.9(0.9)	559(99)	[41]	[41]
15/2	o	38509.07	222.0(1.0)	-1174(31)	[65]	[65]
13/2	e	38513.79	225.1(60)	-2018(28)	[46]	[20]
13/2	o	38598.79	826.7(0.6)	-787(25)	[65]	[65]
15/2	o	38601.75	579.4(0.4)	973(35)	[33]	[33]
21/2	e	38613.34	643.6(1.4)	420(70)	[22]	[37]
13/2	o	38653.82	656.8(0.6)	-620(29)	[65]	[65]
13/2	e	38665.46	901.6(1.8)	-781(218)	[41]	[41]
11/2	o	38703.35	282.6(1.5)	-1120(22)	[32]	[32]
17/2	o	38768.08	928.6(0.7)	2705(11)	[33]	[33]
19/2	e	38785.33			[22]	
17/2	e	38806.69	725.4(0.1)	-65(40)	[41]	[41]
15/2	e	38806.72	808.1(1.8)	-870(100)	[22]	[37]
			725.4(0.1)	-65(40)		[41]
13/2	o	38824.35	872.0(1.0)	452(33)	[65]	[65]
13/2	e	38828.16			[46]	
11/2	o	38896.12	1008.0(3.0)	449(17)	[65]	[65]
15/2	e	38966.58	816.6(2.0)	-520(110)	[22]	[37]
11/2	e	39019.06	1111.8(6.5)	231(26)	[41]	[41]
17/2	e	39071.65			[22]	
15/2	o	39073.71	887.0(0.3)	-239(37)	[65]	[65]
13/2	e	39098.76	10333(4)	-220(240)	[46]	[37]
15/2	e	39098.76	911(4)	960(230)	[46]	[37]
19/2	e	39156.60	693.5(1.6)	-510(80)	[22]	[37]
13/2	e	39171.93			[46]	
15/2	e	39171.93			[46]	
17/2	o	39223.17	899.8(1.7)	1309(72)	[33]	[33]
17/2	e	39273.06	721.781.6)	900(80)	[22]	[37]
15/2	o	39293.04	809.3(0.2)	1144(83)	[33]	[33]
11/2	o	39345.04	859.3(0.8)	1138(49)	[33]	[33]
13/2	e	39554.49			[46]	
13/2	e	39591.01	1260.7(0.8)	26(184)	[41]	[41]
13/2	e	39653.44	767.0(0.6)	575(16)	[63]	[63]
15/2	e	39676.57			[46]	
19/2	e	39700.28	809(3)	-80(160)	[22]	[37]

Table A.1 (continued) : Energy levels of Ho from the literature with their corresponding hfs constants, if available. (Ref 1 and Ref 2 indicate the references of the energy levels and hfs constants, respectively).

J	Parity	E(cm^{-1})	A (MHz)	B (MHz)	Ref 1	Ref 2
13/2	o	39875.45	1203.8(0.4)	957(15)	[32]	[32]
			1204.9(1.2)	940(71)		[41]
15/2	e	39904.45	10688(3)	1400(170)	[46]	[37]
17/2	e	39910.59	524.7(2.5)	2190(140)	[22]	[37]
17/2	o	40023.78	1067.0(2.0)	637(42)	[65]	[65]
17/2	e	40051.48	997(4)	1610(150)	[22]	[37]
13/2	o	40069.22	768.3(1.9)	848(110)	[22]	[67]
			768.8(1.7)	890(90)		[37]
11/2	o	40077.35	1143.8(0.5)	-635(10)	[63]	[63]
15/2	e	40101.22	972.0(2.0)	170(140)	[22]	[37]
15/2	e	40151.13	1040.5(2.2)	620(190)	[22]	[37]
13/2	o	40165.71	1869.9(0.7)	-1043(13)	[63]	[63]
21/2	e	40205.63	600.1(0.3)	-307(5)	[41]	[41]
17/2	e	40220.59	1048.3(1.7)	1733(116)	[41]	[41]
15/2	o	40234.24			[22]	
15/2	e	40265.25	691.6(2.5)	1220(140)	[22]	[37]
17/2	e	40270.03	734.7(2.8)	120(90)	[22]	[37]
13/2	o	40430.49	1067.8(2.3)	-233(210)	[41]	[41]
13/2	e	40438.59	784.8(2.0)	388(91)	[41]	[41]
15/2	e	40446.63	772.9(0.4)	-530(29)	[41]	[41]
13/2	e	40464.79			[22]	
17/2	e	40648.25	660.5(1.6)	-750(80)	[22]	[37]
			663.0(0.8)	-761(151)		[41]
19/2	e	40674.64	642.3(2.4)	-450(130)	[22]	[37]
17/2	o	40701.57	655.9(0.3)	54(8)	[22]	[67]
			656.5(1.7)	70(110)		[37]
17/2	o	40776.90	565.9(0.3)	1234(2)	[22]	[67]
19/2	o	40817.12	797.5(1.3)	1397(77)	[41]	[41]
11/2	o	41088.94	706.3(0.2)	139(170)	[41]	[41]
19/2	e	41124.70	779.3(1.5)	-629(101)	[22]	[31]
			702.4(2.0)	-440(140)		[37]
19/2	o	41255.89	686.0(0.4)	184(41)	[22]	[67]
			682.5(1.6)	40(80)		[37]
13/2	o	41499.79	958(0.2)	45(58)	[41]	[41]
21/2	o	41704.35	649.1(1.1)	663(77)	[22]	[30]
			648.2(1.8)	760(110)		[37]

Table A.1 (continued) : Energy levels of Ho from the literature with their corresponding hfs constants, if available. (Ref 1 and Ref 2 indicate the references of the energy levels and hfs constants, respectively).

J	Parity	E(cm^{-1})	A (MHz)	B (MHz)	Ref 1	Ref 2
17/2	o	41971.91	847.0(2.0)	752(79)	[33]	[33]
9/2	e	42189.40	451.4(1.4)	-698(192)	[41]	[41]
17/2	e	42337.80	1409.6(0.8)	-178(52)	[63]	[63]
23/2	o	42381.97	592.5(1.5)	1039(95)	[22]	[30]
			587.5(1.6)	-1510(90)		[37]
17/2	e	42407.40	980.0(2.1)	-655(110)	[63]	[63]
15/2	e	42770.41	1284.8(0.6)	945(39)	[63]	[63]
19/2	o	43054.38			[22]	
15/2	o	43278.51			[22]	
25/2	o	43505.33	536.2(0.1)	2775(131)	[41]	[41]
23/2	o	44283.99	619.3(1.9)	2481(113)	[41]	[41]
21/2	o	44904.20	653.1(2.2)	2250(250)	[22]	[37]

CURRICULUM VITAE

Name SURNAME: Seda KIN BARKA

EDUCATION:

- **B.Sc.:** 2002, Istanbul University, Faculty of Science, Physics Department
- **M.Sc.:**2005, Miami University of Ohio, Faculty of Science and Letters, Physics Department

PROFESSIONAL EXPERIENCE AND REWARDS:

- 2015-present Lecturer at Acibadem Mehmet Ali Aydinlar University, Vocational School of Health Services, Opticianry Programme.

PUBLICATIONS, PRESENTATIONS AND PATENTS ON THE THESIS:

- **Kın Barka S., Başar Gü, Kröger S. & Başar Gö.** (2024). New energy levels of atomic holmium discovered by laser spectroscopy in the near infrared spectral range *Spectrochimica Acta Part-B Atomic Spectroscopy,* 216,106946
- **Kın Barka S., Başar Gü, Başar Gö., Kanat Öztürk İ. & Kröger S.**, (2024). Laser Spectroscopic Investigations of New Energy Levels of Atomic Holmium in the Range from 690 nm to 830 nm, *ICONAT 2024- International Conference on Natural Sciences and Technologies,* Adrasan (Antalya), Turkey, 30 May- 01 June, Online Oral Presentation, 19-20. (Abstract-Conference Book)

OTHER PUBLICATIONS, PRESENTATIONS AND PATENTS:

- **Zengin, M., Barka, S., İpek Kanat Öztürk, İ., Klincare, I., Kröger, S., & Başar, G.**, (2024). Line identification of atomic and ionic spectra of Holmium in the near infrared spectral range from 700 nm to 1750 nm. *Spectrochimica Acta Part-B Atomic Spectroscopy*, 217, 106950.

- **Kröger, S., BAŞAR, G., KANAT ÖZTÜRK, İ., KIN BARKA, S., Windholz, L. & Ferber, R.**, (2024). Investigation of Transitions to the Atomic Ground State in Fourier Transform Spectra of Holmium. *Physics and Astronomy Reports*, 2(2), 88-93.

- **Bingöl, D., Başar, G., Başar, G., Kanat Öztürk, İ., Güzelçimen, F., Kın Barka, S. & Kröger, S.**, (2023). Verification of the Existence of Recently Published New Energy Levels of Atomic Holmium. *Physics and Astronomy Reports*, 1(2), 85-92.

- **Akyuz, S., Başar, G., Başar, G., Kin, S., & Kroeger, S.** (2009). Studies on kyotorphin and D-kyotorphin in aqueous solution by Raman spectroscopy. *Journal of Molecular Structure*, 924, 42–46.

- **Başar, G., & Kin, S.** (2008). Monitoring of spectroscopic changes of a single trapped fission yeast cell by using a Raman tweezers set-up. *Optics Communications*, 281(19), 4998–5003.

- **Sands, B., Welsh, M., Kin, S., Marhatta, R., Hinkle, J., & Bayram, S.**, (2007). Raman scattering spectroscopy of liquid nitrogen molecules: An advanced undergraduate physics laboratory experiment. *American Journal of Physics*, 75(6), 488–495.

- **Bayram, S. B. and Kin, S. and Welsh, M. J. and Hinkle, J. D.**, (2006). Collisional depolarization of Zeeman coherences in the ^{133}Cs $6p\,^2P_{3/2}$ level: Double-resonance two-photon polarization spectroscopy *Physical Review A*,73, 4, 042713.